NASA Technical Paper 2484

November 1985

Decoupled and Linear Quadratic Regulator Control of a Large, Flexible Space Antenna With an Observer in the Control Loop

Harold A. Hamer,
Katherine G. Johnson,
and John W. Young

NASA

Decoupled and Linear Quadratic
Regulator Control of a Large,
Flexible Space Antenna With an
Observer in the Control Loop

Harold A. Hamer,
Katherine G. Johnson,
and John W. Young

*Langley Research Center*
Hampton, Virginia

Summary

An analysis has been performed to compare decoupled and linear quadratic regulator (LQR) procedures for the control of a large, flexible space antenna. Control objectives involved (1) commanding changes in the rigid-body modes, (2) nulling initial disturbances in the rigid-body modes, or (3) nulling initial disturbances in the first three flexible modes. Control was achieved with two three-axis control-moment gyros located on the antenna column. The results are presented to illustrate various effects on control requirements for the two procedures. These effects include errors in the initial estimates of state variables, variations in the type, number, and location of sensors, and deletions of state-variable estimates for certain flexible modes after control activation. The advantages of incorporating a time lag in the control feedback are also illustrated. In addition, the effects of inoperative-control situations were analyzed with regard to control requirements and resultant modal responses. Comparisons are included which show the effects of perfect state feedback with no residual modes (ideal case). Time-history responses are presented to illustrate the various effects on the control procedures.

Introduction

The advent of the NASA Space Transportation System (STS) has provided the capability of establishing large space structures in Earth orbit for scientific and operational missions. Such structures include large, flexible space antennas and the proposed space station, which may be, in part, flexible. These structures will require control for attitude orientation as well as procedures for controlling the flexible modes. These control problems are considered in this paper for a 122-m (400-ft) diameter hoop-column antenna (ref. 1). A finite-element mathematical model of the antenna is used, which provides an excellent tool for simulated control analysis of realistic large, flexible space structures. Previous control studies of this antenna model include references 2 and 3. The antenna is depicted in sketch A and is described in reference 1.

The present paper is an extension of the study reported in reference 2. This study represented the idealized condition; that is, perfect knowledge of the state vector was assumed for feedback and no residual modes were considered in the mathematical model. Most of the results pertained to a decoupled-control procedure with a brief comparison shown for a linear quadratic regulator (LQR) procedure. The results were presented essentially as a parametric analysis of rigid-body and flexible-mode control require-
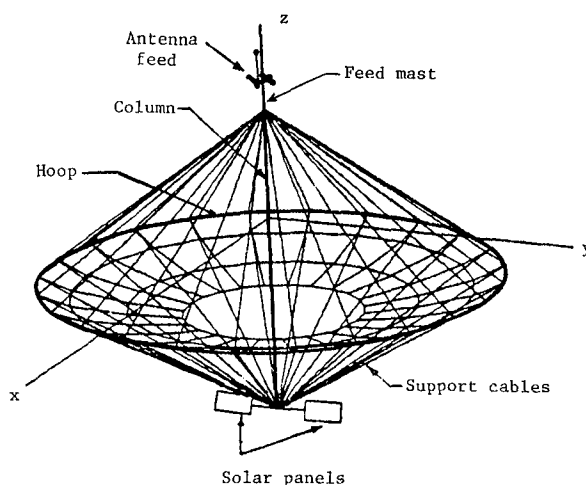
Sketch A

ments over a large range of closed-loop frequencies and damping ratios. Various arrangements and locations for two types of control actuators (control-moment gyros (CMG's) and reaction-control jets) were investigated. Effects of varying the number of controlled flexible modes were also determined.

In the present paper, an observer is used for estimating the state variables. In addition, residual modes are incorporated into the analysis and their effects are investigated. These modes can be assumed to be either unknown (not included in the antenna model) or known but not included in the control law. In reference 2, the control-actuator arrangement which appeared to be the most practical employed one three-axis CMG at the top of the column and one at the bottom. With one exception, this arrangement is used for the present analysis. The values selected for the closed-loop dynamics are based on the results of reference 1. Only the first three flexible modes are included in the control law, because the data in reference 2 showed large increases in the control requirements with additional modes included. It was also shown in reference 2 that the decoupled- and LQR-control procedures gave comparable results; hence, both procedures are analyzed and compared in the present analysis.

Effects on the control requirements are analyzed herein for (1) commanding changes in the rigid-body modes, (2) nulling initial disturbances in the rigid-body modes, or (3) nulling initial disturbances in the first three flexible modes. The study includes the effects of (1) inoperative-control situations, (2) values selected for closed-loop dynamics, (3) errors in initial knowledge of state variables, (4) time lag in control feedback, (5) number and location of sensors, and (6) deletions of estimates in some of the flexible modes. Results are shown in tabular form, in parametric plots, and as sample time histories of modal-

amplitude and control responses. The control system and observer are assumed to be perfect, in that no actuator or sensor dynamics are included in the analysis.

Symbols and Abbreviations

$\mathbf{A}$	system matrix (eq. (4))
A_n	modal amplitude (eq. (2)), where n is the mode number $(1, 2, \ldots, 6)$
$\mathbf{B}$	control influence matrix (eq. (4))
$\mathbf{C}$	observation matrix (eq. (9))
CMG	control-moment gyro
$\mathbf{d}$	displacement vector (eq. (3))
$\mathbf{F}$	decoupled feedback gain matrix (eq. (5))
$\mathbf{G}$	decoupled feedforward gain matrix (eq. (5))
$\mathbf{I}$	moment-of-inertia matrix (eq. (1))
I_x, I_y, I_z, I_{xz}	center-of-gravity moments and product of inertia
J	objective function (eq. (7))
$\mathbf{K}$	LQR feedback gain matrix (eq. (6))
$\mathbf{K}'$	estimator gain matrix (eq. (13))
LQR	linear quadratic regulator
l	distance (see fig. 1)
$M_{i,j}$	angular momentum, where i is the control direction and j is the actuator location
m_n	modal mass
$\mathbf{P}$	control-vector weighting matrix (eq. (7))
$\mathbf{Q}$	state-vector weighting matrix (eq. (7))
r	radius of hoop
$\mathbf{s}$	vector of system input noise (eq. (10))
$\mathbf{T}$	torque vector
$T_{i,j}$	components of torque, where i is the control direction and j is the actuator location
T_{max}	maximum value for actuator requiring largest torque
T_n	natural period
T_{total}	sum of maximum torque values for the six actuators
t	time
$\mathbf{u}$	observation noise (eq. (12))
$\mathbf{v}$	input command vector (eq. (5))
w	weight
x, y, z	coordinates of antenna center of gravity
$\mathbf{x}$	state vector
$\mathbf{y}$	observation vector (eq. (8))
$\mathbf{z}$	sensor output vector without noise
ε	estimator error, $\mathbf{y} - \mathbf{C}'\hat{\mathbf{x}}$
ς_d	desired damping ratio
ς_n	natural damping ratio
θ, ϕ, ψ	rotation angle about x-, y-, and z-axis, respectively
τ	time constant
$\mathbf{\Phi}_{i,j}^{(n)}$	mode-shape matrix, where n is the mode number, i is the direction, and j is the location
$\mathbf{\Phi}_{i,j}'^{(n)}$	mode-slope matrix, where n is the mode number, i is the direction, and j is the location
ω_d	desired frequency
ω_n	natural frequency

Subscripts:

F	feedback
G	feedforward
i, j	control direction and actuator location, respectively

A matrix with a prime relates to the estimator equations. Dots over symbols indicate derivatives with respect to time. A circumflex (^) over a symbol indicates an estimate of the state variable. All matrices are given in units of inches, pounds, and seconds.

Mathematical Model of Antenna

A large space structure such as the hoop-column antenna has, in theory, an infinite number of flexible (vibration) modes. To facilitate analytical treatment of the control problem, a finite-order, linearized model was formulated. For the analysis of this report, the structural model was selected to contain

six of the lowest flexible modes of the 122-m-diameter hoop-column antenna described in reference 1. The three rigid-body rotation modes are included in the analysis.

The equations of motion used to represent the rigid-body and vibration modes of the antenna are given below. Rigid-body rotations (for small angles) about the antenna center of gravity for two three-axis CMG actuators on the column are represented by

$$\begin{pmatrix} \ddot{\theta} \\ \ddot{\phi} \\ \ddot{\psi} \end{pmatrix} = \left[\mathbf{I}^{-1} \mid \mathbf{I}^{-1} \right] \mathbf{T} \qquad (1)$$

where $\mathbf{T} = [T_{x,1}, T_{y,1}, T_{z,1}, T_{x,2}, T_{y,2}, T_{z,2}]^T$. The CMG's were used on the column such that control torques were about the x-, y-, and z-axes, as defined in figure 1. The CMG's are numbered to be consistent with reference 2.

Variations in modal amplitudes of the flexible modes are represented by

$$\ddot{A}_n + 2\varsigma_n \omega_n \dot{A}_n + \omega_n^2 A_n = \frac{1}{m_n} \mathbf{\Phi}'^T \mathbf{T}$$

$$(n = 1, 2, \ldots, 6) \qquad (2)$$

where m_n is the modal mass and $\mathbf{\Phi}'$ is the mode-slope matrix. It should be noted that A_n values in equation (2) are modal-amplitude displacement variables and do not represent actual physical displacements. The physical displacement at some point on the antenna includes linear combinations of the modal amplitudes and the mode shapes and is given by the transformation

$$\mathbf{d}_j = \mathbf{\Phi} A_n \qquad (3)$$

where $\mathbf{\Phi}$ is the mode-shape matrix.

The mode-slope data used in the analysis were taken from unpublished results of a NASTRAN® model of the 122-m-diameter hoop-column antenna system and are provided in reference 2. Table I shows the weight and the inertias of the antenna. The modal masses, the natural frequencies, and the natural damping ratios of the six flexible modes considered in the analysis are also given in table I. As a matter of interest, the unforced transient behavior of these modes is presented in figure 2.

Decoupled and LQR Control

The second-order equations in the analysis (eqs. (1) and (2)) can be reduced to first-order equations (state-vector form) and written as

$$\dot{\mathbf{x}} = \mathbf{A}\mathbf{x} + \mathbf{B}\mathbf{T} \qquad (4)$$

where the state vector

$$\mathbf{x} = [\theta, \phi, \psi, A_1, A_2, \ldots, A_6, \dot{\theta}, \dot{\phi}, \dot{\psi}, \dot{A}_1, \dot{A}_2, \ldots, \dot{A}_6]^T$$

A_1, A_2, and A_3 are the controlled flexible modes, and A_4, A_5, and A_6 are considered as residual modes. The $\mathbf{B}$ matrices used in the present analysis are given in table II. The composition of the $\mathbf{A}$ matrix is defined in reference 2.

Decoupled Control

Since decoupling theory is analyzed extensively in the literature, the discussion of its application in this paper is limited to some general remarks. The decoupling control law is taken as

$$\mathbf{T} = \mathbf{F}\hat{\mathbf{x}} + \mathbf{G}\mathbf{v} \qquad (5)$$

where $\hat{\mathbf{x}}$ is the estimated state vector, $\mathbf{v}$ is the input command vector, and $\mathbf{F}$ and $\mathbf{G}$ are feedback and feedforward gain matrices, respectively. (As noted, estimates of the modal variables are used because these variables cannot be measured directly.) Decoupling theory provides a method for determining the $\mathbf{F}$ and $\mathbf{G}$ matrices such that independent control is maintained for each of the decoupled (controlled) state variables. Different values can be selected for the closed-loop dynamics (ω_d and ς_d) without affecting the independent control capability. Examples are given in reference 2 which illustrate the manner in which the theory was applied to the system equations in determining the $\mathbf{F}$ and $\mathbf{G}$ matrices. The values for the closed-loop dynamics used in the current analysis are given in table III. The "standard" case corresponds to ς_d values which give approximately the same value (10 sec) for time to damp to 1 percent for each of the three flexible modes. The corresponding $\mathbf{F}$ matrix for the standard case is shown in table IV for two control arrangements. The $\mathbf{G}$ matrix is given in table V. An additional $\mathbf{F}$ matrix, used for LQR comparison, is given in table VI. The $\mathbf{F}$ and $\mathbf{G}$ matrices were calculated for a reduced-order model (no residual modes); hence, $\hat{\mathbf{x}} = [\hat{\theta}, \hat{\phi}, \hat{\psi}, \hat{A}_1, \hat{A}_2, \hat{A}_3, \dot{\hat{\theta}}, \dot{\hat{\phi}}, \dot{\hat{\psi}}, \dot{\hat{A}}_1, \dot{\hat{A}}_2, \dot{\hat{A}}_3]^T$. When the residual modes are included in the estimator, zero columns must be added to the $\mathbf{F}$ matrices in order to make the matrices of equation (5) compatible. This has been done in table IV by adding three zero columns after both column 6 and column 12. In this case, $\hat{\mathbf{x}}$ becomes an 18×1 vector. The decoupled and LQR gain matrices, as well as all other matrices in the paper, are given in units of inches, pounds, and seconds.

3

LQR Control

The asymptotic LQR approach of reference 4 was also used to calculate the state feedback control gains. (A computer program is given in ref. 5 for performing these computations.) The control law for the LQR results is given by

$$\mathbf{T} = \mathbf{K}\hat{\mathbf{x}} \qquad (6)$$

The control gain matrix is computed subject to the constraint of equation (4) such that the following function is minimized:

$$J = \lim_{t \to \infty} \int_0^t (\mathbf{x}^T \mathbf{Q} \mathbf{x} + \mathbf{T}^T \mathbf{P} \mathbf{T}) \, dt \qquad (7)$$

where $\mathbf{Q}$ and $\mathbf{P}$ are positive definite symmetric weighting matrices for the states and controls and can be varied in order to achieve desired closed-loop dynamics. For the present analysis, the identity matrix was used for $\mathbf{P}$; the state-vector weighting matrix $\mathbf{Q}$ was adjusted to obtain three different sets (cases) of closed-loop dynamics. (See table III.)

The $\mathbf{K}$ gains were used in the control law (eq. (6)) for the subsequent LQR control analysis. In addition, in order to compare the decoupled- and LQR-control procedures, the resultant LQR closed-loop dynamics (ω_d and ς_d) were used as inputs to the decoupling program to calculate the decoupled gains. Most of the comparison results pertain to case 2 (table III); hence, the gain matrices for the two control procedures (both having identical closed-loop dynamics) are presented in table VI for this case. The weightings $\mathbf{Q}$ used for the LQR procedure are given in reference 2. The $\mathbf{B}$ matrix is the same as that shown at the top of table II. The $\mathbf{K}$ gain matrices for cases 1 and 3 are given in reference 2. (With the observer incorporated into the system, the 6×12 matrix was expanded by adding three zero columns after both column 6 and column 12 to account for the three residual modes.)

Incorporation of Observer

An observer was incorporated into the control procedures in order to calculate estimates of the state variables as required in equations (5) and (6). An attitude-measurement device (e.g., a star tracker) and a rate-measurement device (e.g., a rate gyro) were assumed to be present at certain locations on the column. The sensor output is given by

$$\mathbf{y} = \mathbf{z} + \mathbf{u} \qquad (8)$$

where $\mathbf{z} = \mathbf{C}\mathbf{x}$. As an example, the observation matrix $\mathbf{C}$ is

$$\mathbf{C}_{6 \times 18} = \left[\begin{array}{ccc|c|ccccc} & & & & \Phi_{x,1}^{'(1)} & \Phi_{x,1}^{'(2)} & \cdots & \Phi_{x,1}^{'(6)} \\ & \mathbf{0}_{3 \times 9} & & \mathbf{I}_{3 \times 3} & \Phi_{y,1}^{'(1)} & \Phi_{y,1}^{'(2)} & \cdots & \Phi_{y,1}^{'(6)} \\ & & & & \Phi_{z,1}^{'(1)} & \Phi_{z,1}^{'(2)} & \cdots & \Phi_{z,1}^{'(6)} \\ \hline & \Phi_{x,4}^{'(1)} & \Phi_{x,4}^{'(2)} & \cdots & \Phi_{x,4}^{'(6)} & & & \\ \mathbf{I}_{3 \times 3} & \Phi_{y,4}^{'(1)} & \Phi_{y,4}^{'(2)} & \cdots & \Phi_{y,4}^{'(6)} & & \mathbf{0}_{3 \times 9} & \\ & \Phi_{z,4}^{'(1)} & \Phi_{z,4}^{'(2)} & \cdots & \Phi_{z,4}^{'(6)} & & & \end{array} \right] \qquad (9)$$

where $\mathbf{I}_{3 \times 3}$ is the identity matrix and $\mathbf{z} = [\theta, \phi, \psi, A_1, A_2, \ldots, A_6, \dot{\theta}, \dot{\phi}, \dot{\psi}, \dot{A}_1, \dot{A}_2, \ldots, \dot{A}_6]^T$. The superscripts on the mode slopes refer to the flexible-mode number. The subscripts on the mode slopes refer to the direction and location. For example, the subscript $x, 1$ refers to the mode slope in the x-direction at location 1 on the column (fig. 1). The observation matrix shown in equation (9) senses attitude rate in the x-, y-, and z-directions at location 1 and senses attitude in the x-, y-, and z-directions at location 4. Mode-slope values for various locations on the column are given in reference 2. The values corresponding to equation (9) are presented in table VII.

The complete set of equations required for the control analysis becomes

$$\dot{\mathbf{x}} = \mathbf{Ax} + \mathbf{BT} + \mathbf{s} \tag{10}$$

$$\mathbf{T} = \mathbf{K}\hat{\mathbf{x}} \text{ (for LQR control)} \tag{11a}$$

$$\mathbf{T} = \mathbf{F}\hat{\mathbf{x}} + \mathbf{Gv} \text{ (for decoupled control)} \tag{11b}$$

$$\mathbf{y} = \mathbf{Cx} + \mathbf{u} \tag{12}$$

$$\dot{\hat{\mathbf{x}}} = \mathbf{A}'\hat{\mathbf{x}} + \mathbf{B}'\mathbf{T} + \mathbf{K}'(\mathbf{y} - \mathbf{C}'\hat{\mathbf{x}})$$

$$= (\mathbf{A}' - \mathbf{K}'\mathbf{C}' + \mathbf{B}'\mathbf{K})\hat{\mathbf{x}} + \mathbf{K}'\mathbf{Cx} \text{ (for LQR control)} \tag{13a}$$

$$= (\mathbf{A}' - \mathbf{K}'\mathbf{C}' + \mathbf{B}'\mathbf{F})\hat{\mathbf{x}} + \mathbf{K}'\mathbf{Cx} + \mathbf{B}'\mathbf{Gv} \text{ (for decoupled control)} \tag{13b}$$

The estimator equations (eqs. (13)) calculate the estimates of the states $\hat{\mathbf{x}}$ from the measurement equation $\mathbf{y}$ and the estimator gains $\mathbf{K}'$, which are determined with a full-order, steady-state Kalman-Bucy filter. If all modes are estimated, $\mathbf{C}' = \mathbf{C}$. However, if, for example, the residual modes are not estimated, $\mathbf{C}'$ becomes a 6×12 matrix. The estimator gains were calculated with the technique given in reference 5.

The set of composite equations used for the LQR-control analysis is

$$\begin{pmatrix} \dot{\mathbf{x}} \\ \dot{\hat{\mathbf{x}}} \end{pmatrix} = \left[\begin{array}{c|c} \mathbf{A}_{18\times18} & \mathbf{B}_{18\times6}\,\mathbf{K}_{6\times12} \\ \hline \mathbf{K}'_{12\times6}\,\mathbf{C}_{6\times18} & \mathbf{A}'_{12\times12} - \mathbf{K}'_{12\times6}\,\mathbf{C}'_{6\times12} + \mathbf{B}'_{12\times6}\,\mathbf{K}_{6\times12} \end{array} \right] \begin{pmatrix} x \\ \hat{x} \end{pmatrix} \tag{14}$$

For the decoupled-control analysis, $\mathbf{K}$ is replaced by $\mathbf{F}$ in equation (14) and the term

$$\left[\begin{array}{c} \mathbf{B}_{18\times6}\,\mathbf{G}_{6\times6} \\ \hline \mathbf{B}'_{12\times6}\,\mathbf{G}_{6\times6} \end{array} \right] \mathbf{v}$$

is added to the right side of the equation. The subscripts indicate the dimensions of the various elements for the case in which the three residual modes are not estimated. With precalculated values for $\mathbf{K}'$ and $\mathbf{K}$ (or $\mathbf{K}'$, $\mathbf{F}$, and $\mathbf{G}$), the composite set of equations was integrated to obtain time-history responses for specified initial conditions in the various modes. In determining the estimator gain matrix, the weighting matrices $\mathbf{S}$ and $\mathbf{U}$ for the states and the observations, which are analogous to the covariances of $\mathbf{s}$ and $\mathbf{u}$, were varied until acceptable performance (satisfactory estimator eigenvalues and realistic gain values) was obtained. The resulting matrices were

$$\mathbf{S} = \mathrm{diag}(.1, .1, .1, 10^5, 10^5, 10^5, 10^{11}, 10^7, 10^5, .1, .1, \ldots, .1)$$

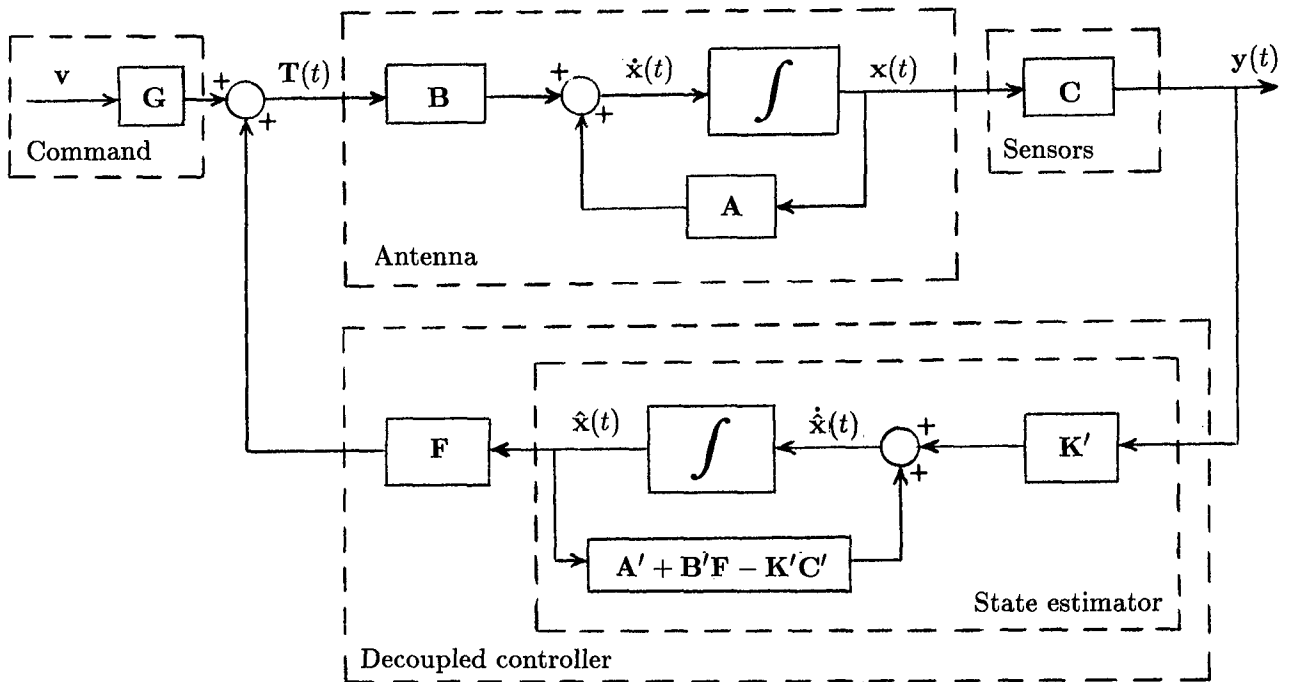$$\mathbf{U} = \mathrm{diag}(1, 1, 1, 1, 1, 10)$$

for the case in which the three residual modes are estimated, and

$$\mathbf{S} = \mathrm{diag}(.1, .1, .1, 10^5, 10^5, 10^5, .1, .1, \ldots, .1)$$

$$\mathbf{U} = \mathrm{diag}(1, 1, 1, 1, 1, 1000)$$

for the case in which the three residual modes are not estimated.

A block diagram for decoupled control is shown in sketch B. (A block diagram for LQR control is the same, with the exclusion of the $\mathbf{G}$ matrix.)

v Command → **G** → + → **T(t)** → **B** → + → **ẋ(t)** → ∫ → **x(t)** → **C** Sensors → **y(t)**

A

Antenna

F ← **x̂(t)** ← ∫ ← **x̂̇(t)** ← + ← **K'** ←

A' + B'F − K'C'

State estimator

Decoupled controller

Sketch B

Results and Discussion

Results of the study are presented to illustrate various effects on the control requirements. The effects are analyzed for (1) commanding changes in the rigid-body modes, (2) nulling initial disturbances in the rigid-body modes, or (3) nulling initial disturbances in the first three flexible modes. The cases for (1) and (2) are referred to as rigid-body command and rigid-body control, respectively, even though control is being applied to maintain the first three flexible modes at zero. Likewise, the cases for (3) are referred to as flexible-mode control. Comparisons are made between the decoupled- and LQR-control procedures, with the results shown in tabular form, parametric plots, and sample time histories of modal-amplitude and control responses. All time histories are for the observer in the control-system loop.

Momentum and the maximum value for torque input are used as measures of control requirements when making various comparisons. The momentum time histories represent the area under the torque-response curves. The momentum values in the tables and parametric plots are the values at the end of each computer run, when the torque responses have been essentially zeroed out. The total torque is the sum of the maximum absolute values for the six actuators. Maximum torque is the value for that actuator requiring the highest absolute value of torque.

General Considerations

For simulation, two three-axis CMG's were used as actuators to control initial disturbances of 0.01 rad in the rigid-body modes or of 1 in. in the three flexible modes. Since the system equations are linear, the results can be scaled to any constant positive multiple of these initial conditions. Initial disturbances were also included in the three residual modes, even though it was determined that the results were not materially affected by their inclusion. Except where noted, the CMG's were placed at the top and bottom of the antenna column at locations 1 and 2 as shown in figure 1. It was assumed that three-axis attitude sensors and three-axis attitude-rate sensors were available at various locations on the column for determining estimates of the state variables. Except where noted, one three-axis attitude sensor at location 1 was used for rigid-body control, and one three-axis attitude-rate sensor at location 1 and one three-axis attitude sensor at location 4 were used for flexible-mode control.

In general, it was assumed that the control system was not activated until the initial estimates were known to 90 percent of the true values for the rigid-body modes and for the first three flexible modes. The initial estimates are actually the initial conditions in the estimator equations. Except where noted, estimates of the residual modes were included in the control procedure. No initial knowledge was assumed for the residual modes, inasmuch as these modes were not included in the control law. It was

6

found that the initial estimate in these modes was of little significance to the control requirements.

Various sets of values were used for the closed-loop dynamics (ω_d and ζ_d). The standard case refers to those values listed in table III, in which the damping ratios for the three flexible modes were selected such that the time required to damp the three flexible modes to 1 percent was approximately 10 sec. The LQR closed-loop values are included in table III. The values for case 2 are close to the standard values. As stated previously, these values were used in the decoupling procedure for most of the comparisons with the LQR procedure.

Effect of Observer

In reference 2, the effect of an observer was not studied; that is, perfect knowledge of the state variables was assumed for feedback. Also, the effect of residual modes was not included. The present paper is an extension to the work of this reference and includes both effects. Results with and without an observer for three cases of closed-loop dynamics are presented in table VIII. The three cases correspond to the closed-loop values in table III, in which it is shown that the three sets of values are essentially the same except for the flexible-mode damping ratios, which represent high, medium, and low damping cases. The procedure used in arriving at these values is described in the section entitled "LQR Control." It should be noted that the same closed-loop eigenvalues for the decoupled and LQR controls were used to obtain the results given in table VIII. Note that the closed-loop flexible-mode frequencies in table III are close to the natural frequencies (table I).

The data in table VIII show that the control requirements are appreciably higher when the observer is used for decoupled or LQR rigid-body control than when the observer is not used. For flexible-mode control, the requirements are generally lower with the observer than they are without. Typical time histories of control without an observer are shown in reference 2, and time histories of control with an observer are shown and discussed subsequently in this report.

In comparing the three cases in table VIII, the requirements for rigid-body control are not affected by flexible-mode closed-loop damping. The requirements for flexible-mode control, however, decrease as the damping is lowered. Also, the momentum requirements are lower for LQR control than for decoupled control, with a pronounced reduction shown for low damping (case 3).

For case 2, data are also included for flexible-mode control with one three-axis attitude sensor at location 1. The results show that one sensor is sufficient, especially for LQR control.

Transient Effects

For ideal (no observer) decoupled control, there are no transients in the undisturbed modes. With the incorporation of an observer, transients are introduced, and they are compared in this section with LQR transients, which are present in either case.

As far as control requirements are concerned, the LQR procedure appears to be the better, especially for flexible-mode control. However, LQR control has more of an effect on the modes that are not initially disturbed, that is, the modes that are intended to remain at zero. These transient effects, with the observer in the system, are presented in table IX and in figures 3 and 4. The data in the table show that the flexible-mode transients for cases 1 and 2 are 2 to 6 times higher for LQR control than for decoupled control. For low damping (case 3), these transients are more than an order of magnitude higher. The flexible-mode transients increase with reduced damping for LQR control and decrease with reduced damping for decoupled control. In all three cases, the rigid-body transients are about an order of magnitude higher for LQR control than for decoupled control. For decoupled control, these transients are not affected by damping; however, for LQR control, they decrease substantially as the damping is reduced. The transient effects may be important to the overall performance of the control system. Examples of the transients are shown in figures 3 and 4.

Figure 3 illustrates the transient response in the third flexible mode for rigid-body control. Results were similar for the first and second modes. Results are shown in which a time lag has been introduced into the control feedback by multiplying the feedback gain matrix by $1 - e^{-t/\tau}$. An important characteristic of decoupled control is that columns of the feedback (or feedforward) gain matrix can be altered without affecting the decoupling process. The desired dynamics will be changed, but the system will still be decoupled. For example, multiplying a column corresponding to a particular rate feedback by a constant changes the desired damping ratio by that constant. Columns of the gain matrix can also be multiplied by time-varying quantities without affecting the decoupling. The overall effect is that, as time increases, the damping ratios increase from their natural values to the closed-loop values, the flexible-mode frequencies change from their natural frequencies to the closed-loop values, and the rigid-body frequencies increase from zero to the closed-loop values. Introducing lag

into the LQR-control feedback matrix gives a similar effect. (The stability of the system with lag added cannot be analytically guaranteed; however, the system was always stable for the magnitudes of lag used in the present analysis.) Additional data concerning the effect of lag on the control requirements are shown subsequently.

Examination of figure 3 shows that the small transient in A_3 for decoupled control is virtually eliminated with the inclusion of lag in the control feedback; the transient for LQR control is reduced by about 50 percent. Similar effects are obtained in the rigid-body transients for flexible-mode control, shown in figure 4. In this case, lag reduces the transient for LQR control by about 75 percent.

Effects on Decoupled Control Requirements

Table X contains various effects of sensor combinations on decoupled-control requirements. These effects include type and number of sensors as well as their location. Also, the effects of using different conditions for estimating the flexible modes are presented.

The standard values for the closed-loop dynamics were used to generate the data in table X. For these data, initial estimates were assumed to have been determined prior to turning on the control system, as described previously. The different conditions for estimating the flexible modes, as listed in the columns of table X, represent conditions after the control system has been activated.

The upper half of table X corresponds to rigid-body control and the lower half to flexible-mode control. Values selected for the initial disturbances in the residual modes have negligible effect on the overall results. (The values shown in the table were determined from data given in table IV of ref. 2.) A scan of table X shows that the type, number, and location of sensors have, for the stable cases, only a small effect on rigid-body control requirements, with differences between the cases being about 10 percent. The effect on flexible-mode control requirements is larger, with differences being about 20 percent. The use of two three-axis CMG's produces the lowest control requirements.

In table X, the data in the first columns under the torque requirements and under the momentum requirements apply to the condition wherein both the controlled and the residual modes are estimated. (Subsequent results in this paper pertain to this condition.) In the second columns, no estimates are used for any of these modes, and in the third columns, only the controlled modes are estimated. Naturally, the second columns for the flexible-mode requirements

are blank because estimates of the controlled modes are required.

When all of the flexible modes are estimated, all cases shown in table X are stable. However, when certain modes are not estimated, some sensor arrangements produce unstable control. For rigid-body control, the lowest momentum requirements are obtained when none of the flexible modes are estimated, but an additional unstable case resulted. The case which gives the lowest momentum requirement ($M = 9712$ ft-lb-sec) needs about 120 sec for the rigid-body mode ψ to null. For all other cases shown in table X, the rigid-body modes null in 60 sec. For flexible-mode control, the control requirements are lowest when all the flexible modes are estimated. Also, smoother control time histories are produced when all modes are estimated, as shown by the example in figure 5.

In the bottom half of table X, the case giving the lowest requirement ($M = 2602$ ft-lb-sec) would seem to be the best for flexible-mode control, but figure 6 shows that this case results in poor modal response. Only the first and third modes are shown; however, a similar effect is produced in the second mode. The oscillations shown eventually die out because of the small amount of natural damping. In all other cases shown for flexible-mode control in table X, the flexible modes null within about 10 sec.

For control of the rigid-body modes, the inclusion of flexible-mode initial disturbances produces only small increases in the momentum requirements (results in parentheses in table X). The maximum torque requirements, however, increase by about 25 percent.

Determination of Initial Estimates

As previously stated, the results presented herein are determined with the assumption that the initial estimates of the modal displacements are 90 percent of the true values. Figures 7 and 8 show the length of time required for the observer (with controls off) to determine estimates to this accuracy. Figure 7 shows time histories of the errors in the estimates for rigid-body control; that is, initial disturbances are included only in the rigid-body modes. Inspection of the figure shows that about 20 sec are required to obtain good estimates. Excessive errors can be noted for the residual-mode estimates; however, as previously stated, initial estimates for the residual modes are not necessary inasmuch as these modes are not in the control law. For flexible-mode control, good estimates are obtained after about 10 sec. (See fig. 8.)

Example Time Histories for Rigid-Body Control

Three-axis control. Time histories are given in figures 9 to 16 to compare the responses for the decoupled and LQR procedures and to show the effects of inoperative control for these procedures. The results pertain to rigid-body control and also illustrate the effects of lag in the system. As previously noted, the observer is in the loop for all cases. The initial conditions are given in the "General Considerations" section. Figure 9 contains the control responses for the two control procedures; lag is not included in the system. The modal responses resulting from the two control procedures are essentially identical; examples of these responses are shown in figure 10(c). Examination of figure 9 shows that the LQR procedure basically relies on all six control actuators. For the decoupled procedure, the bulk of the control effort is performed by the three-axis CMG at the bottom of the column; hence, the CMG at the top may not be essential.

Figure 10 shows the effect of assuming that the three-axis actuator at the top of the column is inoperative. This condition was simulated on the computer by zeroing out the first three rows in the feedback gain matrix. The other gains in the matrix were left unchanged; that is, the control law was not altered. As shown in figure 10, control of the system is still maintained by the one three-axis CMG. Comparison of the two cases for this CMG shows only small differences in the torque time histories as illustrated by the small oscillations in two of the curves. The momentum time histories show that the one remaining CMG automatically compensates for the inoperative CMG. The rigid-body modal responses are essentially the same for both cases (fig. 10(c)). The magnitudes of the flexible-mode transients for the inoperative-control case remain relatively low; however, the first flexible mode develops a slowly damped oscillation of very low magnitude. (As expected, when the three-axis actuator at the bottom of the column is assumed to fail, the system becomes unstable.)

The results of incorporating a time lag τ of 10 sec into the two rigid-body control procedures are presented in figures 11 and 12. The lag is incorporated in the control input which enters both the plant and the estimator. Comparison of the time histories in figure 11 with those of the no-lag case (fig. 9) shows that the control requirements are considerably reduced when lag is included. The rigid-body modal responses for the cases in figure 11 are essentially identical to those shown in figure 12(c).

As in figure 9, figure 11 indicates the CMG at the top of the antenna column is used sparingly for decoupled control. Hence, this case was investigated for the effect of an inoperative CMG at the top of the column. (See fig. 12.) The simulation procedure was the same as that used for figure 10. The results in figure 12 are similar to those in figure 10. However, note that the small oscillations in the torque time histories for the no-lag case (fig. 10(a)) are eliminated by including lag. Comparing figure 12(c) with figure 10(c) shows that with lag included, more time is required to null the rigid-body responses. The comparison also shows that the magnitudes of the flexible-mode transients are substantially reduced when lag is included. The slowly damped oscillation in the first flexible mode (fig. 10(c)) is virtually nonexistent in the case with lag.

Single-axis control. Figures 13 to 17 are examples of time histories relating to decoupled control of single-axis rigid-body modes. The control requirements are summarized in table XI. In figure 13, the control responses are presented for control of the rigid-body mode θ. Results are similar for control of ϕ and ψ. The resulting θ response for figure 13 is the same as that shown in figure 10(c). The other two rigid-body modes, as well as the flexible modes, are not materially affected. The data in figure 13 correspond to the use of one three-axis attitude sensor at the top of the column. In the figure, the small torques for the z-axis control are required because of the antenna product of inertia I_{xz}. The normal control arrangement for the two CMG's was changed by moving the bottom CMG to location 4. (See fig. 1.) This arrangement produces much smaller effects in the second residual mode A_5, as shown in figure 14.

It should be noted that for single-axis rigid-body control, the residual modes were not estimated. Eliminating these estimates has little effect on the control requirements. (See table XI.) Also, comparing figure 13(a) with figure 15 shows that the z-axis control time histories are smoother when the residual modes are not estimated. (The effects are similar for the other z-axis control actuator.)

Control (about the x- and y-axes) was maintained when the two z-axis control actuators for the case considered in figure 13 were assumed to be inoperative. This condition was simulated on the computer by zeroing out the third and sixth rows in the feedback gain matrix. The other gains in the matrix were left unchanged; that is, the control law was not altered. (It should be noted that the system becomes unstable if only one z-axis actuator is inoperative.) The only noticeable effects of the inoperative actuators are illustrated in figure 16. As shown, a slowly damped oscillation of very small magnitude developed for the first flexible mode A_1. In addition,

an extremely small steady-state offset results in the rigid-body mode ψ.

The effect of eliminating the y- and z-axis attitude sensors for the case considered in figure 13 was studied. (See fig. 17.) Rigid-body control is maintained; however, the z-axis control requirements increase, as shown by the example in figure 17. The peak torques increase from about 4 to about 30 ft-lb, with a slowly damped oscillation. The overall control requirements increase by about 10 percent. The other effect noticed is in the first flexible mode, as shown by the oscillations in figure 17(b). As for the other flexible modes, A_2 is not affected and the small transient in A_3 damps out rapidly.

As previously mentioned, the summary in table XI shows that for single-axis rigid-body control, the control requirements are about the same whether or not the residual modes are estimated. Also, the control-actuator arrangement is not of importance, except for control of the rigid-body mode ψ. For this case, the excessive requirements for locations 1 and 4 were caused by large gains on ψ in the feedback gain matrix **F**. (See table IV.) These gains resulted from the fact that the z-mode slope values at locations 1 and 4 for the first flexible mode A_1 are about the same magnitude.

Rigid-Body Command Requirements

Decoupled-control requirements for 0.01-rad commands in the three rigid-body modes are presented in figure 18. The initial estimates are assumed to be 0.001 rad, or 10 percent of the commanded values. For the computer simulations, it was necessary to scale the rigid-body command values **v** by multiplying them by the squares of their respective closed-loop frequencies.

Except where noted, the results in figure 18 correspond to the use of one three-axis attitude-rate sensor at location 1 and one three-axis attitude sensor at location 4. The single data point on figures 18(a) and 18(b) for the one three-axis attitude sensor (at location 1), normally used for nulling rigid-body disturbances, shows about the same control requirements; however, the control time histories are not as smooth. As noted in figures 18(a) and 18(b), various values of time lag were incorporated into the feedforward gain matrix **G**. (This matrix is shown in table V.)

The curves in figures 18(a) and 18(b) depict the control requirements plotted against the amount of time lag used in the control feedback gains with $\tau_G = 10$ sec. When compared with the curves, the data points for both τ_F and $\tau_G = 0$ sec illustrate the benefits of incorporating lag into the system. Also, the data points (open symbols) for $\tau_G = 0$ and $\tau_G = 5$ sec indicate that feedforward lag is more

effective than feedback lag. (For $\tau_G = 0$ sec, large overshoot occurs in the rigid-body responses.) For reduced closed-loop frequencies, the solid symbols for $\tau_G = 0$ show a marked decrease in the control requirements and there is no overshoot; however, this condition requires instantaneous values for torque at $t = 0$ sec. The solid symbols at $\tau_F = 6$ sec show lower control requirements, but the time required to reach rigid-body steady state is doubled.

The curves in figures 18(a) and 18(b) do not apply to $\tau_F = 0$. Data for this value are shown by single data points (for $\tau_F = 0$, $\tau_G = 10$) in these figures. The point in figure 18(b) shows a lower momentum requirement but, here again, this condition requires instantaneous values for torque at $t = 0$ sec.

The curve in figure 18(a) shows that the torque $|T_{\max}|$ is insensitive to τ_F over a wide range of values. This is not the case for momentum (fig. 18(b)), for which the best result occurs at about $\tau_F = 6$ sec.

Example Time Histories for Flexible-Mode Control

Time histories are given in figures 19 to 23 to show various effects on the decoupled and LQR procedures for flexible-mode control. The results pertain to the effects of (1) initial estimate, (2) lag, and (3) inoperative controls.

Effect of accuracy of initial estimate. Figures 19 and 20 illustrate the effect of the initial estimates of the flexible-mode disturbances for the decoupled and LQR procedures, respectively. Parametric data on this effect are presented in a subsequent section which includes the effect on rigid-body control. In figures 19 and 20, comparison of the data for the two values of the initial estimate shows that perfect knowledge of the initial disturbances (initial estimate of 100 percent) results in the higher control requirements for both control procedures. The differences in the torque and momentum requirements are not as great, however, for the LQR procedure as they are for the decoupled procedure. As shown in figures 19(c) and 20(c), the flexible-mode responses are essentially unaffected by the value of the initial estimate. Noticeable differences are apparent in the rigid-body transient responses for decoupled control (fig. 19(c)). In figure 20(c), the rigid-body transients are relatively large for the LQR-control procedure, regardless of the value used for the initial estimate.

Effect of lag. The effect of incorporating lag into the system for flexible-mode control can be seen by comparing figures 21 and 22. Comparisons of the two control procedures are also shown in each figure. Figure 21 is an example of a no-lag case, whereas for

figure 22 a time lag of 10 sec is included in the control feedback gains.

Comparison of figures 21 and 22 shows that the lag reduces the maximum torque values by about 50 percent. The momentum values are reduced by a lesser amount because of the additonal torque oscillations induced by the lag.

Examination of figure 21(c) shows that the flexible-mode responses (no lag included) are about the same for the two control procedures. Although not shown, this result is the same for the case in which lag is included. In the lag case, the responses require a longer time to null than in the no-lag case. (An example of the responses is shown in fig. 23.) As shown in figure 22(a) for the actuator at the top of the antenna column, inclusion of lag resulted in virtually identical torque responses for the two control procedures. Comparing the rigid-body responses in figure 21(c) for the two control procedures shows relatively large transients for the LQR procedure.

Effect of inoperative controls. Results in figures 21 and 22 show that the decoupled procedure basically relies on all six control actuators, whereas, for the LQR procedure, the bulk of the control effort is performed by the three-axis CMG at the top of the antenna column. (The presence or absence of lag did not affect these results.) These results are opposite to those for rigid-body control with regard to both actuator location and control procedure. It is shown in figure 22 that for LQR control, lag virtually cancels the control effort for the three-axis CMG at the bottom of the antenna column. Figure 23 shows the effect of assuming that this CMG is inoperative when LQR control is used. The method used for this simulation was discussed in a previous section on rigid-body control. As shown in figure 23, control is still maintained by the one three-axis CMG, with only negligible changes in both the control requirements and modal responses. (As expected, when the three-axis actuator at the top of the column is assumed to fail, the system becomes unstable.)

Effect of Control on Residual Modes

Figure 24 shows the effect of decoupled control on the residual modes. The LQR-control results are similar in appearance to those shown for decoupled control, with one exception. For rigid-body control with no lag (compare fig. 24(b)), LQR control reduces the maximum peaks in A_4 and A_6 by greater than 50 percent and in A_5 by about 20 percent.

Figure 24(a) pertains to flexible-mode control with no lag. Figures 24(b) and 24(c) pertain to rigid-body control with and without lag. Standard

closed-loop dynamics were used for figure 24(a); LQR closed-loop dynamics were used for figures 24(b) and 24(c). The results of figure 24 are essentially the same, regardless of the set of closed-loop dynamics used.

Flexible-mode control. In figure 24(a), the initial disturbances are selected as 0.1, 0.5, and 0.1 in. for modes 4, 5, and 6, respectively. As shown, these disturbances damp out because of the small values of natural damping in these modes (table I). The behavior of these modes is the same regardless of the magnitudes of the initial disturbances. Under certain conditions, such as type, number, and location of sensors and number of flexible modes estimated, one or more of the residual modes may become unstable, leading to an unstable control system. (See table X.) As far as flexible-mode control is concerned, the inclusion of lag in the system had little or no effect on the residual-mode time histories.

Rigid-body control. The results in figures 24(b) and 24(c) apply to either rigid-body commands or nulling rigid-body disturbances. No initial disturbances are assumed to exist in any of the flexible modes, including the residual modes. (Similar results are obtained even when initial disturbances are present.) Although the disturbances damp out for the no-lag case, it is shown in figure 24(b) that relatively large amplitudes occur initially in the second residual mode (mode 5). With lag included (fig. 24(c)), the maximum amplitudes in all three residual modes are reduced by an order of magnitude. As mentioned above, under certain conditions one or more of the residual modes may become unstable. (See table X.)

Parametric Summary of Control Requirements

Effect of initial estimate. Some time-history examples were previously presented (figs. 19 and 20) on the effect of the accuracy of the initial estimates. Figure 25 presents results of control requirements plotted against initial estimates. The rigid-body results (fig. 25(a)) are shown for decoupled control only; results are similar for LQR control. For rigid-body control, the lowest torque requirements occur at an initial-estimate value of about 90 percent. Over the range of initial estimates, the $|T_{max}|$ values are produced, for the most part, by the x-axis control actuator (at location 2) at a time of about 2 sec. (For initial estimates of 95 percent and above, the y-axis actuator produces the maximum torque.) As for momentum, figure 25(a) shows the best results for an

overestimate of about 10 percent. (This result would change somewhat by altering the estimator feedback gains.) The overestimate could be determined by taking the value of a "good" estimate, say 85 to 90 percent, and adding 20 percent. A good estimate could be based on a priori information such as that shown in figures 7 and 8. A good estimate could also be established by monitoring the estimator error $\varepsilon = \mathbf{y} - \mathbf{C}'\hat{\mathbf{x}}$.

The data for flexible-mode control (fig. 25(b)) are shown for the three conditions noted in the key. All data for $|T_{\max}|$ up to an initial estimate of about 100 percent apply to the z-axis control actuator at location 1. The $|T_{\max}|$ values are about 10 percent higher for decoupled control with the standard closed-loop dynamics. Also, $|T_{\max}|$ for decoupled control is insensitive to the initial estimate over the range up to about 100 percent. The curve for LQR control does not vary appreciably, with the lowest value of $|T_{\max}|$ occurring at an initial estimate of 75 percent.

The lowest momentum requirements occur at initial estimates of 50 to 70 percent, depending upon the control procedure used. Also, for initial estimates from 0 to 100 percent, the LQR-control momentum requirements are 3 to 15 percent lower than those for decoupled control.

Effect of lag. Figure 26 presents results showing the effect of lag on control requirements. (As previously noted, the lag was incorporated into the control input which enters both the plant and the estimator.) The data are shown for decoupled control only in figure 26(a); LQR-control momentum results are about the same but $|T_{\max}|$ results are lower than decoupled-control results. (See table XII.) As a matter of interest, results are also included for the ideal case (no estimator). Perfect knowledge of the state variables for feedback was assumed and no residual modes were included in the model.

Results for flexible-mode control are presented for the two control procedures in figure 26(b). Standard closed-loop dynamics were used for the decoupled control; results with LQR closed-loop values were about the same. (See case 2C in table XII.) Results for the ideal case were the same as those shown, except that the decoupled-control requirements were several percent higher at lag values of $0 < \tau < 2$ sec.

The data in figure 26(b) pertain to use of initial estimates of 90 percent. The value used for the initial estimate is not crucial, however, when lag is included in the system. For example, with a lag of 10 sec, a value of 60 percent for the initial estimate results in approximately the same magnitudes as those shown for both torque and momentum.

In comparing the two control procedures in figure 26(b), note the pronounced decrease in momentum for the LQR-control procedure as τ varies from 0 to 5 sec. This effect of lag is similar to the effect of decreasing the flexible-mode closed-loop damping ratios for this procedure, as previously discussed for table VIII. The disadvantage of the LQR-control procedure, as previously discussed regarding the transient responses, is evident when lag is included. Table XIII (case 2C) shows rigid-body transients of about one order of magnitude higher than those for decoupled control. Table XIII also shows that for rigid-body control, the flexible-mode transients are one to two orders of magnitude higher for the LQR control procedure.

In table XII, it is shown that for rigid-body control, use of the two three-axis sensors produces the lowest control requirements. Case 2D is included in table XII to indicate the lower control requirements for LQR flexible-mode control when only the one three-axis CMG (at location 1) is in operation. (See also fig. 23.) Table XIII, however, shows that for this case the rigid-body transients are close to one order of magnitude higher. (Compare cases 2D and 2C.)

Concluding Remarks

An analysis has been performed to compare decoupled and linear quadratic regulator (LQR) procedures for the control of a large, flexible space antenna. A state estimator is used in the loop for both procedures. Control involved (1) commanding changes in the rigid-body modes, (2) nulling initial disturbances in the rigid-body modes, or (3) nulling initial disturbances in the first three flexible modes. Control was achieved with two three-axis control-moment gyros (CMG's) located on the antenna column. The results illustrated various effects on control requirements for the two procedures. These effects included errors in the initial estimates of state variable, variations in the type, number, and location of sensors, and deletions of state-variable estimates for certain flexible modes after control activation. The advantages of incorporating a time lag in the control feedback were also illustrated. In addition, the effects of inoperative-control situations were analyzed with regard to control requirements and resultant modal responses. Comparisons were included which showed the effects of perfect state feedback with no residual modes (ideal case). Time-history responses were presented to illustrate the various effects on the control procedures. Results of the study indicate the following:

1. Compared with the ideal case (perfect estimates of state variables and no residual modes),

control requirements were appreciably higher when an observer was incorporated in rigid-body control. Further, for flexible-mode control, the requirements were generally somewhat lower than for rigid-body control.

2. Accuracy of the initial estimates of the state variables had a significant effect on control requirements, especially for rigid-body control. In fact, an overestimate of about 10 percent for rigid-body control produced the lowest momentum requirements. For flexible-mode control, initial estimates of from 50 to 75 percent resulted in the lowest control requirements. About 10 sec were required before control activation to obtain good estimates for flexible-mode control, and 20 sec were required for rigid-body control.

3. For flexible-mode control, the LQR-control requirements were less than those for decoupled control, with a pronounced reduction for low values of closed-loop damping. For rigid-body control, the momentum requirements were about the same for both control procedures; however, the LQR maximum torque requirements were much less.

4. Linear quadratic regulator (LQR) control had more of an effect on the transients which occur in the initially undisturbed modes. For either rigid-body control or flexible-mode control, the LQR transients were generally an order of magnitude larger than those for decoupled control. Incorporation of lag into the system can be used to reduce the transients considerably.

5. The type, number, and location of sensors had only a small effect on control requirements when the control system was stable. Rate sensors cannot be used alone because the system is unobservable without attitude sensors. Two three-axis sensors (one for attitude and one for attitude rate) produced lower control requirements than one three-axis attitude sensor. For single-axis rigid-body control, a one-axis attitude sensor was adequate; however, a three-axis attitude sensor produced better results. (In practice, three-axis control is usually required.)

6. With certain sensor arrangements, instability occurred when the residual modes were not estimated after control activation. This was also true when none of the flexible modes were estimated. For flexible-mode control, the torque and momentum requirements were generally lower when all the flexible modes were estimated.

7. Under certain conditions, for either control procedure, one three-axis CMG could be made inoperative without materially changing the control requirements or the resultant modal responses from the normal case.

8. A time lag incorporated into the system led to large reductions in the control requirements. The reduction was pronounced in the LQR momentum requirements for flexible-mode control. Incorporating lag in the control input automatically included lag in the estimator. For rigid-body control, lag was also effective in reducing the residual-mode amplitudes by one order of magnitude.

9. For either rigid-body or flexible-mode control of initial disturbances, the control requirements decreased as lag increased. For rigid-body commands, the requirements were essentially invariant with lag values of up to about 10 sec. For command control, it was essential that lag be included in both the feedforward and feedback control gains.

References

1. Sullivan, Marvin R.: *LSST (Hoop/Column) Maypole Antenna Development Program.* NASA CR-3558, Part 2, 1982.

2. Young, John W.; Hamer, Harold A.; and Johnson, Katherine G.: *Decoupled-Control Analysis of a Large Flexible Space Antenna With Linear Quadratic Regulator Comparisons.* NASA TP-2293, 1984.

3. Joshi, Suresh M.: Control Systems Synthesis for a Large Flexible Space Antenna. *Acta Astronaut.*, vol. 10, no. 5–6, May–June 1983, pp. 365–380.

4. Kwakernaak, Huibert; and Sivan, Raphael: *Linear Optimal Control Systems.* John Wiley & Sons, Inc., c.1972.

5. Armstrong, Ernest S.: *ORACLS—A System for Linear-Quadratic-Gaussian Control Law Design.* NASA TP-1106, 1978.

TABLE I. ANTENNA CHARACTERISTICS

$$\begin{bmatrix} I_x = 1.9577 \times 10^{10} \text{ lb-in}^2; \ I_y = 1.9657 \times 10^{10} \text{ lb-in}^2; \\ I_z = 1.499 \times 10^{10} \text{ lb-in}^2; \ I_{xz} = 0.8357 \times 10^8 \text{ lb-in}^2; \\ w = 10\,020.3 \text{ lb} \end{bmatrix}$$

Mode	ω_n, rad/sec	T_n, sec	ς_n	m_n, lb-sec^2/in.	Description
1	0.7466	8.42	0.01	153.157	First torsion
2	1.3460	4.67	.01	5.233	First bending, x-z plane
3	1.7025	3.69	.01	3.073	First bending, y-z plane
4	3.1813	1.98	.01	.305	Surface torsion
5	4.5294	1.39	.02	1.993	Second column bending, y-z plane
6	5.5905	1.12	.02	723.522	Surface-hoop torsion, feed mast torsion

TABLE II. B MATRICES USED IN CURRENT ANALYSIS

(a) Three-axis CMG's at locations 1 and 2

$$\mathbf{B}_{18\times6}$$

0.	0.	0.	0.	0.	0.
0.	0.	0.	0.	0.	0.
0.	0.	0.	0.	0.	0.
0.	0.	0.	0.	0.	0.
0.	0.	0.	0.	0.	0.
0.	0.	0.	0.	0.	0.
0.	0.	0.	0.	0.	0.
0.	0.	0.	0.	0.	0.
0.	0.	0.	0.	0.	0.
.19737917E-07	0.	.11003987E-09	.19737917E-07	0.	.11003987E-09
0.	.19658120E-07	0.	0.	.19658120E-07	0.
.11003987E-09	0.	.25777798E-07	.11003987E-09	0.	.25777798E-07
.14712325E-05	0.	-.11745441E-03	-.42320542E-06	0.	-.37776195E-06
0.	-.36681003E-03	0.	0.	.31838614E-04	0.
.61143590E-03	0.	.89756447E-04	-.61885513E-04	0.	.20098311E-05
-.39176798E-06	0.	.44199044E-05	.88746034E-07	0.	-.10276237E-03
-.12693521E-03	0.	-.11452151E-04	-.21981567E-02	0.	-.83552937E-06
.59589099E-07	0.	-.34274029E-05	.71689636E-07	0.	-.13551496E-03

(b) Three-axis CMG's at locations 1 and 4

$$\mathbf{B}_{18\times6}$$

0.	0.	0.	0.	0.	0.
0.	0.	0.	0.	0.	0.
0.	0.	0.	0.	0.	0.
0.	0.	0.	0.	0.	0.
0.	0.	0.	0.	0.	0.
0.	0.	0.	0.	0.	0.
0.	0.	0.	0.	0.	0.
0.	0.	0.	0.	0.	0.
0.	0.	0.	0.	0.	0.
.19737917E-07	0.	.11003987E-09	.19737917E-07	0.	.11003987E-09
0.	.19658120E-07	0.	0.	.19658120E-07	0.
.11003987E-09	0.	.25777798E-07	.11003987E-09	0.	.25777798E-07
.14712325E-05	0.	-.11745441E-03	-.77163021E-06	0.	-.71560219E-04
0.	-.36681003E-03	0.	0.	.10334324E-03	0.
.61143590E-03	0.	.89756447E-04	-.16473635E-03	0.	.55520430E-04
-.39176798E-06	0.	.44199044E-05	.78522547E-07	0.	.12148418E-03
-.12698521E-03	0.	-.11452151E-04	.15432331E-03	0.	-.74294476E-05
.59589099E-07	0.	-.34274029E-05	-.59473221E-08	0.	-.33933624E-04

TABLE III. SPECIFIED CLOSED-LOOP EIGENVALUES

Case	Mode	$\omega_d,$ rad/sec	ς_d
Standard	θ	0.1	0.90
	ϕ	.1	.90
	ψ	.1	.90
	A_1	ω_n	.59
	A_2	ω_n	.34
	A_3	ω_n	.24
1	θ	0.099	0.903
	ϕ	.112	.900
	ψ	.112	.901
	A_1	.748	.885
	A_2	1.342	.898
	A_3	1.681	.897
2	θ	0.098	0.904
	ϕ	.112	.900
	ψ	.112	.901
	A_1	.745	.502
	A_2	1.345	.511
	A_3	1.700	.502
3	θ	0.098	0.904
	ϕ	.112	.900
	ψ	.113	.901
	A_1	.747	.099
	A_2	1.346	.106
	A_3	1.703	.107

TABLE IV. **F** MATRICES FOR DECOUPLED CONTROL

[Standard closed-loop dynamics used]

(a) Three-axis CMG's at locations 1 and 2

$$\mathbf{F}_{6\times18}$$

Row no.						
1	-.45712427E+05	0.	.11921449E+04	0.	0.	0.
	0.	0.	0.	-.84082369E+06	0.	.21458608E+05
	-.96193614E+03	0.	-.11606671E+04	0.	0.	0.
2	0.	-.40627667E+05	0.	0.	0.	0.
	0.	0.	0.	0.	-.73129801E+06	0.
	0.	.22284285E+04	0.	0.	0.	0.
3	.10685880E+04	0.	.12632075E+04	0.	0.	0.
	0.	0.	0.	.19234584E+05	0.	.22737735E+05
	.73817760E+04	0.	-.18780960E+02	0.	0.	0.
4	-.45993871E+06	0.	.97063982E+03	0.	0.	0.
	0.	0.	0.	-.82788968E+07	0.	.17471517E+05
	.96193614E+03	0.	.11606671E+04	0.	0.	0.
5	0.	-.46806799E+06	0.	0.	0.	0.
	0.	0.	0.	0.	-.84252238E+07	0.
	0.	-.22284285E+04	0.	0.	0.	0.
6	.10941967E+04	0.	-.38920317E+06	0.	0.	0.
	0.	0.	0.	.19695540E+05	0.	-.70056570E+07
	-.73817760E+04	0.	.18780960E+02	0.	0.	0.

(b) Three-axis CMG's at locations 1 and 4

$$\mathbf{F}_{6\times18}$$

Row no.						
1	-.10768223E+06	0.	.15260150E+04	0.	0.	0.
	0.	0.	0.	-.19382801E+07	0.	.27468270E+05
	-.83057383E+03	0.	-.10068196E+04	0.	0.	0.
2	0.	-.11181514E+06	0.	0.	0.	0.
	0.	0.	0.	0.	-.20126726E+07	0.
	0.	.18895115E+04	0.	0.	0.	0.
3	-.11632138E+03	0.	.60493111E+06	0.	0.	0.
	0.	0.	0.	-.20937849E+04	0.	.10888760E+08
	.18830121E+05	0.	-.49203577E+02	0.	0.	0.
4	-.30896891E+06	0.	.63676967E+03	0.	0.	0.
	0.	0.	0.	-.71814404E+07	0.	.11461854E+05
	.83057383E+03	0.	.10068196E+04	0.	0.	0.
5	0.	-.39688051E+06	0.	0.	0.	0.
	0.	0.	0.	0.	-.71438492E+07	0.
	0.	-.18895115E+04	0.	0.	0.	0.
6	.22701061E+04	0.	-.99287107E+06	0.	0.	0.
	0.	0.	0.	.41023909E+05	0.	-.17871679E+08
	-.18830121E+05	0.	.49203577E+02	0.	0.	0.

TABLE V. G MATRIX USED FOR RIGID-BODY COMMANDS

[Three-axis CMG's at locations 1 and 2]

$$\mathbf{G}_{6\times6}$$

.46712427E+07	0.	−.11921449E+06	.11107667E+04	0.	.14820496E+04
0.	.40627667E+07	0.	0.	−.25084746E+04	0.
−.10685880E+06	0.	−.12632075E+06	−.85234396E+04	0.	.23981307E+02
.45993371E+08	0.	−.97063982E+05	−.11107667E+04	0.	−.14820496E+04
0.	.46806799E+08	0.	0.	.25084746E+04	0.
−.10941967E+06	0.	.38920317E+08	.85234396E+04	0.	−.23981307E+02

TABLE VI. F AND K MATRICES FOR DECOUPLED- AND LQR-CONTROL COMPARISONS FOR CASE 2 OF TABLE III

[LQR closed-loop dynamics used]

$$\mathbf{F}_{6\times18}$$

Row no. 1
-.4532156EE+05	0.	.14900905E+04	.21542986E+01	0.	.13614419E+02
0.	0.	0.	-.83152418E+06	0.	.24020045E+05
-.81474542E+03	0.	-.24803124E+04	0.	0.	0.

2
0.	-.50590072E+05	0.	0.	-.80997642E+01	0.
0.	0.	0.	0.	-.81649130E+06	0.
0.	.33827820E+04	0.	0.	0.	0.

3
.10367708E+04	0.	.15789134E+04	-.16530955E+02	0.	.22029732E+00
0.	0.	0.	.19021840E+05	0.	.25451858E+05
.62519281E+04	0.	-.40134373E+02	0.	0.	0.

4
-.44624404E+06	0.	.12132260E+04	-.21542986E+01	0.	-.13614419E+02
0.	0.	0.	-.81873322E+07	0.	.19557030E+05
.81474542E+03	0.	.24803124E+04	0.	0.	0.

5
0.	-.58295808E+06	0.	0.	.80997642E+01	0.
0.	0.	0.	0.	-.94067286E+07	0.
0.	-.33827820E+04	0.	0.	0.	0.

6
.10616170E+04	0.	-.48647438E+06	.16530955E+02	0.	-.22029732E+00
0.	0.	0.	.19477708E+05	0.	-.78418974E+07
-.62519281E+04	0.	.40134373E+02	0.	0.	0.

$$\mathbf{K}_{6\times18}$$

Row no. 1
-.29895400E+06	0.	.54927800E+04	-.16430800E+03	0.	-.21718500E+03
0.	0.	0.	-.49691600E+07	0.	.10590600E+06
-.37985200E+03	0.	-.26596200E+04	0.	0.	0.

2
0.	-.29397700E+06	0.	0.	.29870400E+03	0.
0.	0.	0.	0.	-.49383200E+07	0.
0.	.36385900E+04	0.	0.	0.	0.

3
-.64377600E+04	0.	-.16643500E+06	.44618800E+03	0.	-.16038200E+03
0.	0.	0.	-.11149400E+06	0.	-.32711900E+07
.61915100E+04	0.	-.32459400E+03	0.	0.	0.

4
-.33254100E+06	0.	-.92131600E+03	.91541000E+00	0.	-.23435600E+03
0.	0.	0.	-.53549900E+07	0.	-.13441100E+05
.80414800E+02	0.	.28173600E+03	0.	0.	0.

5
0.	-.33701200E+06	0.	0.	.31977000E+03	0.
0.	0.	0.	0.	-.54360600E+07	0.
0.	-.34250000E+03	0.	0.	0.	0.

6
-.12852600E+04	0.	-.20559200E+06	.51996500E+03	0.	-.22174100E+02
0.	0.	0.	-.12442100E+05	0.	-.38013700E+07
-.93569700E+02	0.	-.36261200E+01	0.	0.	0.

TABLE VII. C MATRIX FOR THREE-AXIS ATTITUDE-RATE SENSOR AT LOCATION 1
AND THREE-AXIS ATTITUDE SENSOR AT LOCATION 4

$$C_{6\times18}$$

Row no. 1	0.	0.	0.	0.	0.	0.
	0.	0.	0.	.10000000E+01	0.	0.
	.22532850F-03	0.	.19790460E-02	-.11935500E-06	-.25308020E-03	.43113600E-04
2	0.	0.	0.	0.	0.	0.
	0.	0.	0.	0.	.10000000E+01	0.
	0.	-.19195410E-02	0.	0.	0.	0.
3	0.	0.	0.	0.	0.	0.
	0.	0.	0.	0.	0.	.10000000E+01
	-.17988610F-01	0.	.27583180E-03	.13464720E-05	-.22823800F-04	-.24797850E-02
4	.10000000E+01	0.	0.	-.11818080E-03	0.	-.50625030E-03
	.23921470E-07	.30756450E-03	-.43030160E-05	0.	0.	0.
	0.	0.	0.	0.	0.	0.
5	0.	.10000000E+01	0.	0.	.54079040E-03	0.
	0.	0.	0.	0.	0.	0.
	0.	0.	.10000000E+01	-.10959970E-01	0.	.17061950E-03
6	.37009500E-04	-.14806800E-04	-.24551710E-01	0.	0.	0.
	0.	0.	0.	0.	0.	0.

TABLE VIII. DECOUPLED- AND LQR-CONTROL REQUIREMENTS WITH AND WITHOUT OBSERVER

[Numbers in parentheses indicate control with observer; residuals estimated]

Case	No. of three-axis sensors	Initial disturbances of—		LQR-control requirements for—		Decoupled-control requirements for—	
		Rigid-body modes, rad	Flexible modes, in.	$\lvert T_{max}\rvert$, ft-lb	Momentum, ft-lb-sec	$\lvert T_{max}\rvert$, ft-lb	Momentum, ft-lb-sec
1	1	0.01	0	292 (318)	9 895 (11 736)	488 (509)	9 910 (12 056)
	2	0	1	276 (258)	3 543 (3 440)	278 (270)	3 850 (3 678)
2	1	0.01	0	281 (301)	9 945 (11 768)	486 (501)	9 876 (11 798)
	2	0	1	210 (202)	2 400 (2 373)	212 (209)	2 850 (2 750)
	1	0	1	(195)	(2 228)	(230)	(3 091)
3	1	0.01	0	267 (276)	9 976 (11 707)	485 (495)	9 860 (11 555)
	2	0	1	63 (68)	1 355 (1 367)	65 (61)	2 378 (2 312)

TABLE IX. MAXIMUM TRANSIENTS DURING DECOUPLED AND LQR CONTROL WITH OBSERVER IN SYSTEM

Case	No. of three-axis sensors	Initial disturbances of— Rigid-body modes, rad	Flexible modes, in.	Maximum transients for LQR control, rad or in. (absolute)	Maximum transients for decoupled control, rad or in. (absolute)
1	1	0.01	0	$A_1 = 0.16$ $A_2 = 0.37$ $A_3 = 0.50$	$A_1 = 0.047$ $A_2 = 0.164$ $A_3 = 0.170$
	2	0	1	$\theta = 0.27 \times 10^{-3}$ $\phi = 0.35 \times 10^{-3}$ $\psi = 0.91 \times 10^{-3}$	$\theta = 0.10 \times 10^{-4}$ $\phi = 0.35 \times 10^{-4}$ $\psi = 0.42 \times 10^{-4}$
2	1	0.01	0	$A_1 = 0.25$ $A_2 = 0.54$ $A_3 = 0.60$	$A_1 = 0.036$ $A_2 = 0.126$ $A_3 = 0.127$
	2	0	1	$\theta = 0.16 \times 10^{-3}$ $\phi = 0.23 \times 10^{-3}$ $\psi = 0.58 \times 10^{-3}$	$\theta = 0.10 \times 10^{-4}$ $\phi = 0.35 \times 10^{-4}$ $\psi = 0.42 \times 10^{-4}$
	1	0	1	$\theta = 0.15 \times 10^{-3}$ $\phi = 0.19 \times 10^{-3}$ $\psi = 0.50 \times 10^{-3}$	$\theta = 0.40 \times 10^{-5}$ $\phi = 0.70 \times 10^{-5}$ $\psi = 0.76 \times 10^{-4}$
3	1	0.01	0	$A_1 = 0.47$ $A_2 = 0.94$ $A_3 = 1.06$	$A_1 = 0.011$ $A_2 = 0.058$ $A_3 = 0.055$
	2	0	1	$\theta = 0.40 \times 10^{-4}$ $\phi = 0.76 \times 10^{-4}$ $\psi = 0.15 \times 10^{-3}$	$\theta = 0.10 \times 10^{-4}$ $\phi = 0.35 \times 10^{-4}$ $\psi = 0.42 \times 10^{-4}$

TABLE X. DECOUPLED-CONTROL REQUIREMENTS FOR VARIOUS COMBINATIONS OF SENSORS
WITH AND WITHOUT ESTIMATES IN FLEXIBLE MODES

[U indicates unstable; numbers in parentheses indicate initial disturbances included in flexible modes]

| Initial disturbances | Three-axis sensors | | $\lvert T_{max}\rvert$, ft-lb, determined— | | | Momentum, ft-lb-sec, determined— | | |
	Type	Location	With estimates in flexible modes	Without estimates in flexible modes	Without estimates in residual modes	With estimates in flexible modes	Without estimates in flexible modes	Without estimates in residual modes
$\theta, \phi, \psi = 0.01$ rad	Attitude	1	418	443	418	11 033	10 546	10 984
$(A_n = 0)$	Attitude	2	436	U	U	11 094	U	U
	Attitude	4	429	U	447	11 103	U	10 890
	Attitude	1, 2	511	U	U	10 773	U	U
	Attitude	1, 4	475	480	475	10 762	10 407	10 845
	Attitude	2, 4	470	U	U	10 765	U	U
	Attitude, attitude rate	2, 1	418	U	U	10 456	U	U
	Attitude, attitude rate	4, 1	417 (529)	414	429 (540)	10 438 (10 505)	9 712	9 916 (10 667)
$A_1, A_2, A_3 = 1.0$ in.;	Attitude	1	247		246	3 030		3 066
$A_4, A_6 = 0.1$ in.;	Attitude	2	219		U	2 602		U
$A_5 = 0.5$ in.	Attitude	4	241		275	2 890		3 570
$(\theta, \phi, \psi = 0)$	Attitude	1, 2	237		U	2 844		U
	Attitude	1, 4	241		246	2 917		2 977
	Attitude	2, 4	228		U	2 767		U
	Attitude, attitude rate	2, 1	226		U	2 700		U
	Attitude, attitude rate	4, 1	227		243	2 716		2 919

TABLE XI. CONTROL REQUIREMENTS FOR CONTROLLING SINGLE-AXIS RIGID-BODY MODES

Initial disturbances	Control locations	Residuals estimated	$|T_{max}|$, ft-lb	Momentum, ft-lb-sec
$\theta = 0.01$	1, 4	No	362	3 905
	1, 4	Yes	363	3 907
	1, 2	No	395	3 848
	1, 2	Yes	418	3 868
$\phi = 0.01$	1, 4	No	354	3 880
	1, 4	Yes	354	3 880
	1, 2	No	418	3 888
	1, 2	Yes	418	3 888
$\psi = 0.01$	1, 4	No	767	13 158
	1, 4	Yes	765	13 209
	1, 2	No	300	3 343
	1, 2	Yes	300	3 371

TABLE XII. DECOUPLED- AND LQR-CONTROL REQUIREMENTS FOR CASE 2 WITH OBSERVER AND LAG

$[\tau = 10$ sec; LQR closed-loop dynamics used]

Case	No. of three-axis sensors	Initial disturbances of—		LQR-control requirements for—		Decoupled-control requirements for—	
		Rigid-body modes, rad	Flexible modes, in.	$|T_{max}|$, ft-lb	Momentum, ft-lb-sec	$|T_{max}|$, ft-lb	Momentum, ft-lb-sec
2A	1	0.01	0	108	9070	184	9164
2B	2	0.01	0	96	8894	169	8948
2C	2	0	1	91	1401	96	2470
2D	2*	0	1	90	1292		

*One three-axis control actuator inoperative.

TABLE XIII. MAXIMUM TRANSIENTS DURING DECOUPLED AND LQR CONTROL
FOR CASE 2 WITH OBSERVER AND LAG

$[\tau = 10$ sec; LQR closed-loop dynamics used]

Case	No. of three-axis sensors	Initial disturbances of—		Maximum transients for LQR control, rad or in. (absolute)	Maximum transients for decoupled control, rad or in. (absolute)
		Rigid-body modes, rad	Flexible modes, in.		
2A	1	0.01	0	$A_1 = 0.16$ $A_2 = 0.27$ $A_3 = 0.28$	$A_1 = 0.018$ $A_2 = 0.075$ $A_3 = 0.060$
2B	2	0.01	0	$A_1 = 0.19$ $A_2 = 0.22$ $A_3 = 0.22$	$A_1 = 0.004$ $A_2 = 0.010$ $A_3 = 0.007$
2C	2	0	1	$\theta = 0.17 \times 10^{-4}$ $\phi = 0.24 \times 10^{-4}$ $\psi = 0.16 \times 10^{-3}$	$\theta = 0.22 \times 10^{-5}$ $\phi = 0.79 \times 10^{-5}$ $\psi = 0.17 \times 10^{-4}$
2D	2*	0	1	$\theta = 0.90 \times 10^{-4}$ $\phi = 0.15 \times 10^{-3}$ $\psi = 0.50 \times 10^{-3}$	

*One three-axis control actuator inoperative.
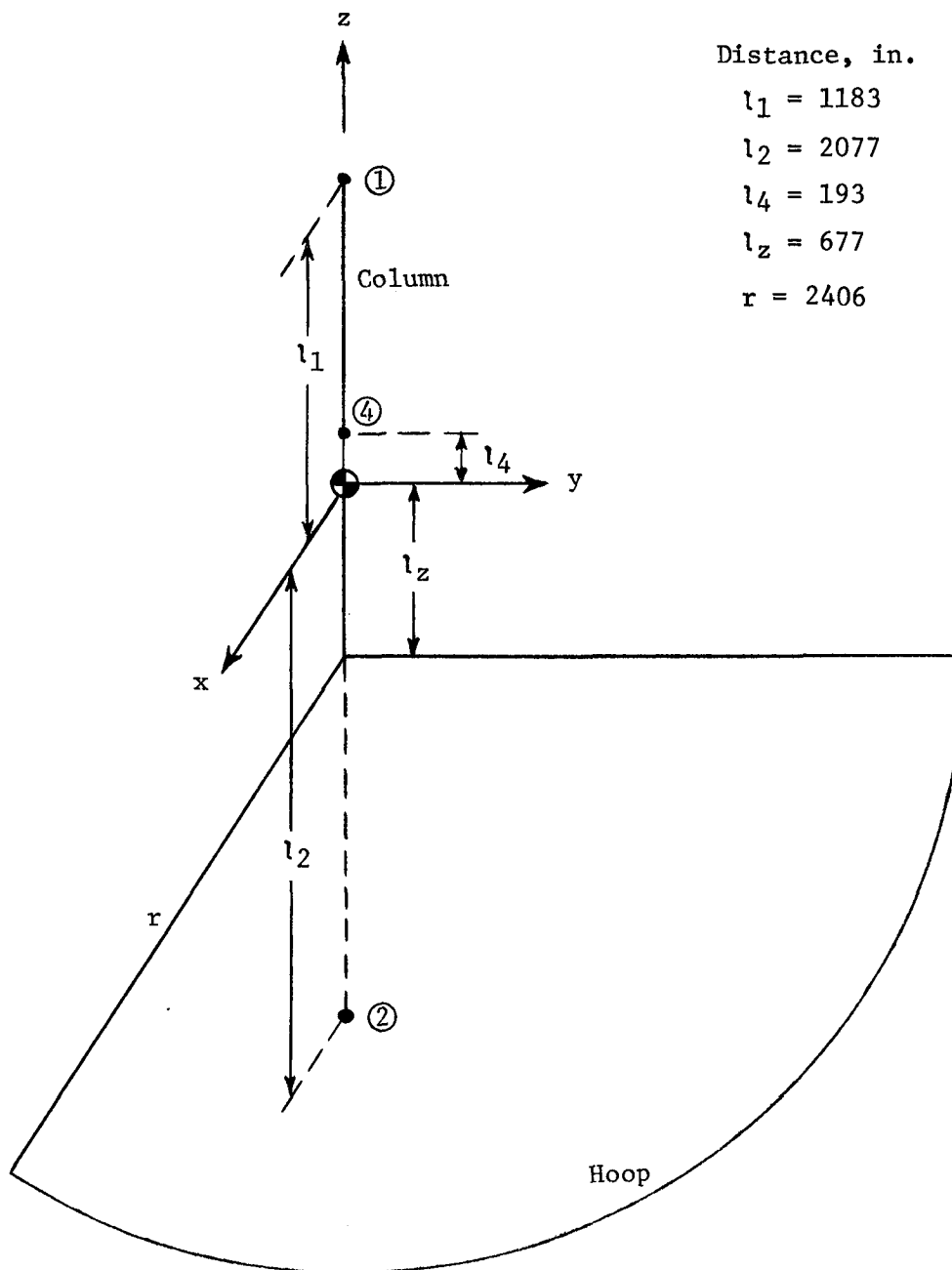
Figure 1. Antenna coordinates and actuator or sensor locations.
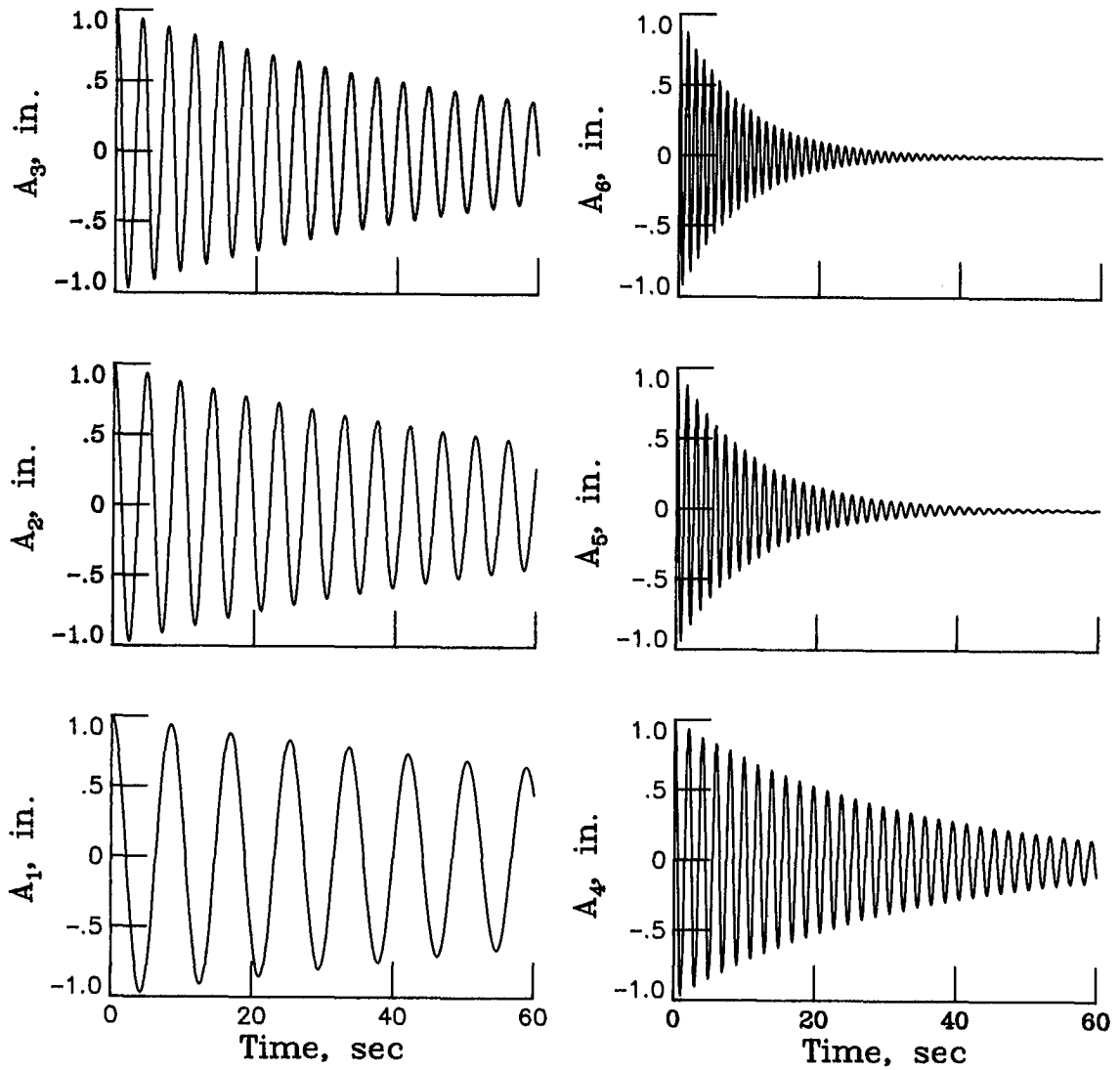
Figure 2. Unforced responses of natural vibration modes.
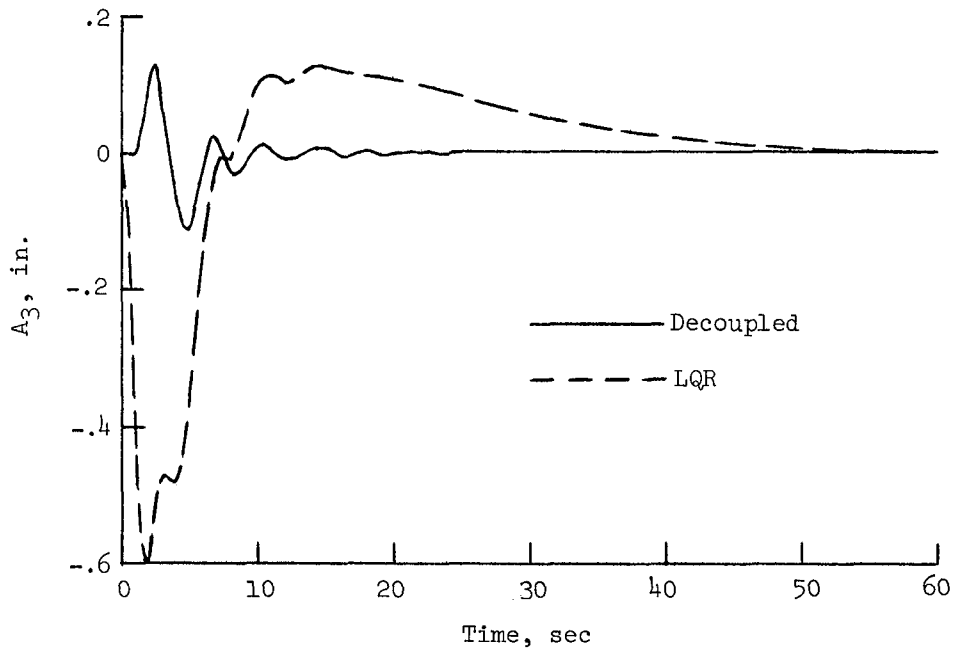
(a) No lag.
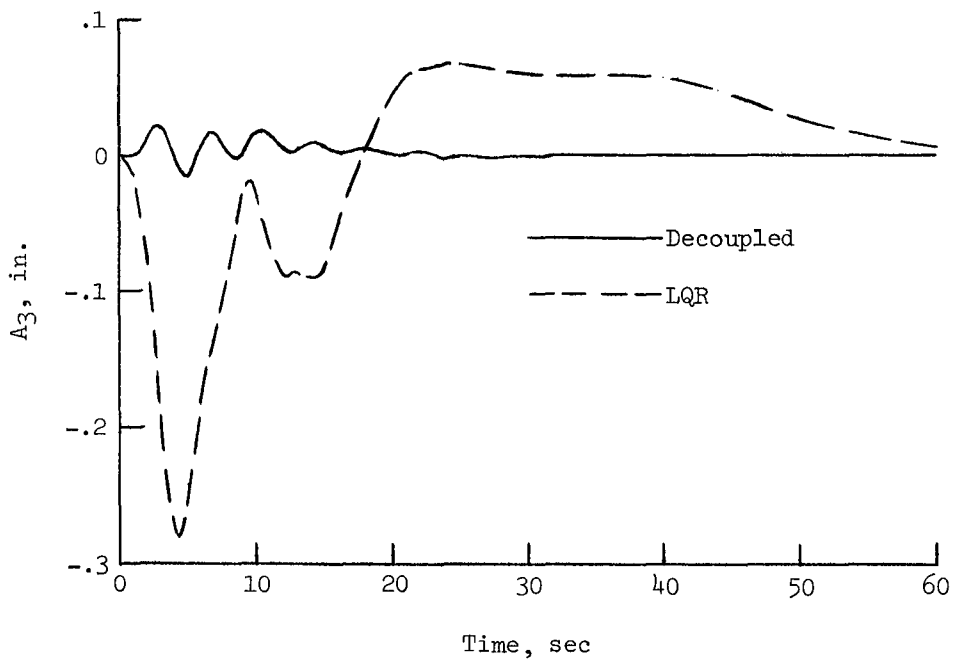
(b) With lag; $\tau = 10$ sec.

Figure 3. Flexible-mode transient response for decoupled and LQR control of rigid-body modes with observer in system.
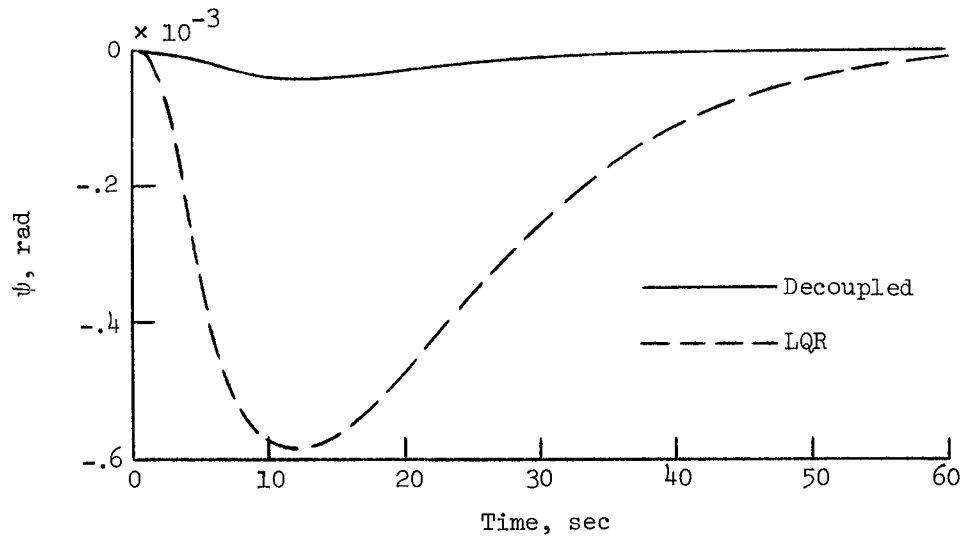
(a) No lag.
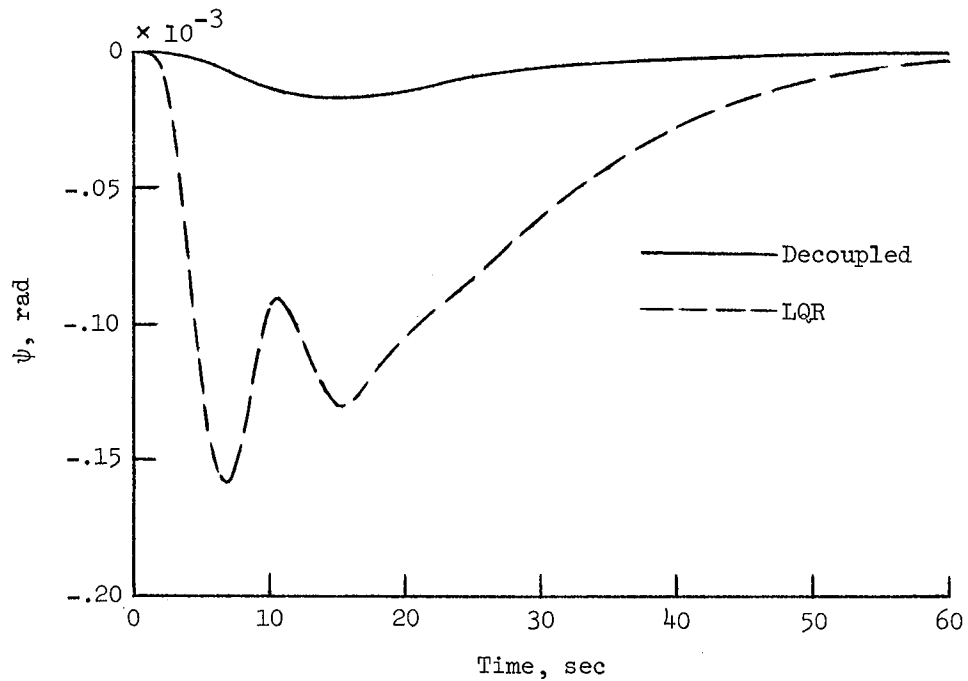
(b) With lag; $\tau = 10$ sec.

Figure 4. Rigid-body-mode transient response for decoupled and LQR control of flexible modes with observer in system.
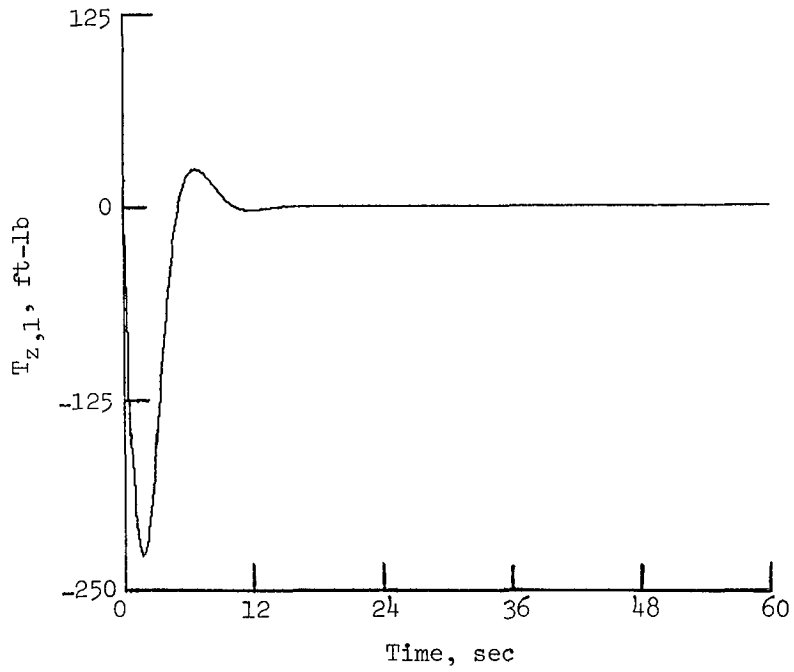
(a) All modes estimated.
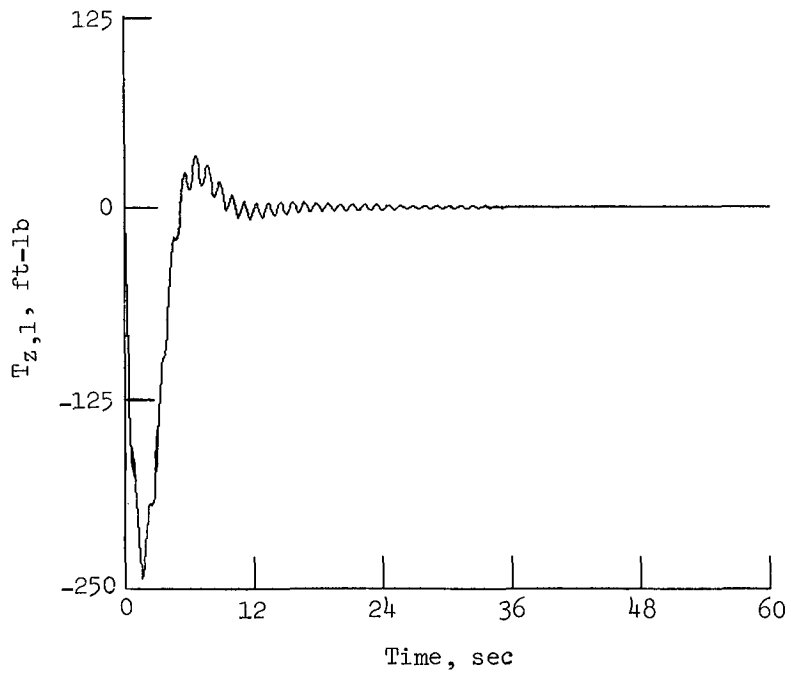
(b) Rigid-body and first three flexible modes estimated.

Figure 5. Effect of omitting estimates of residual modes.
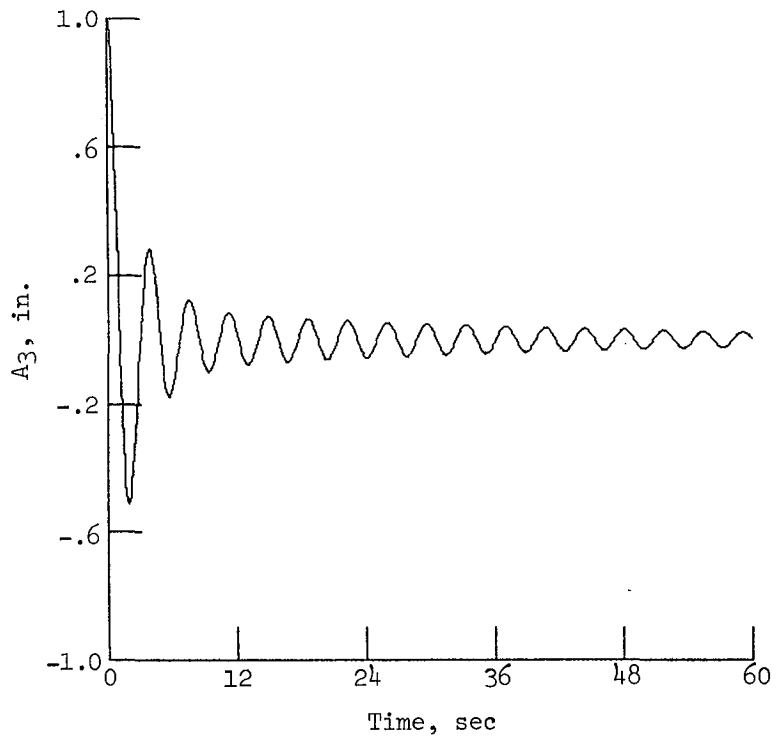
(a) Third-flexible-mode response.
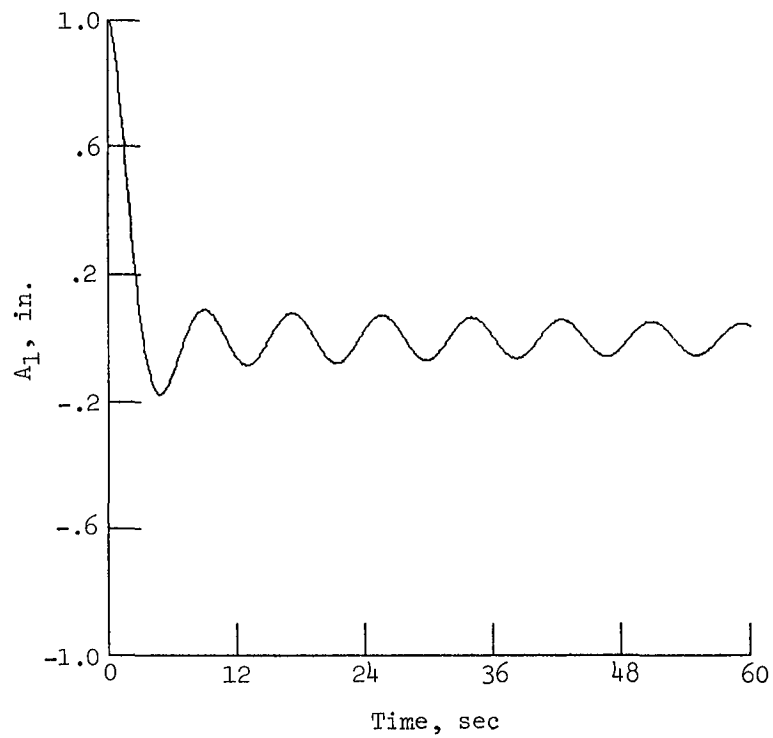
(b) First-flexible-mode response.

Figure 6. Example of poor performance for one three-axis attitude sensor located at bottom of column.
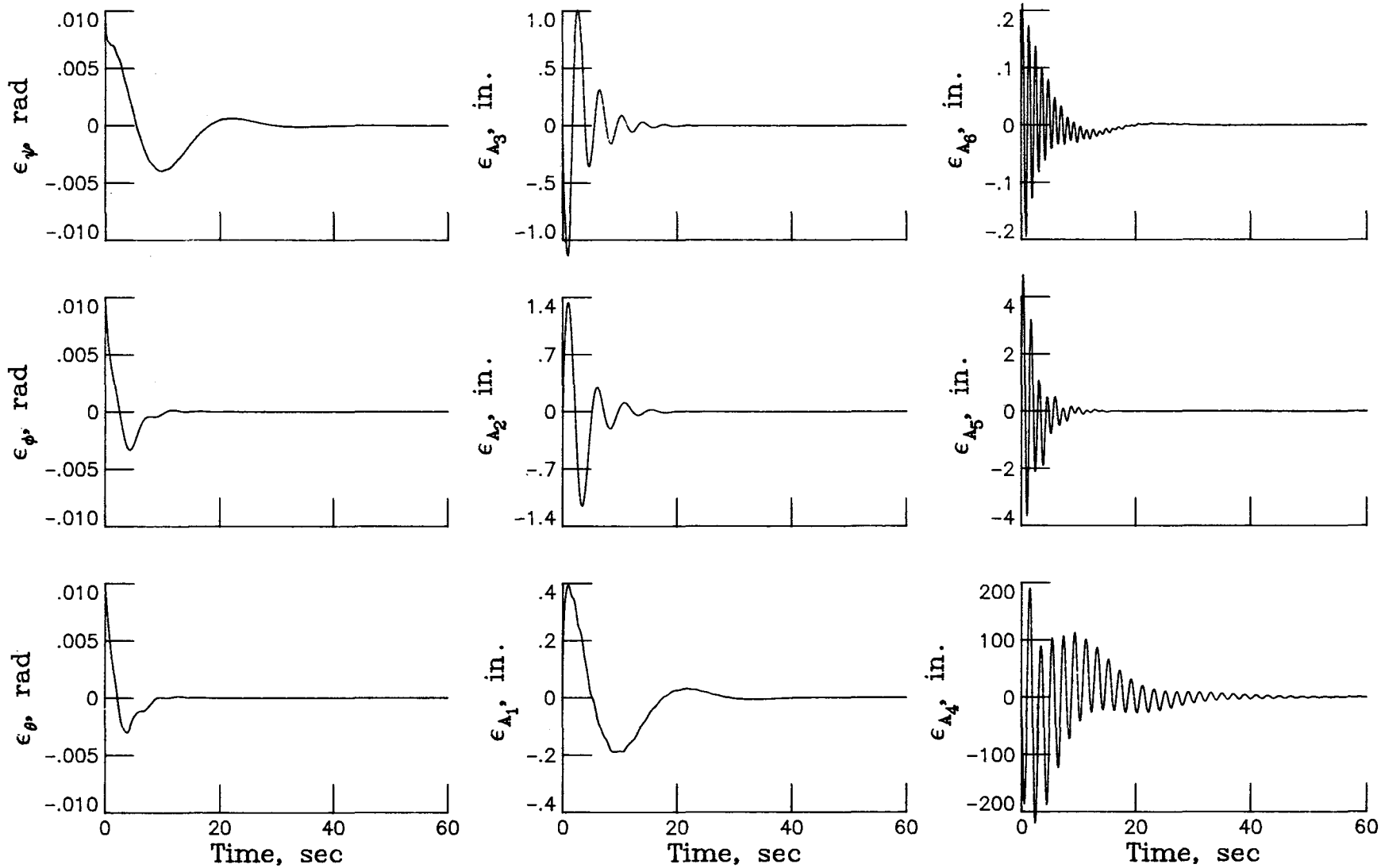
Figure 7. Example of estimator error for rigid-body control (controls off).
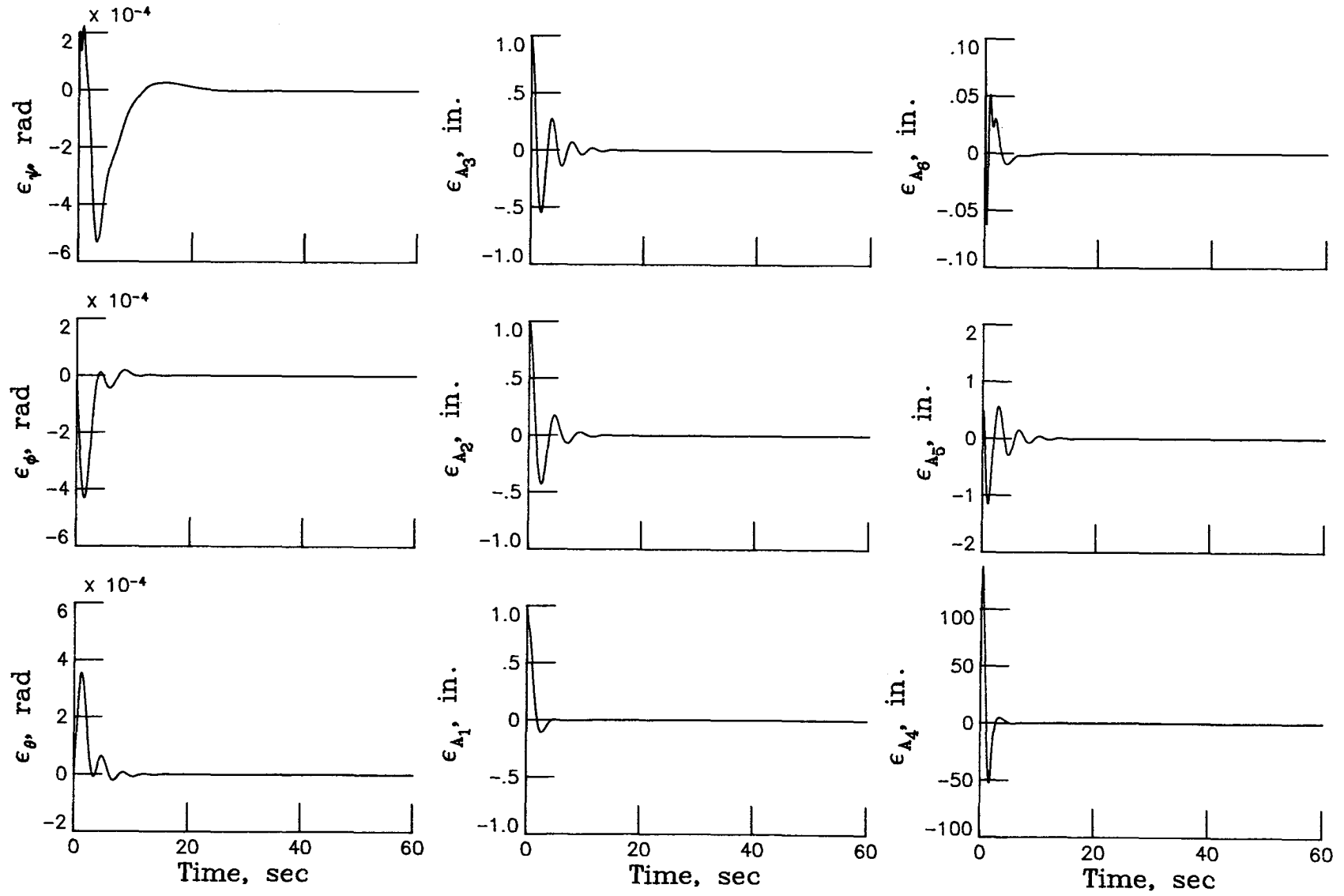
Figure 8. Example of estimator error for flexible-mode control (controls off).
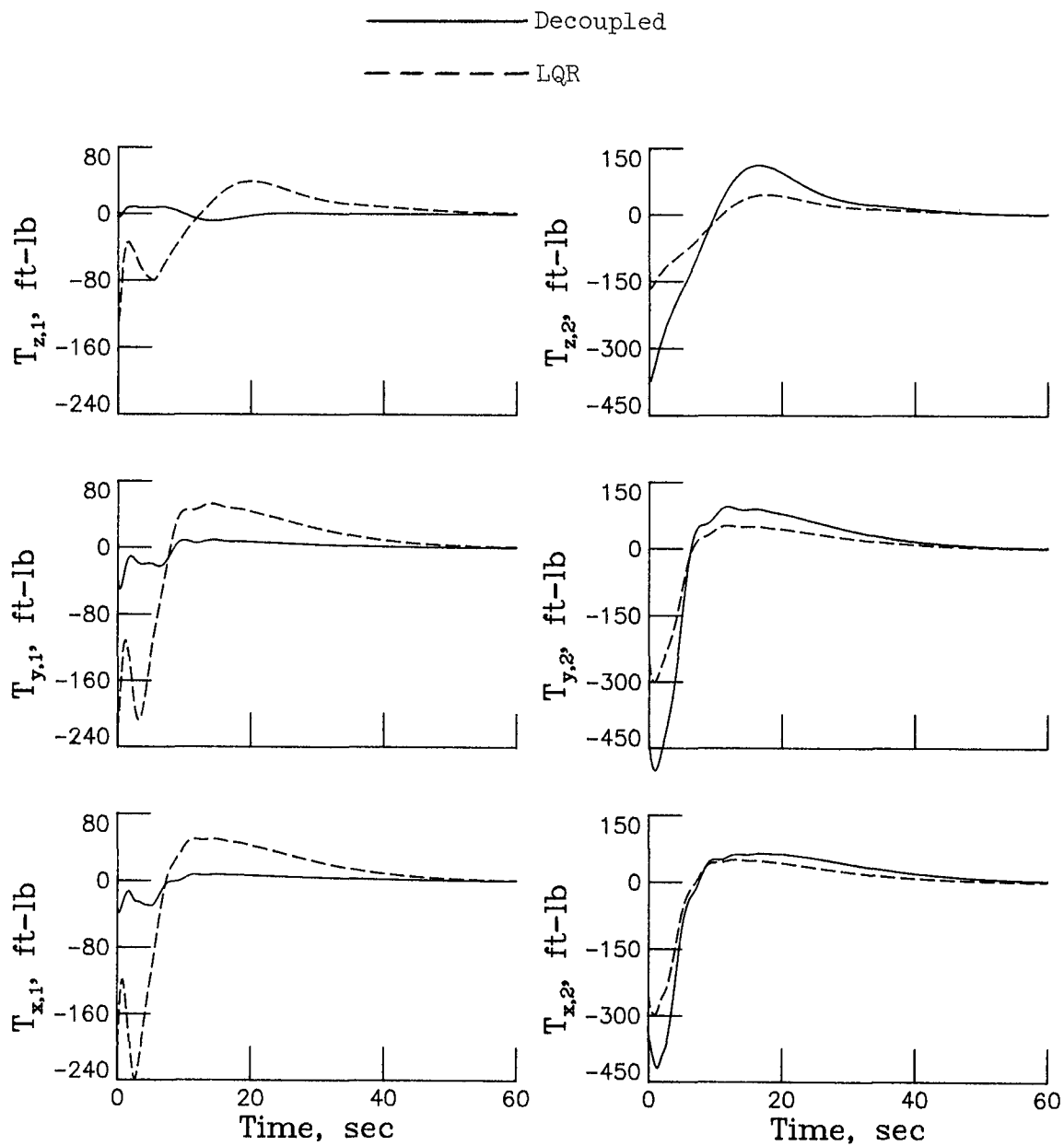
(a) Torque response.

Figure 9. Decoupled- and LQR-control responses for rigid-body control with no lag. (LQR closed-loop dynamics used.)
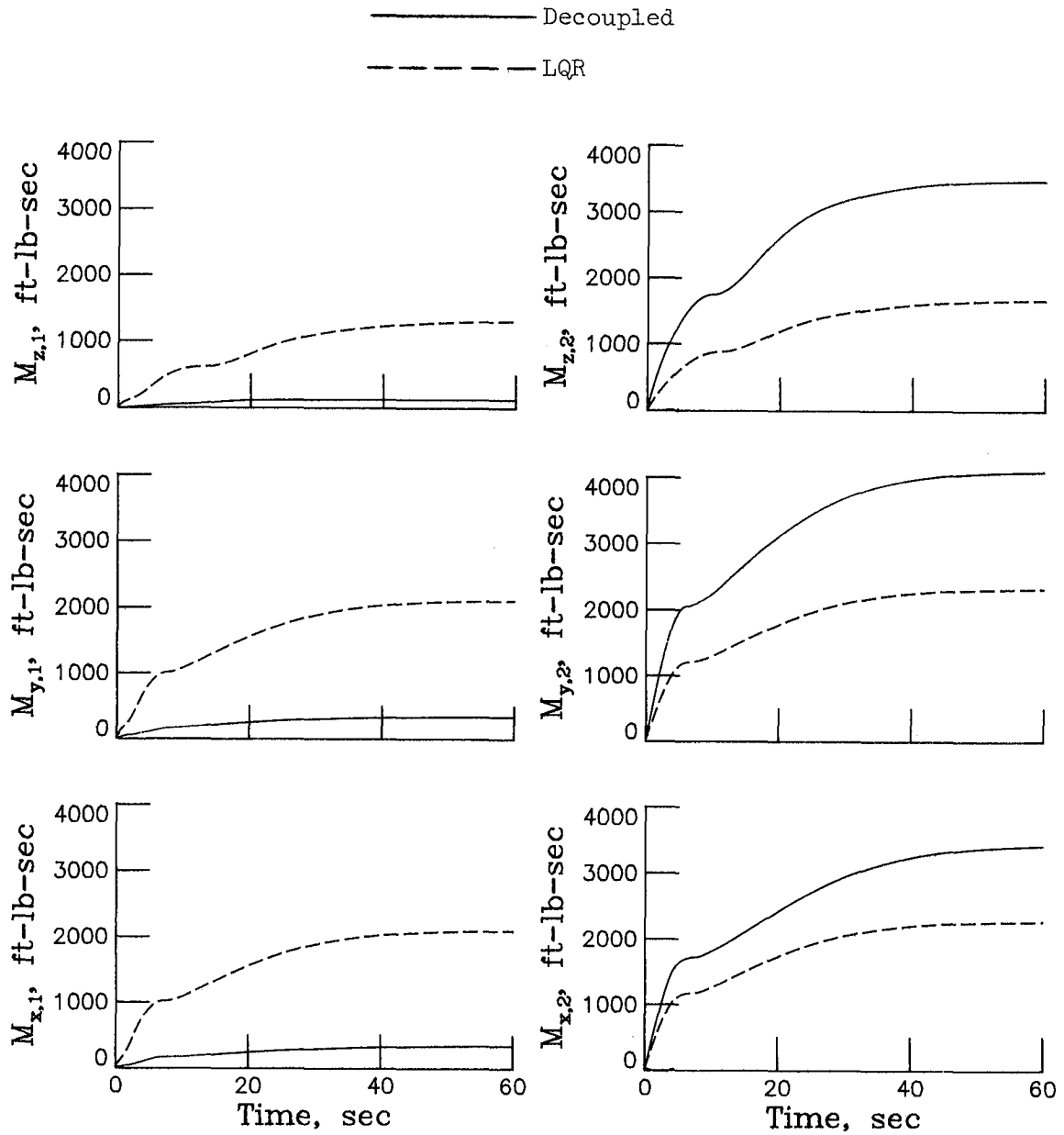
(b) Momentum required.

Figure 9. Concluded.
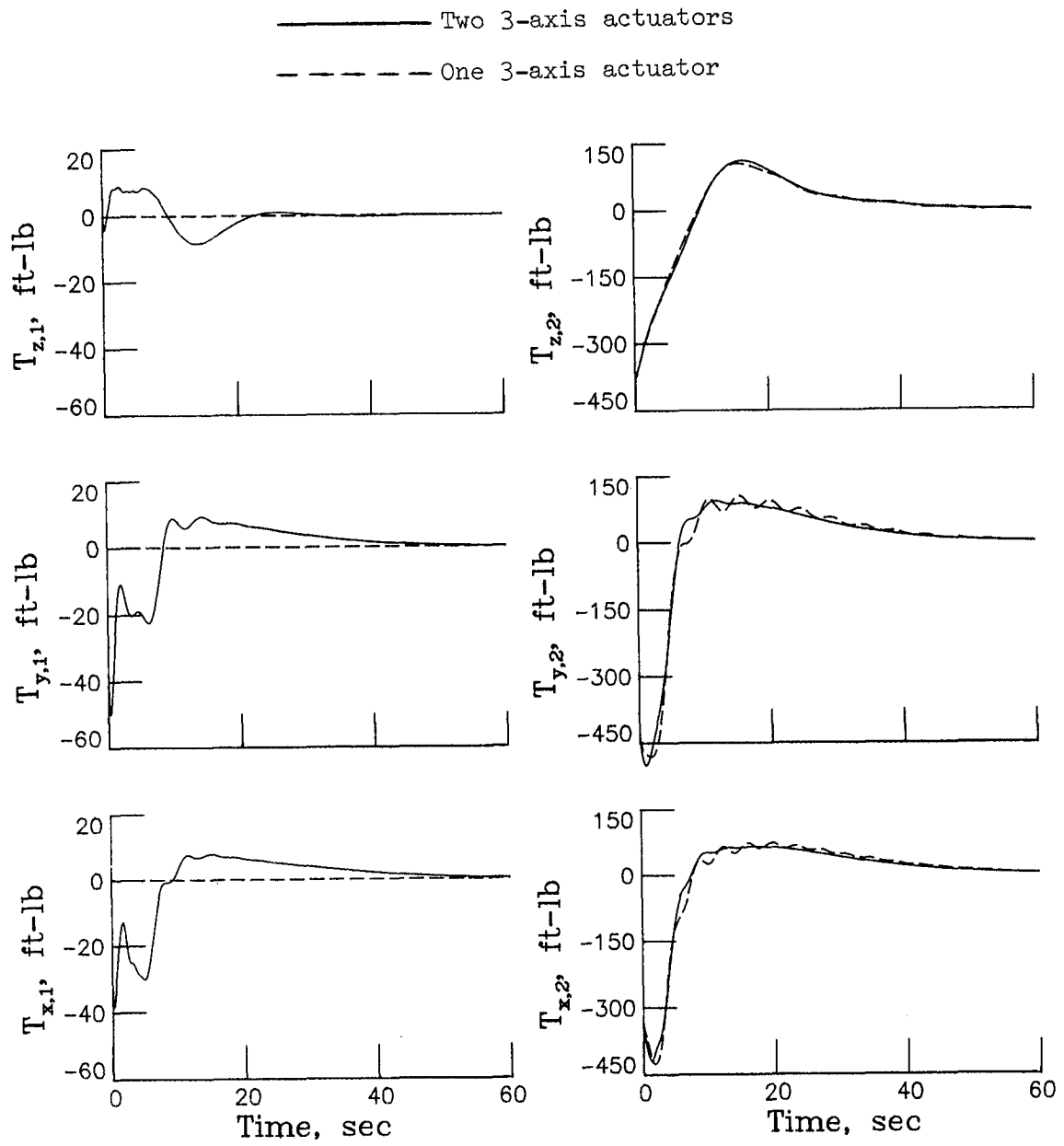
(a) Torque response for decoupled control.

Figure 10. Effect of inoperative CMG at top of antenna column for rigid-body control with no lag. (LQR closed-loop dynamics used.)

Two 3-axis actuators
One 3-axis actuator
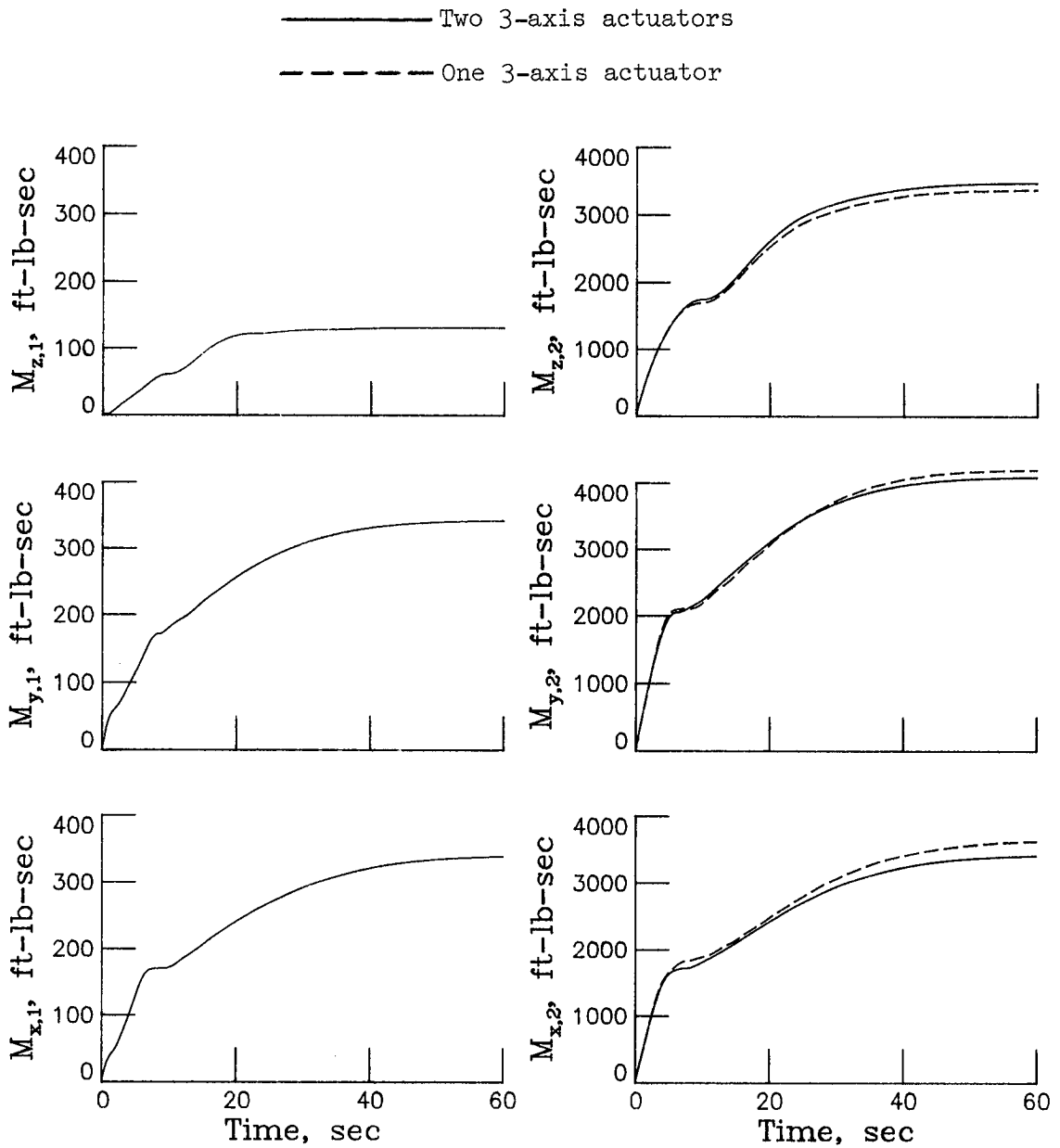
(b) Momentum required for decoupled control.

Figure 10. Continued.
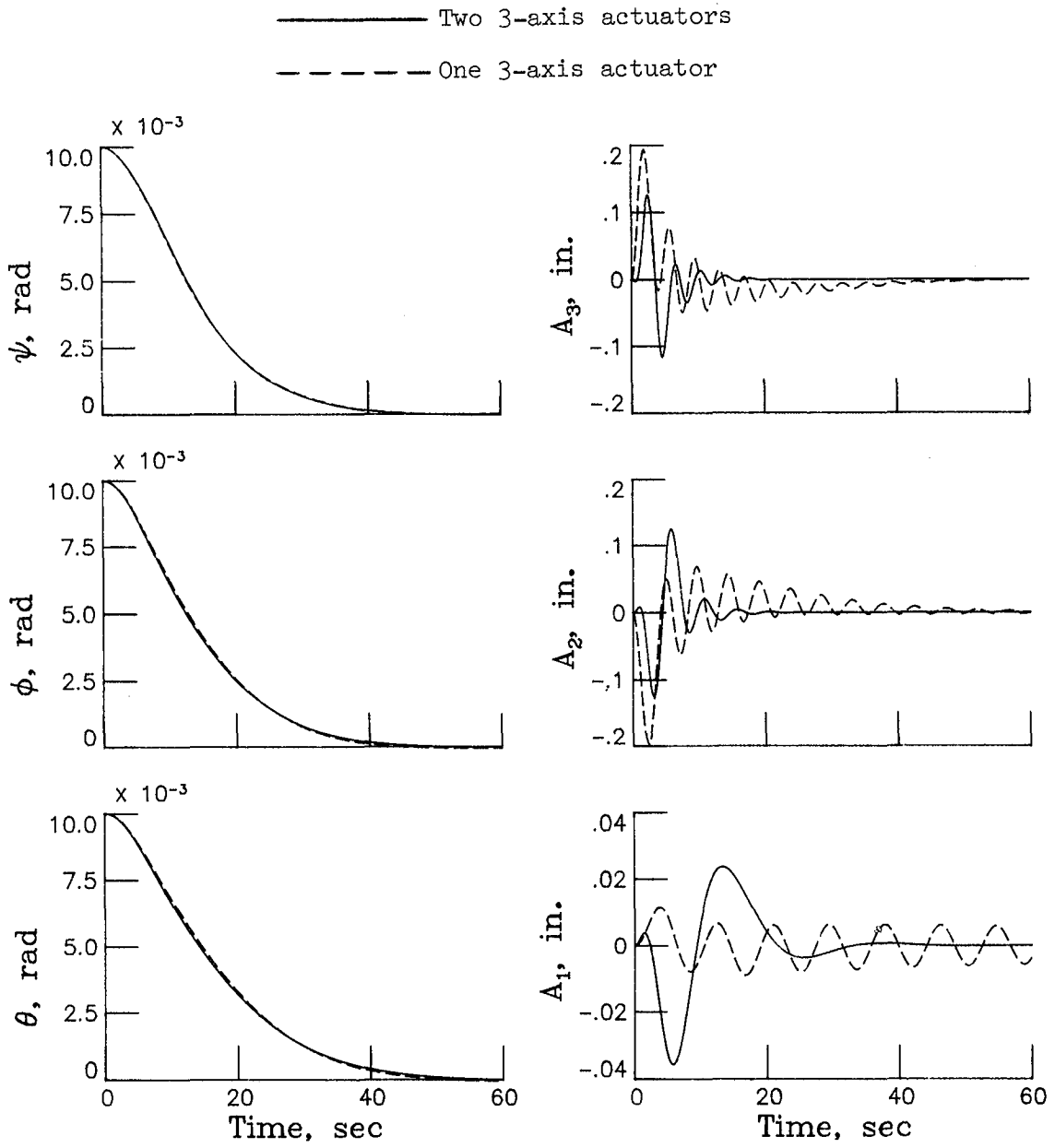
(c) Modal response for decoupled control.
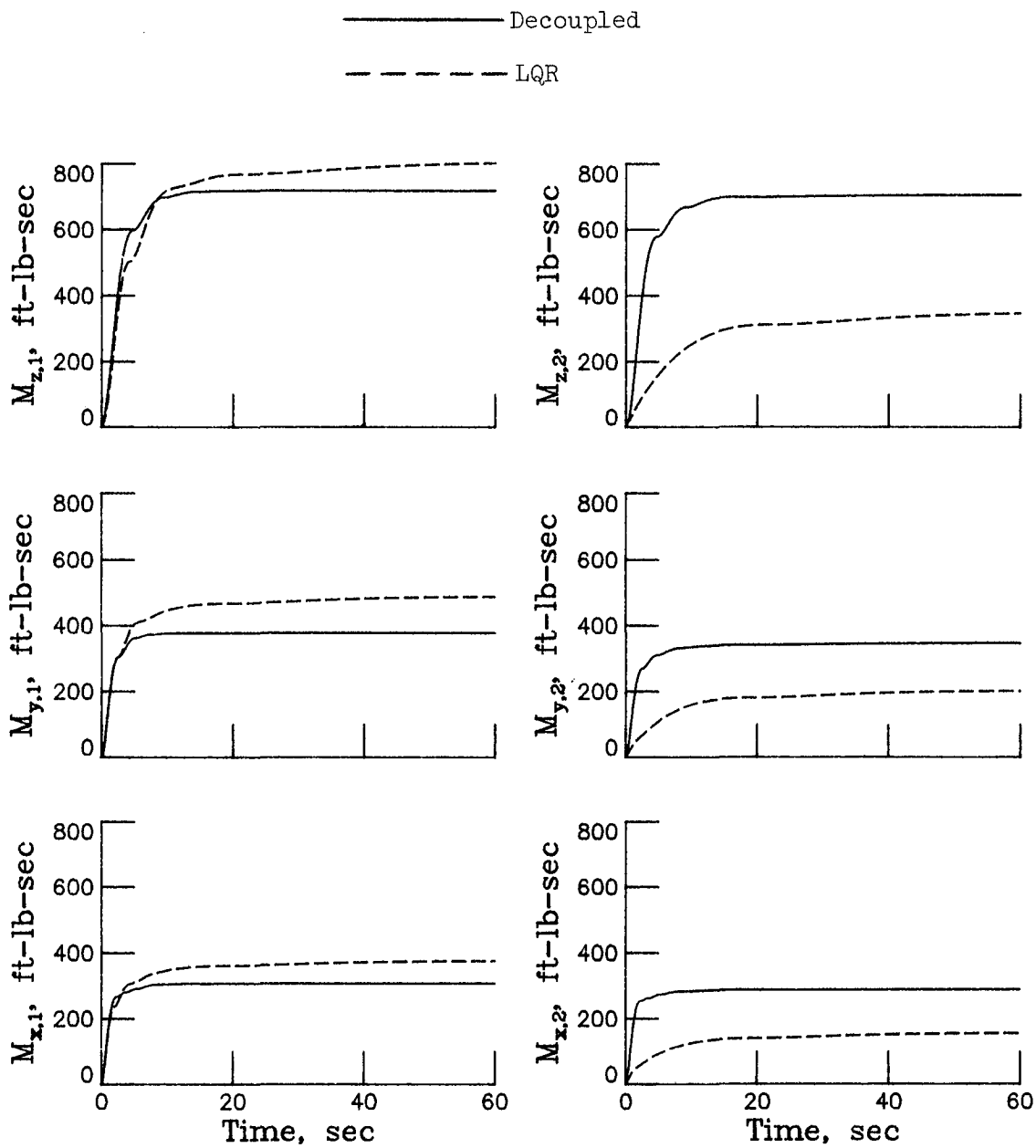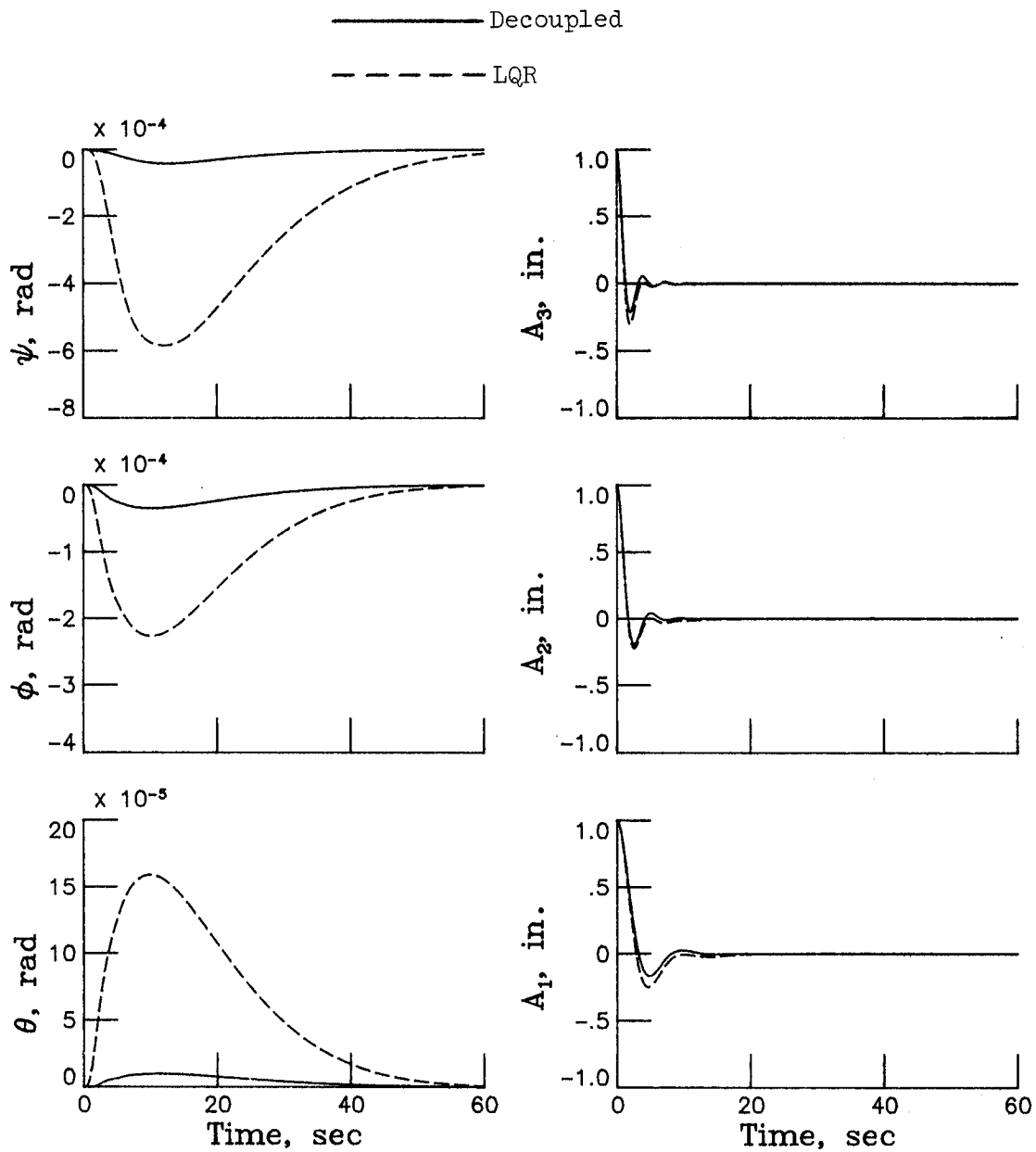
Figure 10. Concluded.
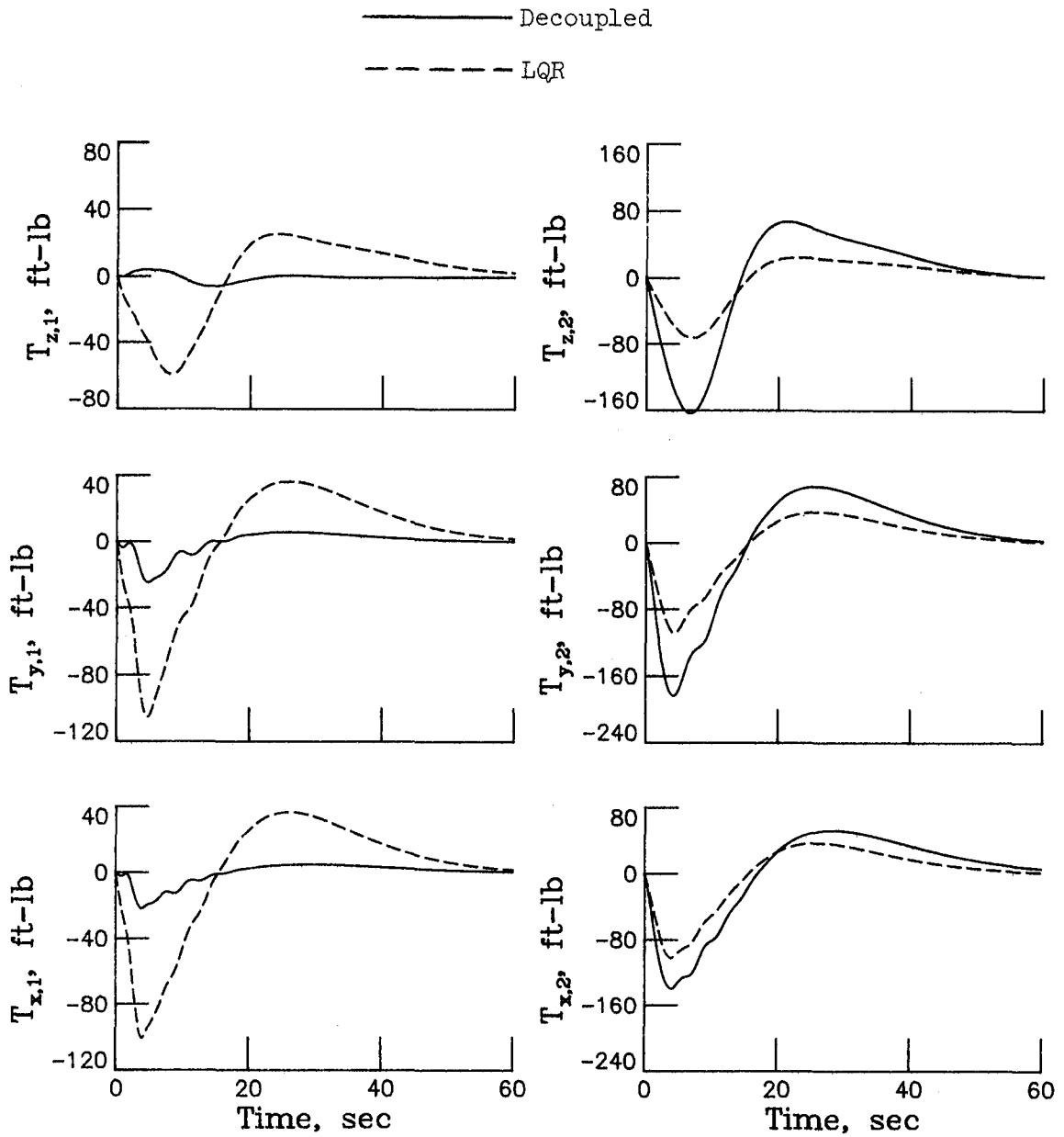
(a) Torque response.

Figure 11. Decoupled- and LQR-control responses for rigid-body control with lag. (LQR closed-loop dynamics used.)
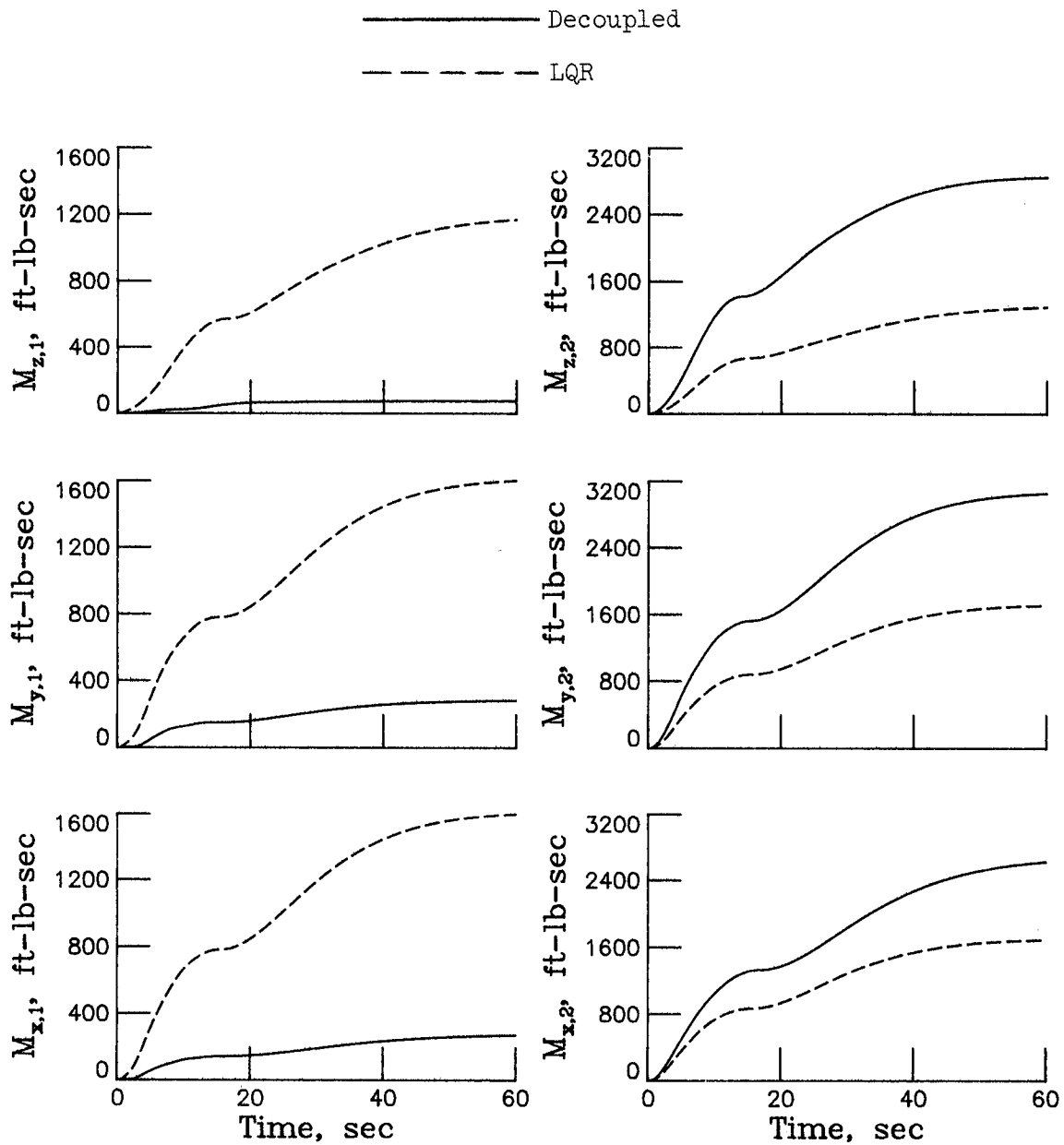
(b) Momentum required.

Figure 11. Concluded.

(a) Torque response for decoupled control.
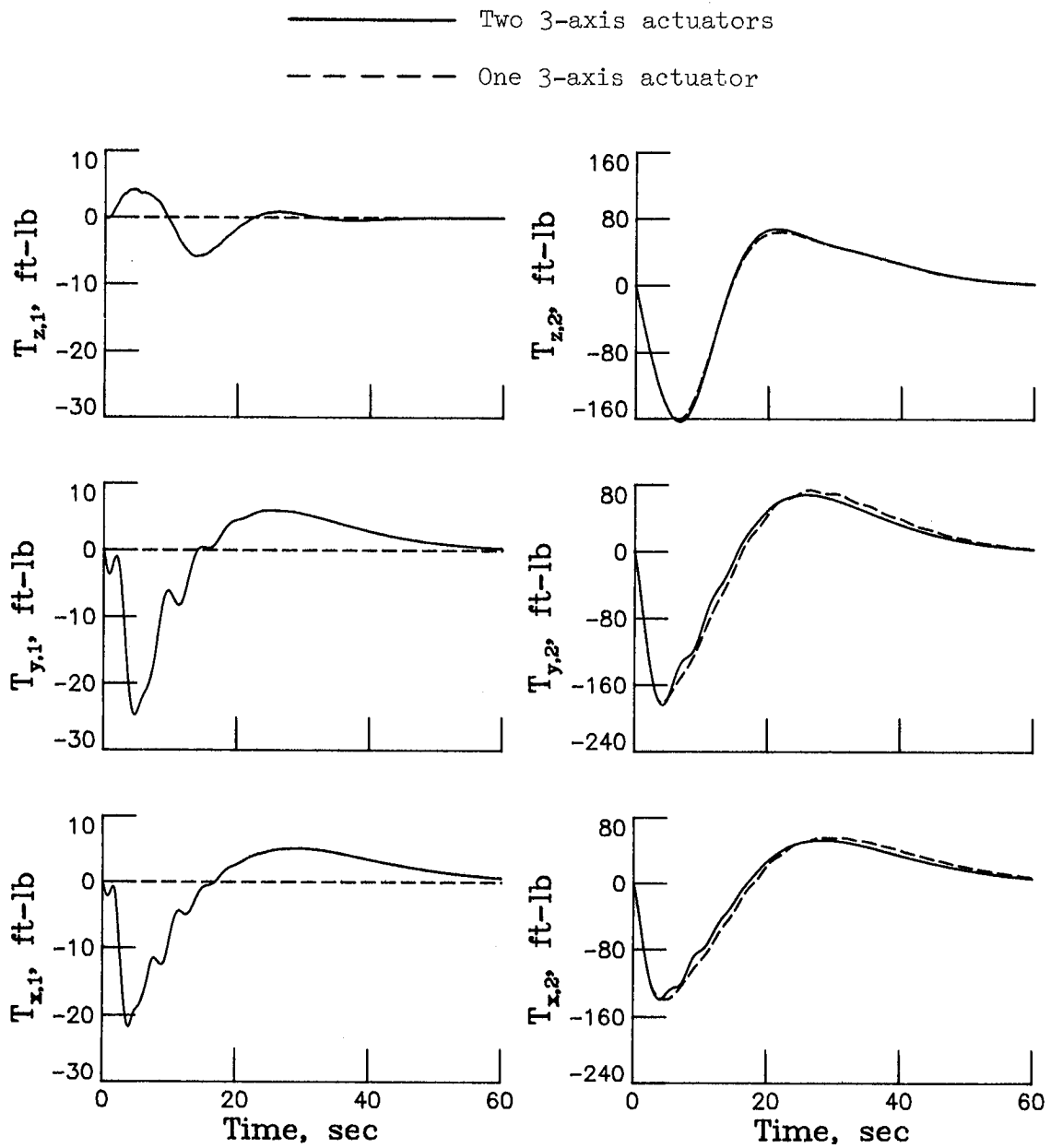
Figure 12. Effect of inoperative CMG at top of antenna column for rigid-body control with lag. (LQR closed-loop dynamics used.)
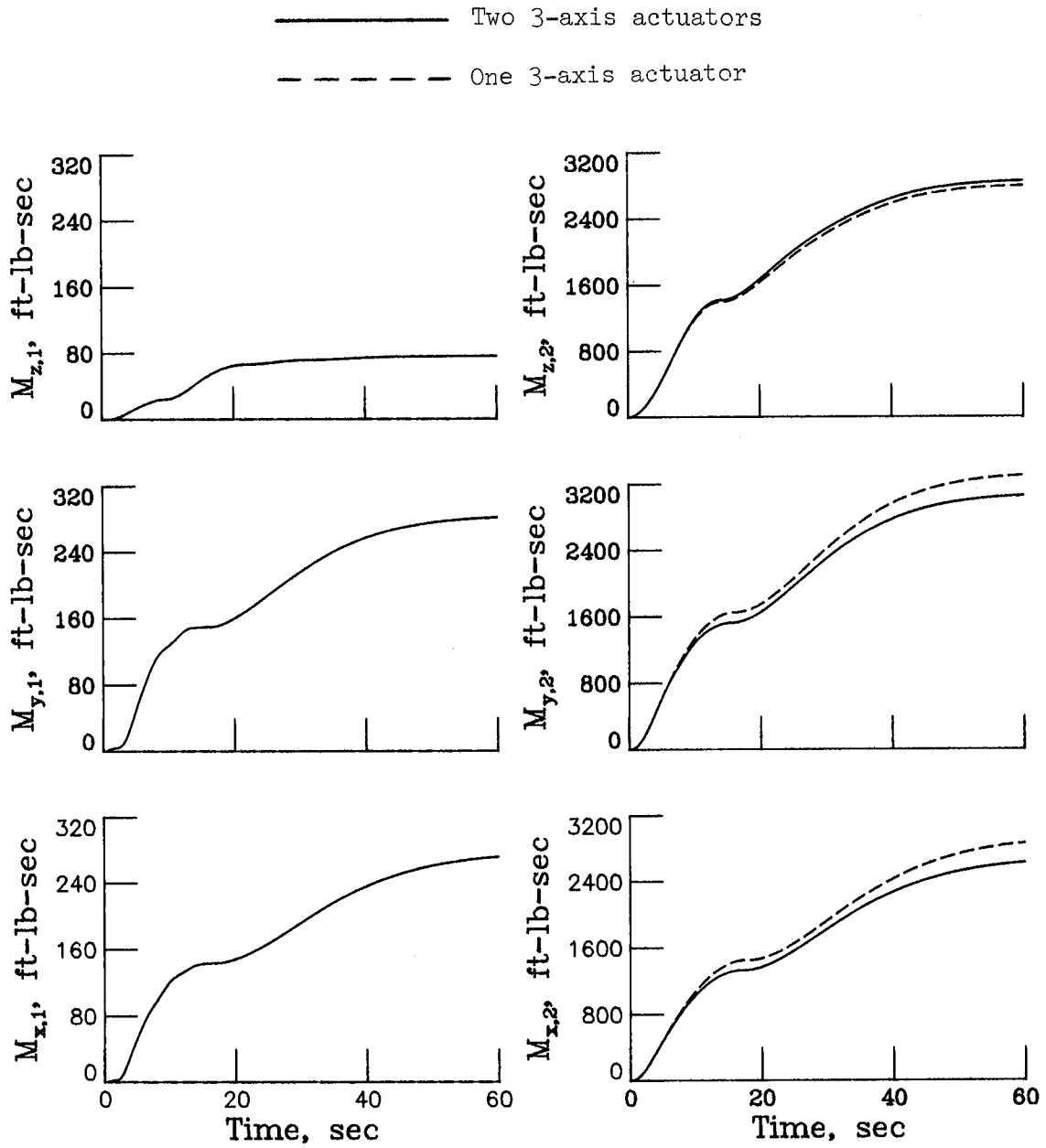
(b) Momentum required for decoupled control.

Figure 12. Continued.
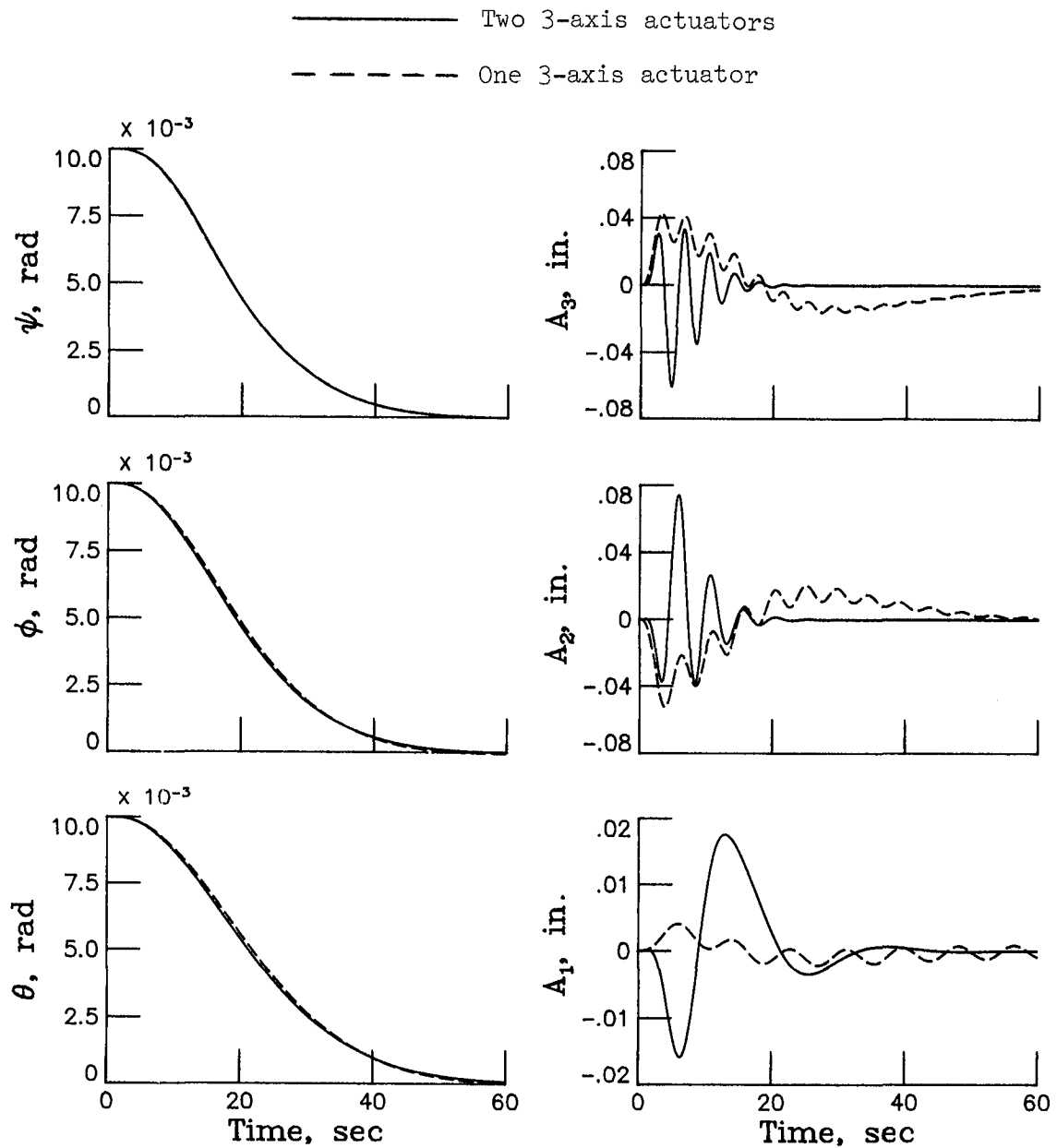
(c) Modal response for decoupled control.

Figure 12. Concluded.
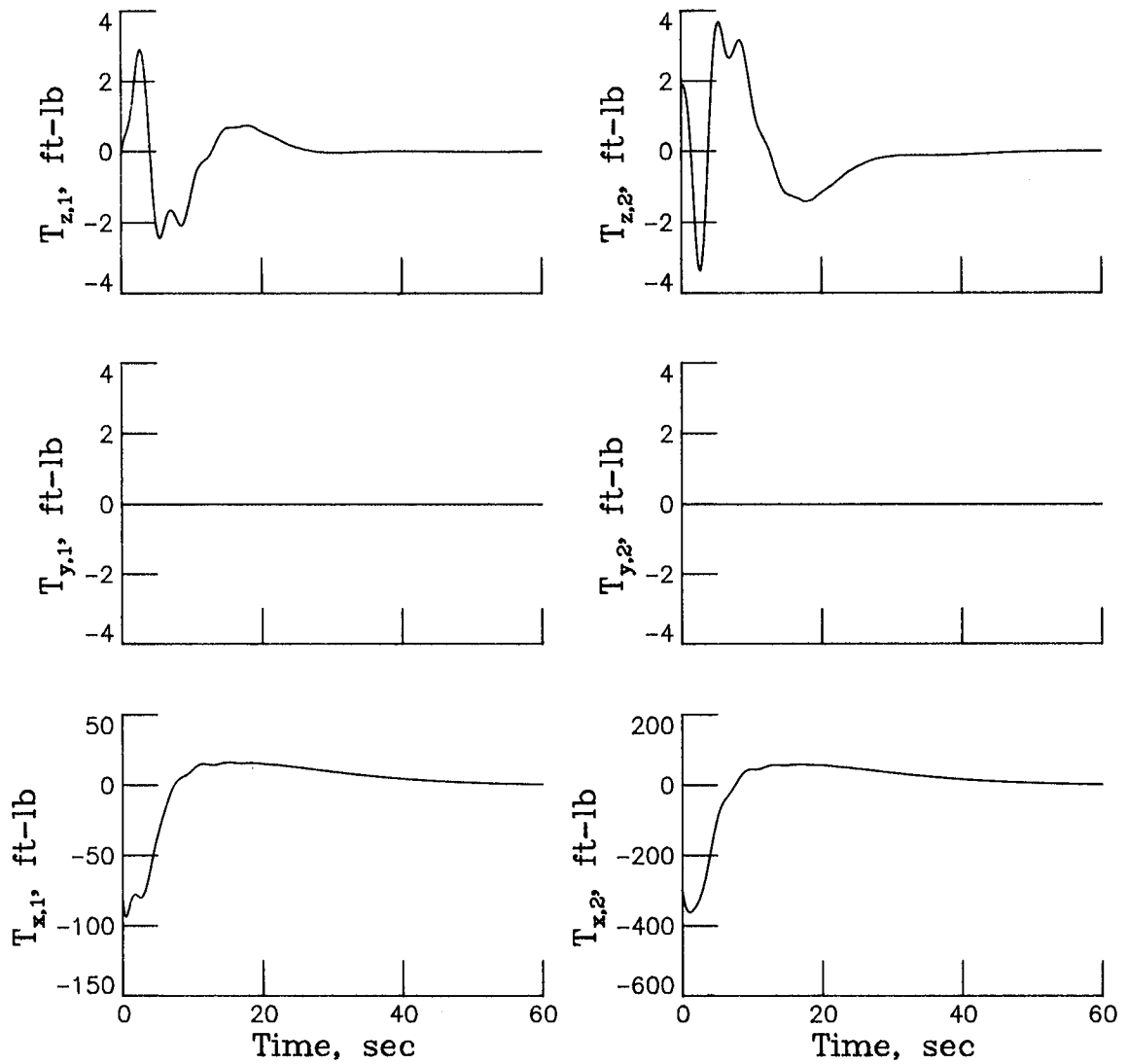
(a) Torque response.

Figure 13. Decoupled-control responses for rigid-body control about the x-axis. (Standard closed-loop dynamics used.)
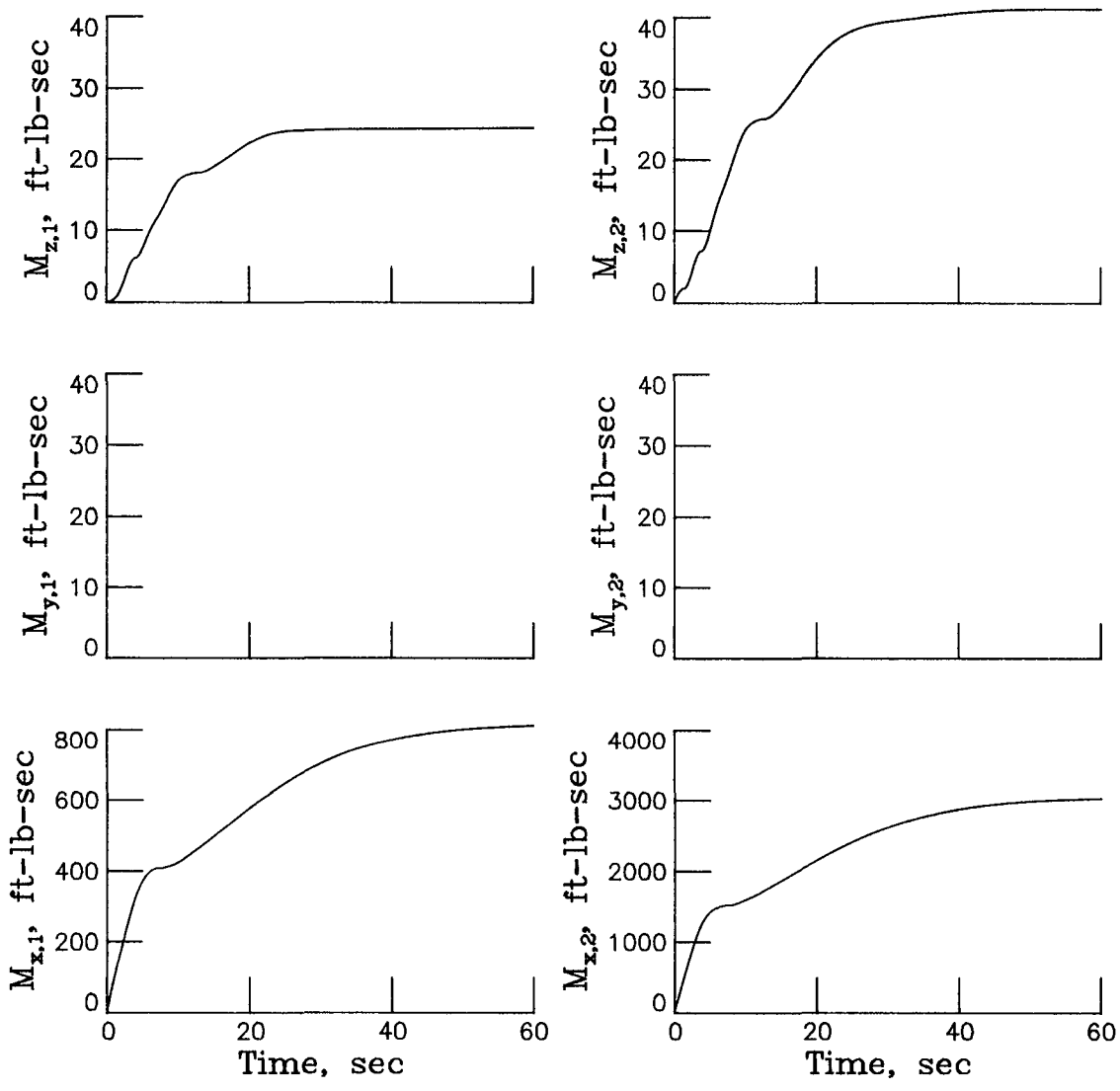
(b) Momentum required.

Figure 13. Concluded.
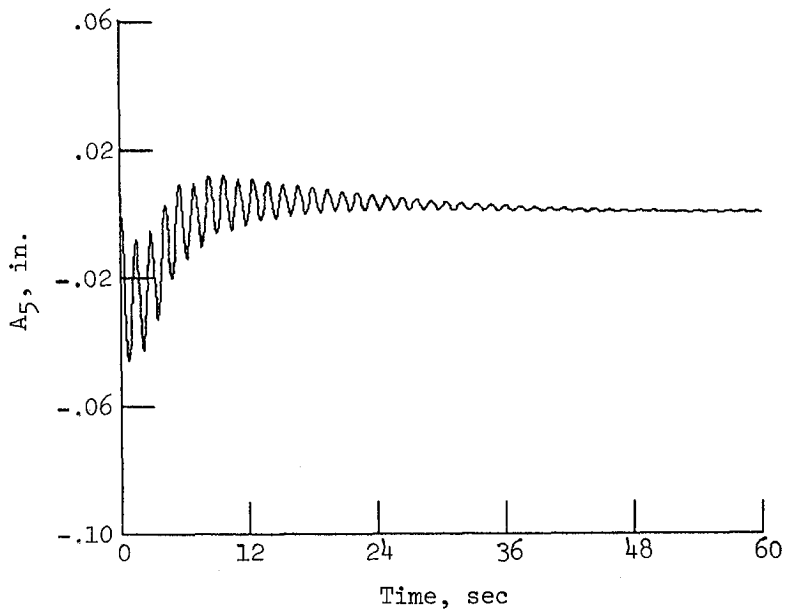
(a) Three-axis actuators at locations 1 and 4.
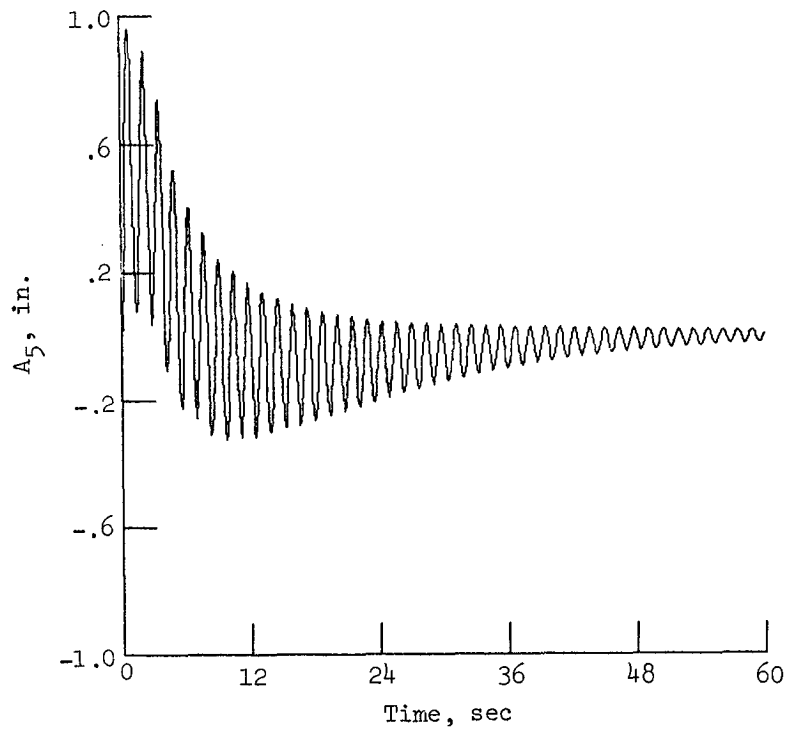
(b) Three-axis actuators at locations 1 and 2.

Figure 14. Effect of control-actuator location for single-axis rigid-body decoupled control.
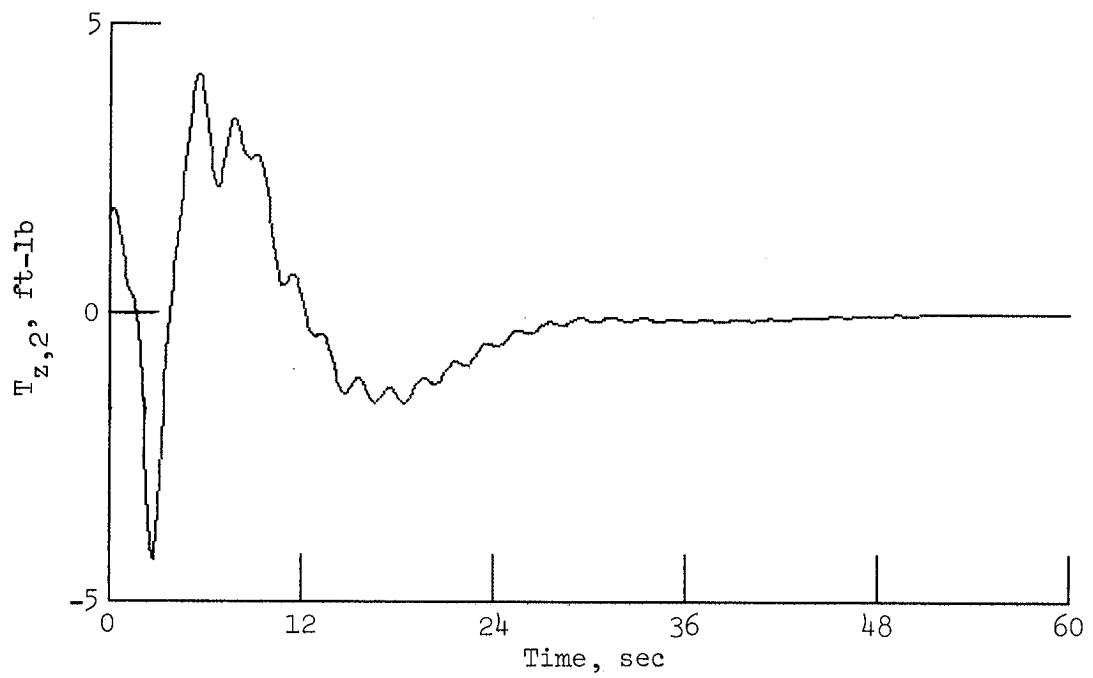
Figure 15. Example of z-axis control response when residual modes are estimated for single-axis rigid-body decoupled control.
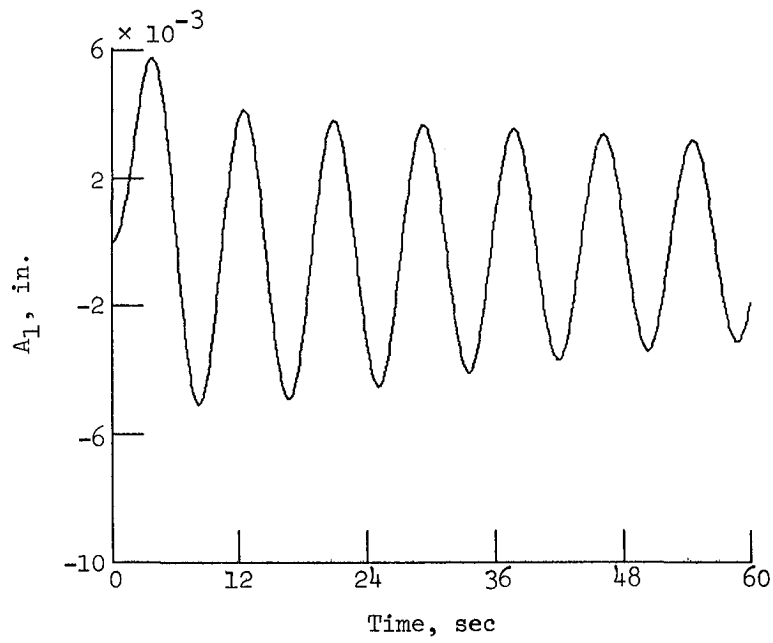
(a) First-flexible-mode response.
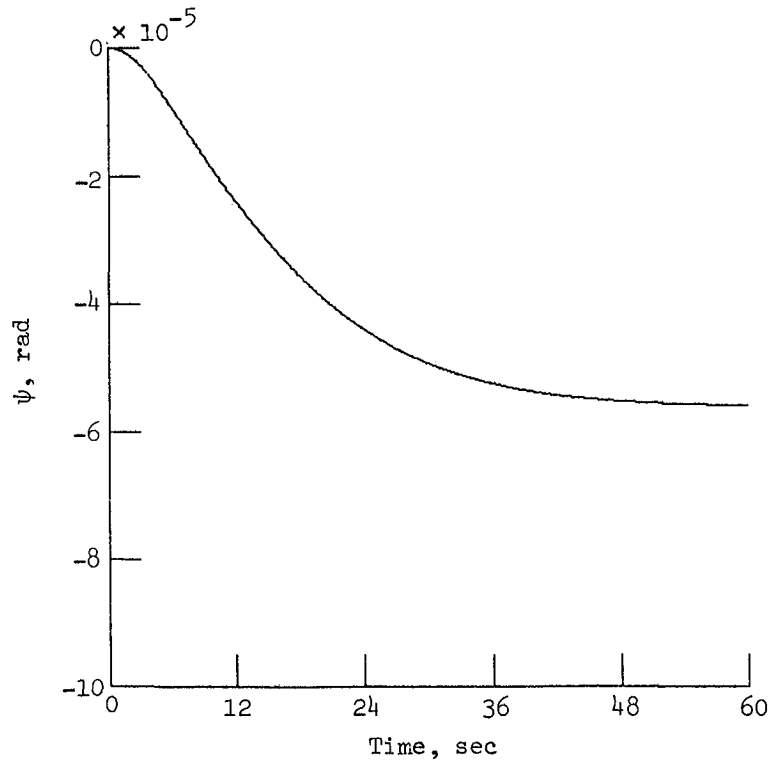
(b) Yaw rigid-body modal response.

Figure 16. Effects of inoperative z-axis control actuators for single-axis rigid-body decoupled control.
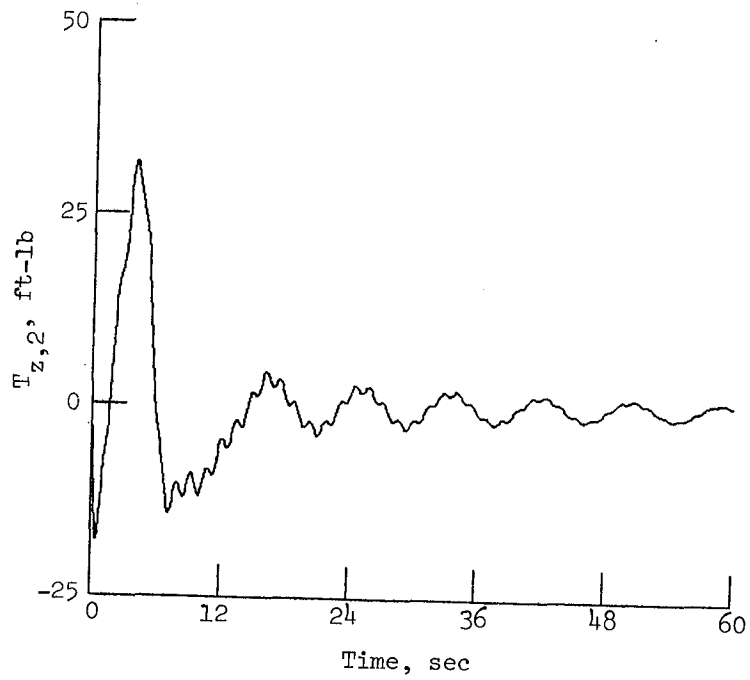
(a) z-axis torque response at location 2.
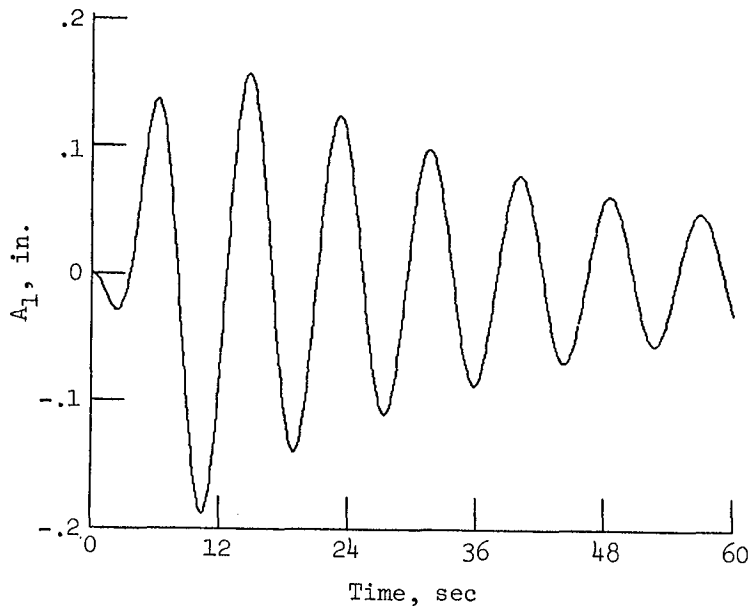
(b) First-flexible-mode response.

Figure 17. Effects of inoperative y- and z-axis attitude sensors for single-axis rigid-body decoupled control.
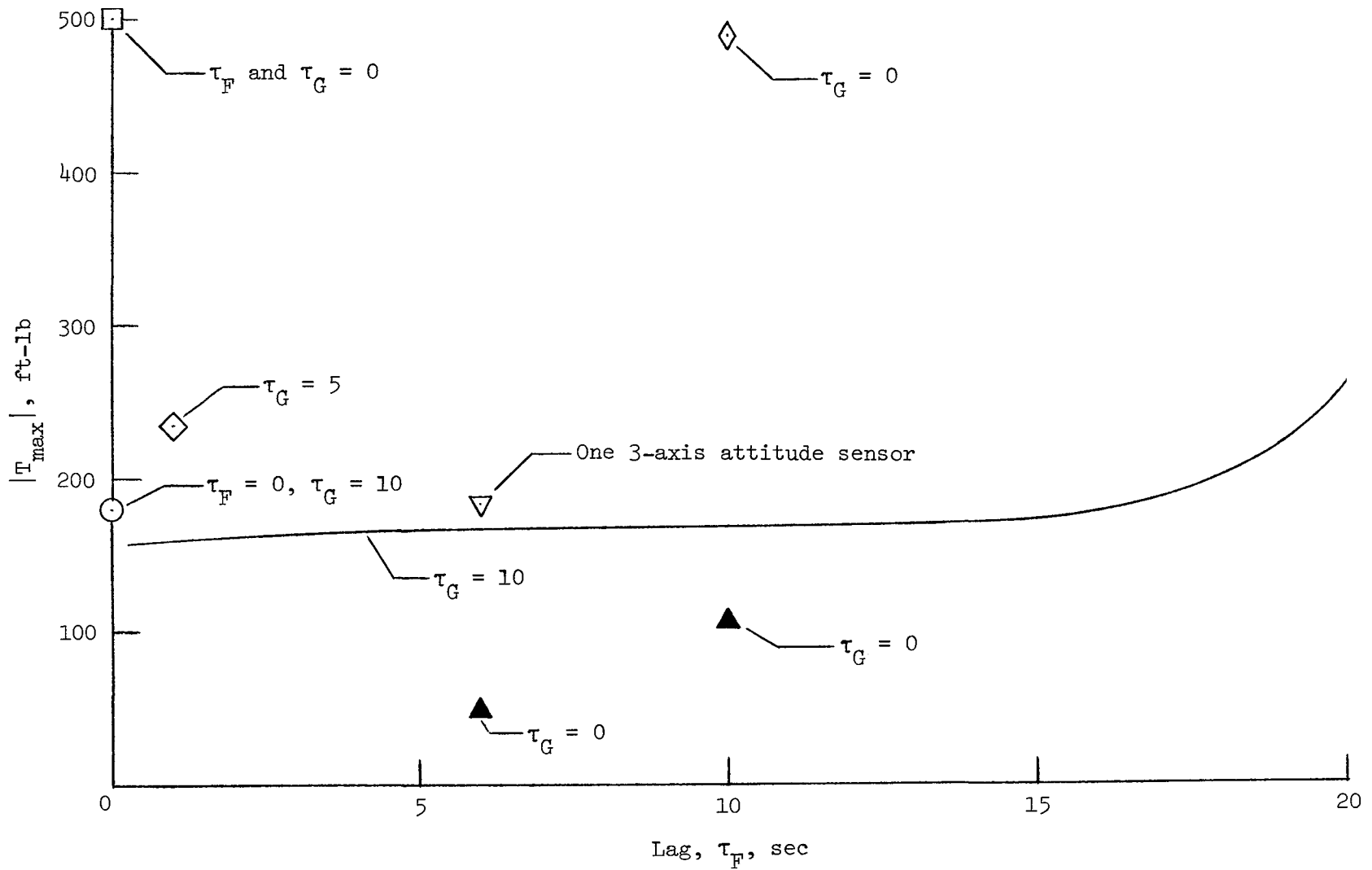
(a) Maximum torque requirements.

Figure 18. Decoupled-control requirements for 0.01-rad commands in three rigid-body modes. Solid symbols represent 50-percent reduction in closed-loop rigid-body frequencies. (LQR closed-loop dynamics used.)
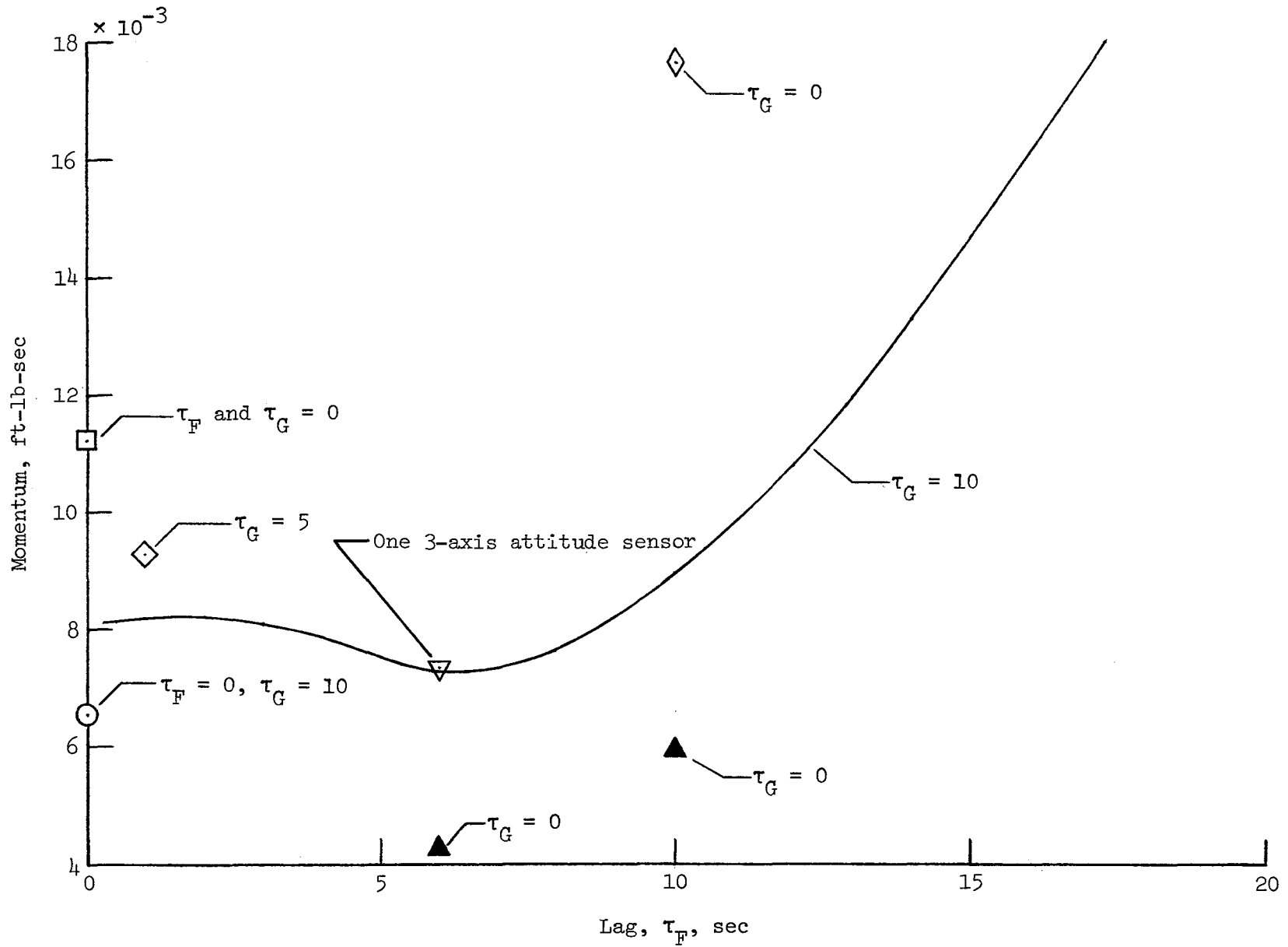
(b) Momentum requirements.

Figure 18. Concluded.
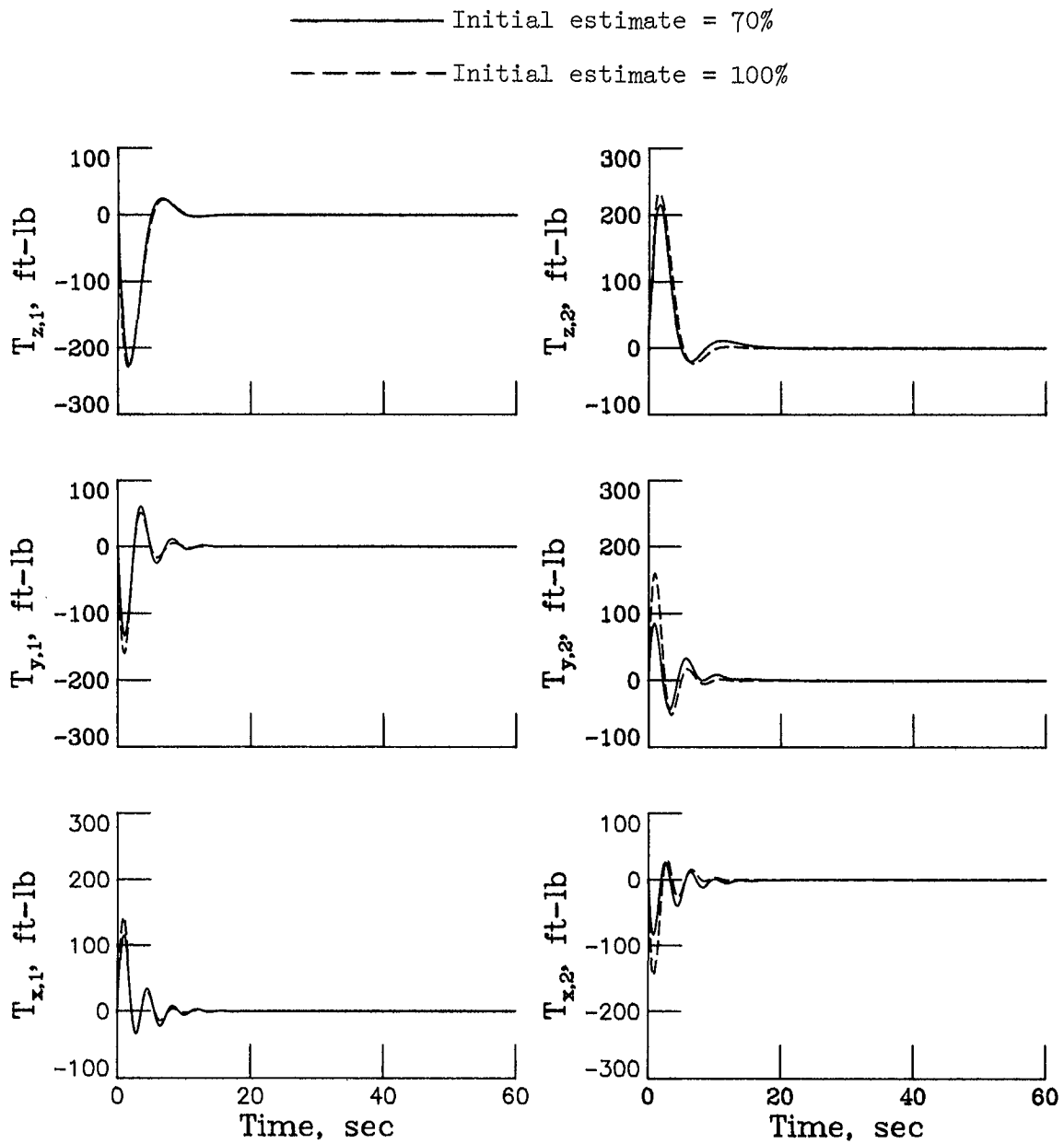
(a) Torque response.

Figure 19. Effect of accuracy of initial estimate for flexible-mode decoupled control. (Standard closed-loop dynamics used.)

(b) Momentum required.

Figure 19. Continued.

Initial estimate = 70%

Initial estimate = 100%
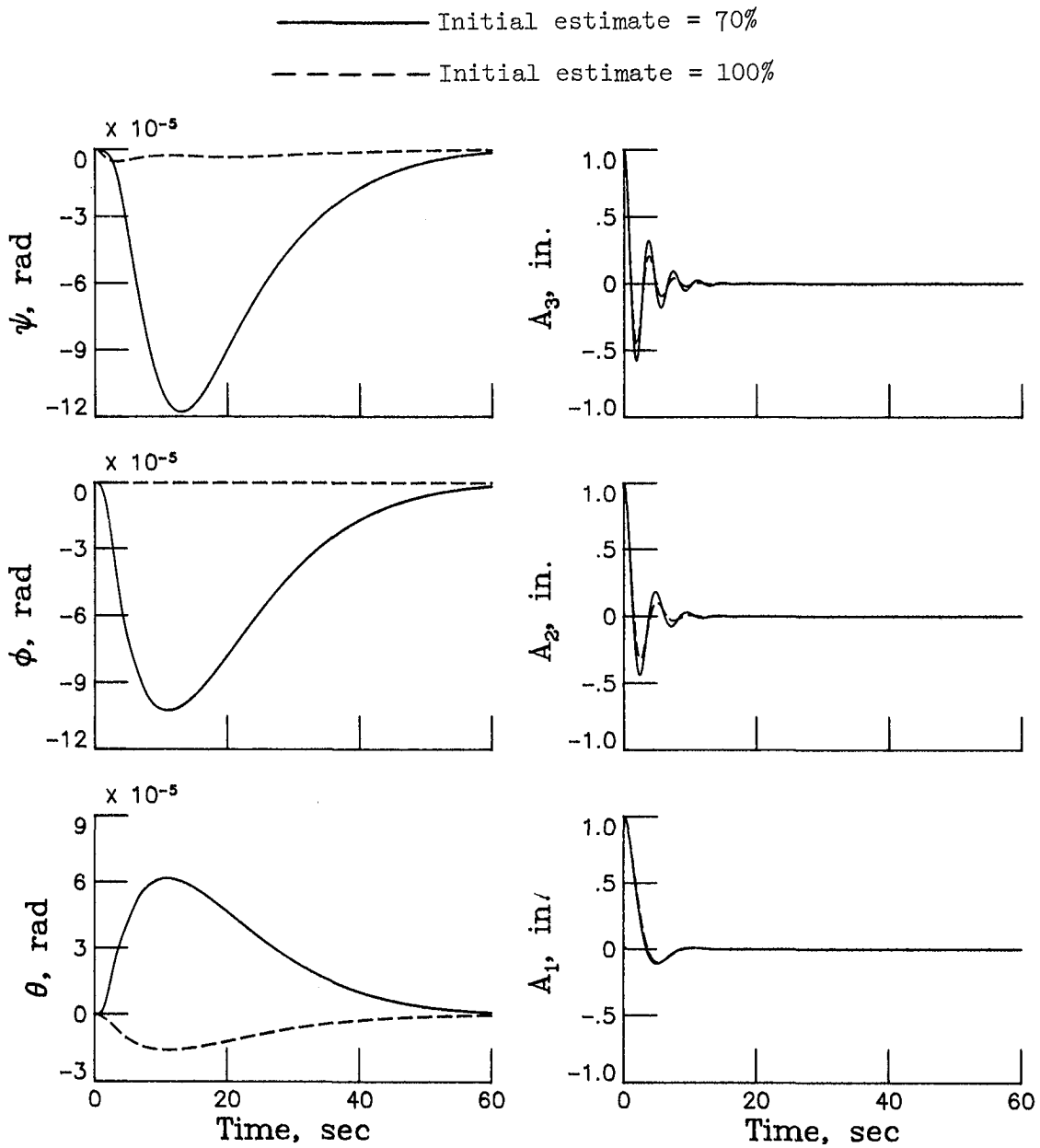
(c) Modal response.

Figure 19. Concluded.
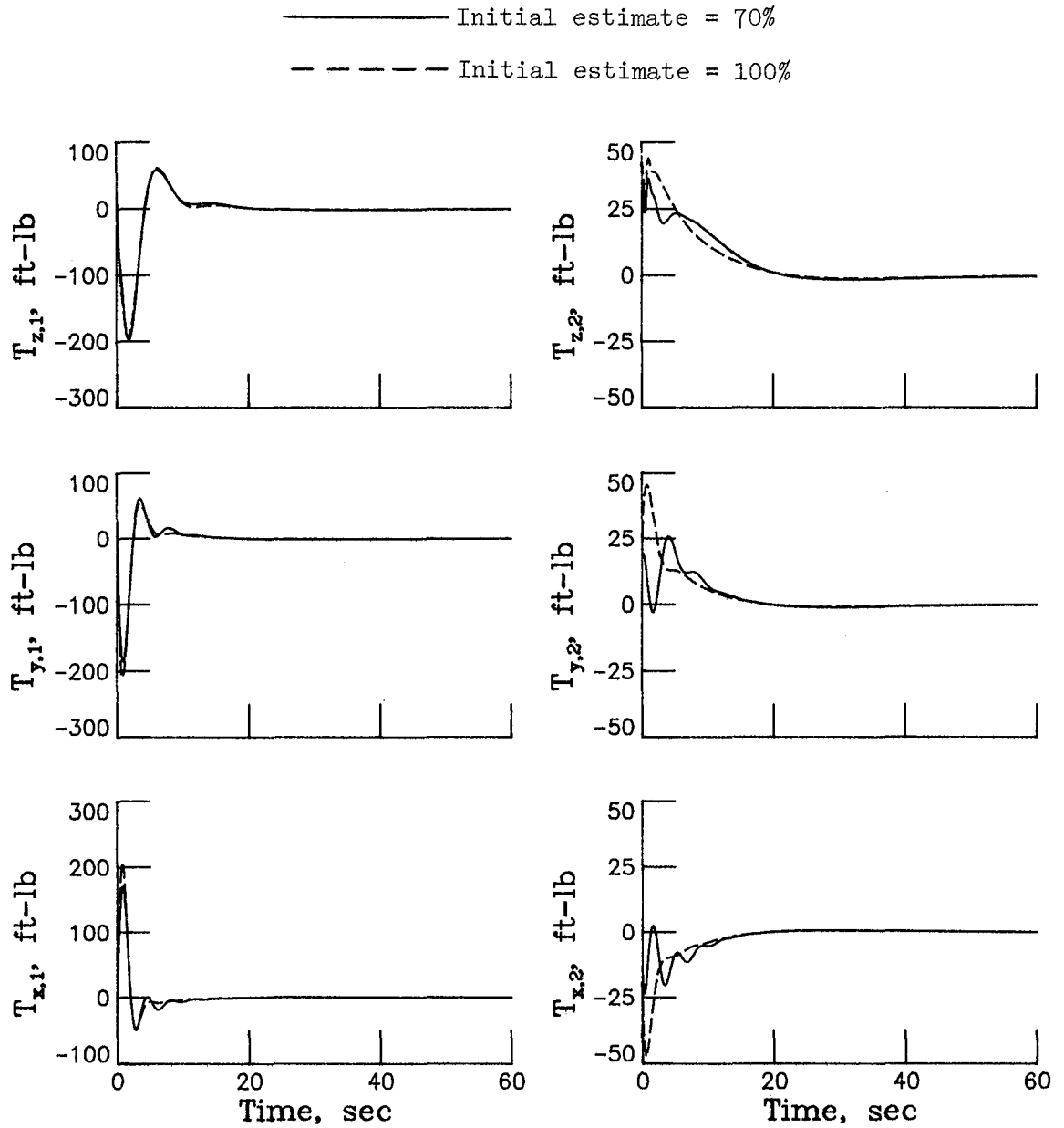
(a) Torque response.

Figure 20. Effect of accuracy of initial estimate for flexible-mode LQR control. (LQR closed-loop dynamics used.)
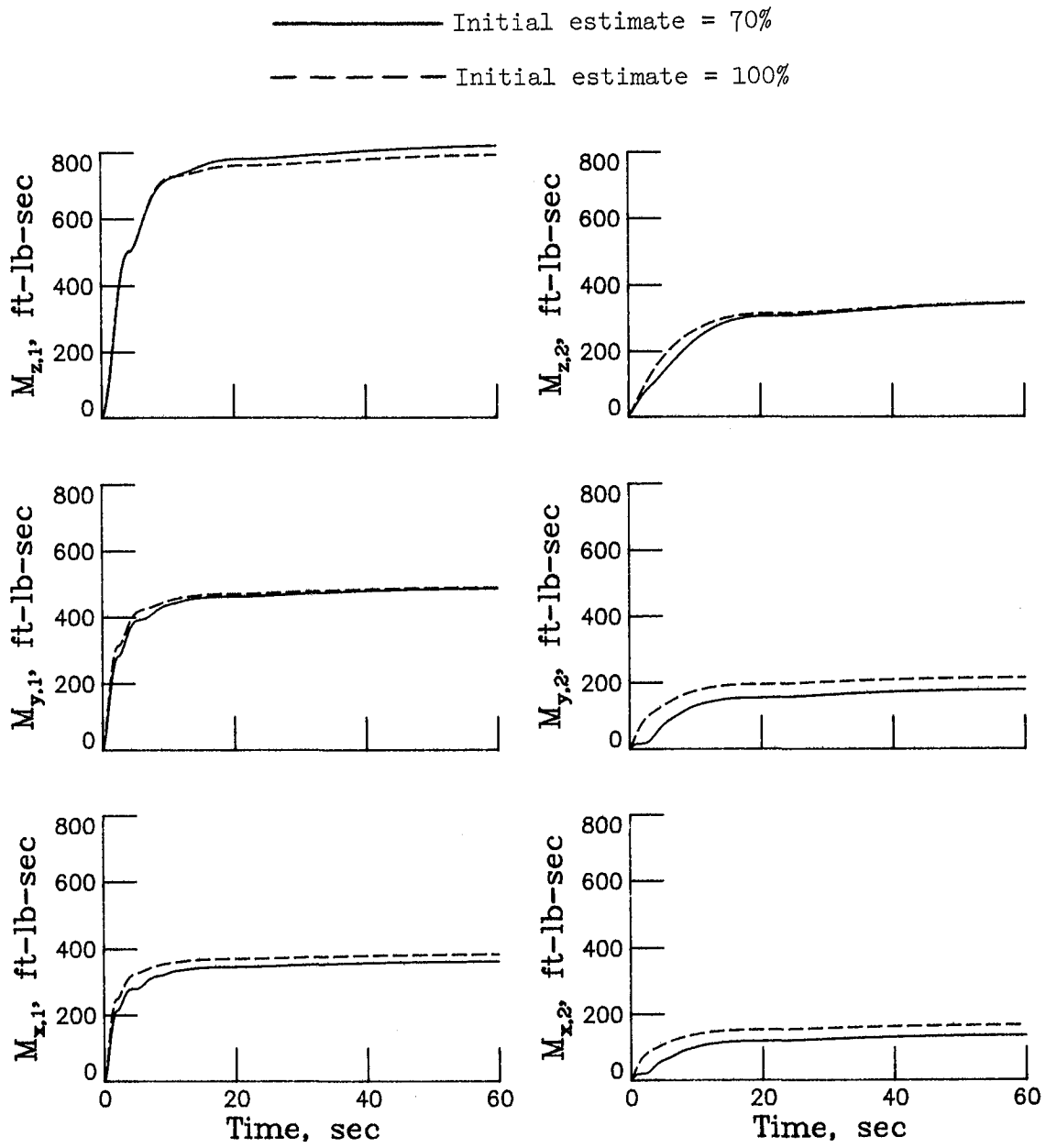
(b) Momentum required.

Figure 20. Continued.
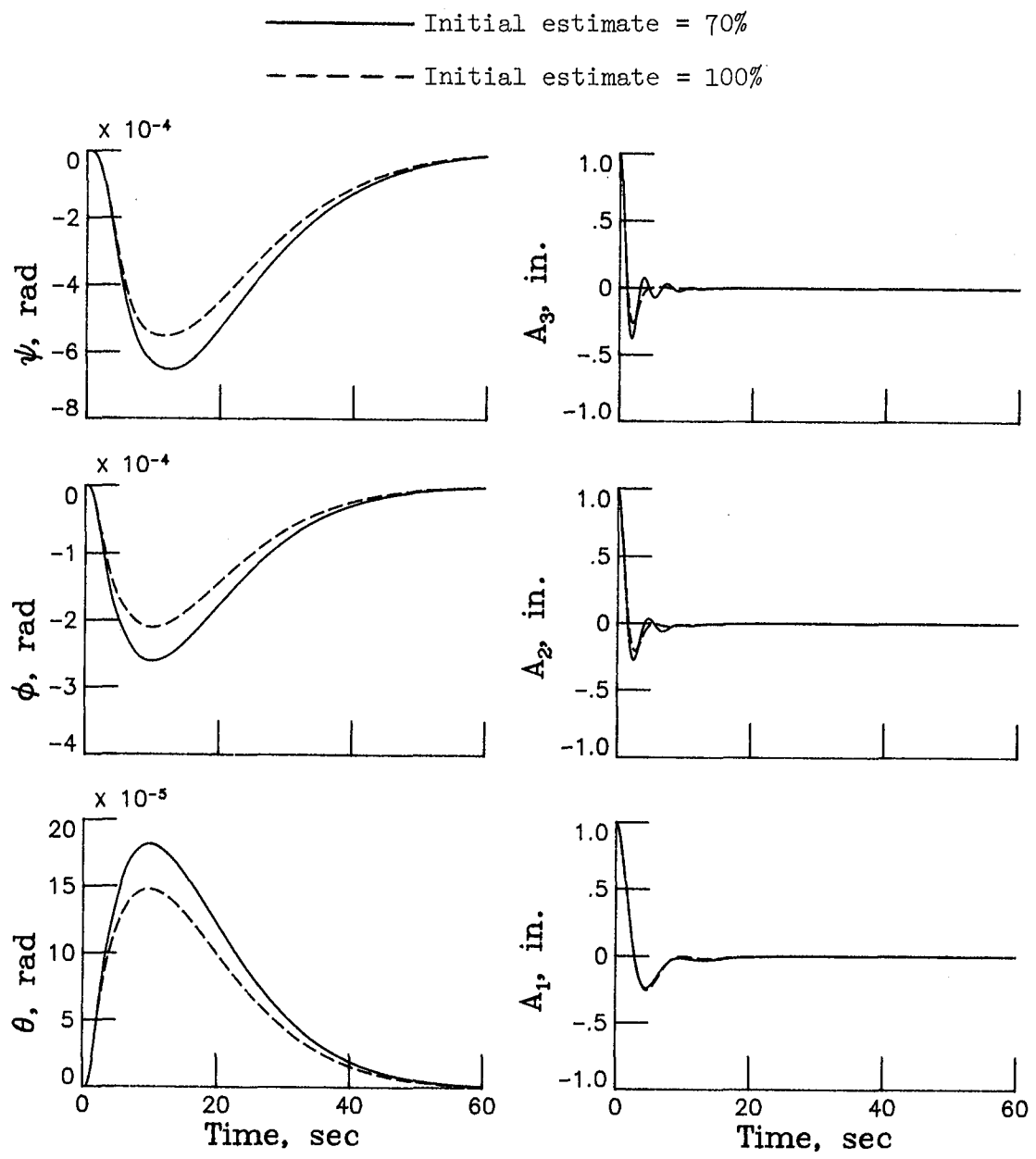
(c) Modal response.

Figure 20. Concluded.
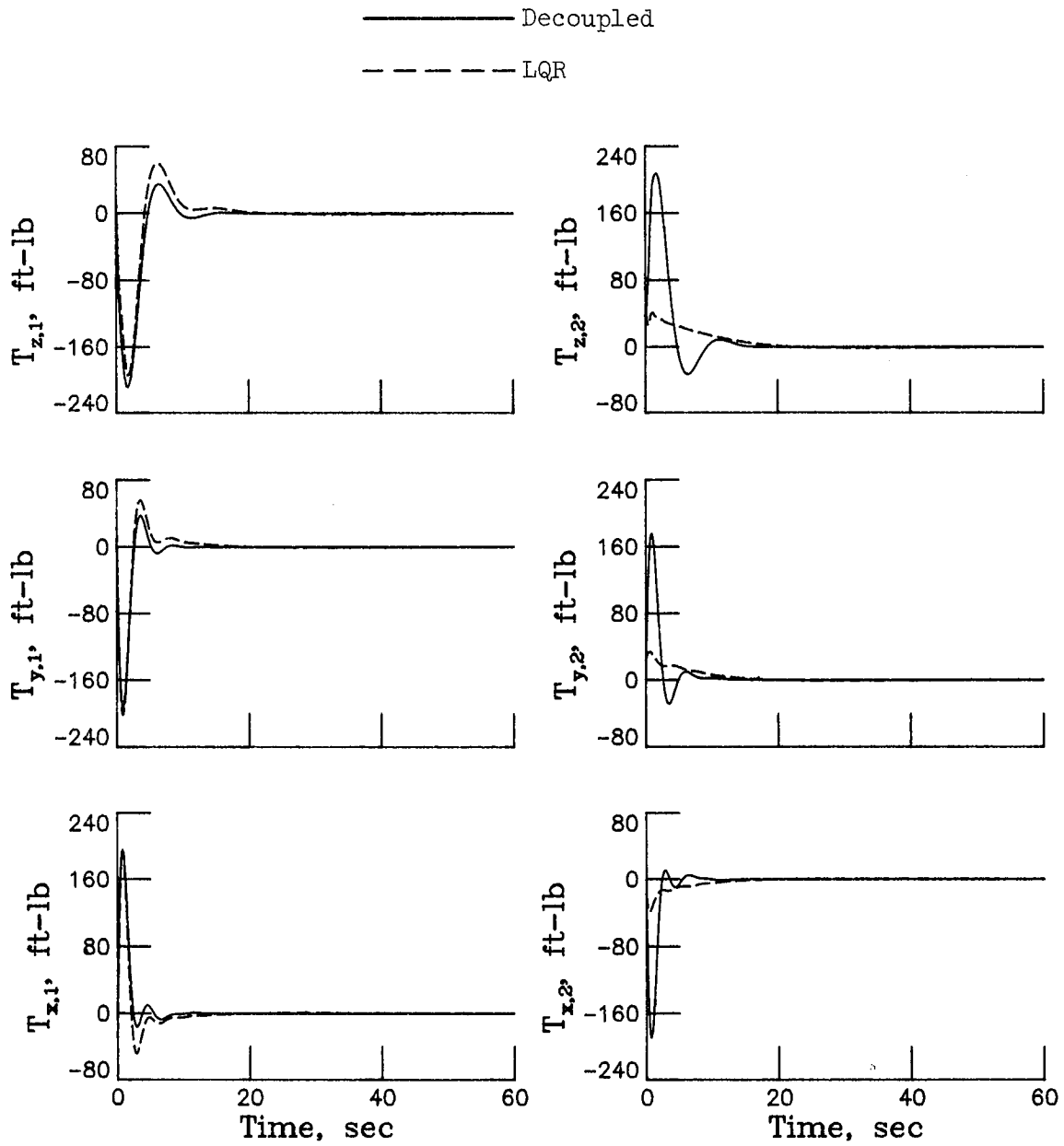
(a) Torque response.

Figure 21. Decoupled and LQR control responses for flexible-mode control with no lag. (LQR closed-loop dynamics used.)

(b) Momentum required.

Figure 21. Continued.

(c) Modal response.

Figure 21. Concluded.
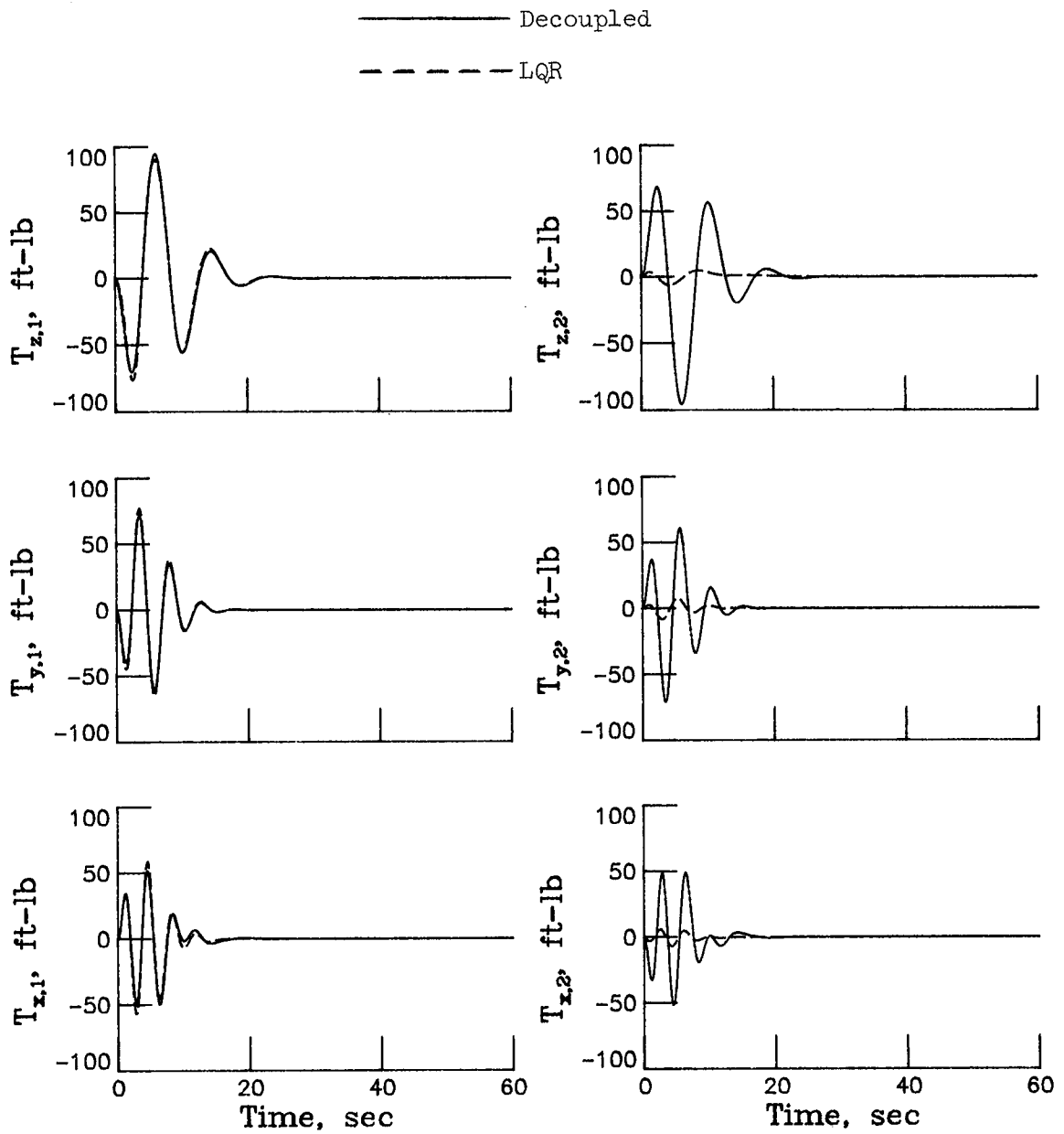
(a) Torque response.

Figure 22. Decoupled and LQR control responses for flexible-mode control with lag. (LQR closed-loop dynamics used.)
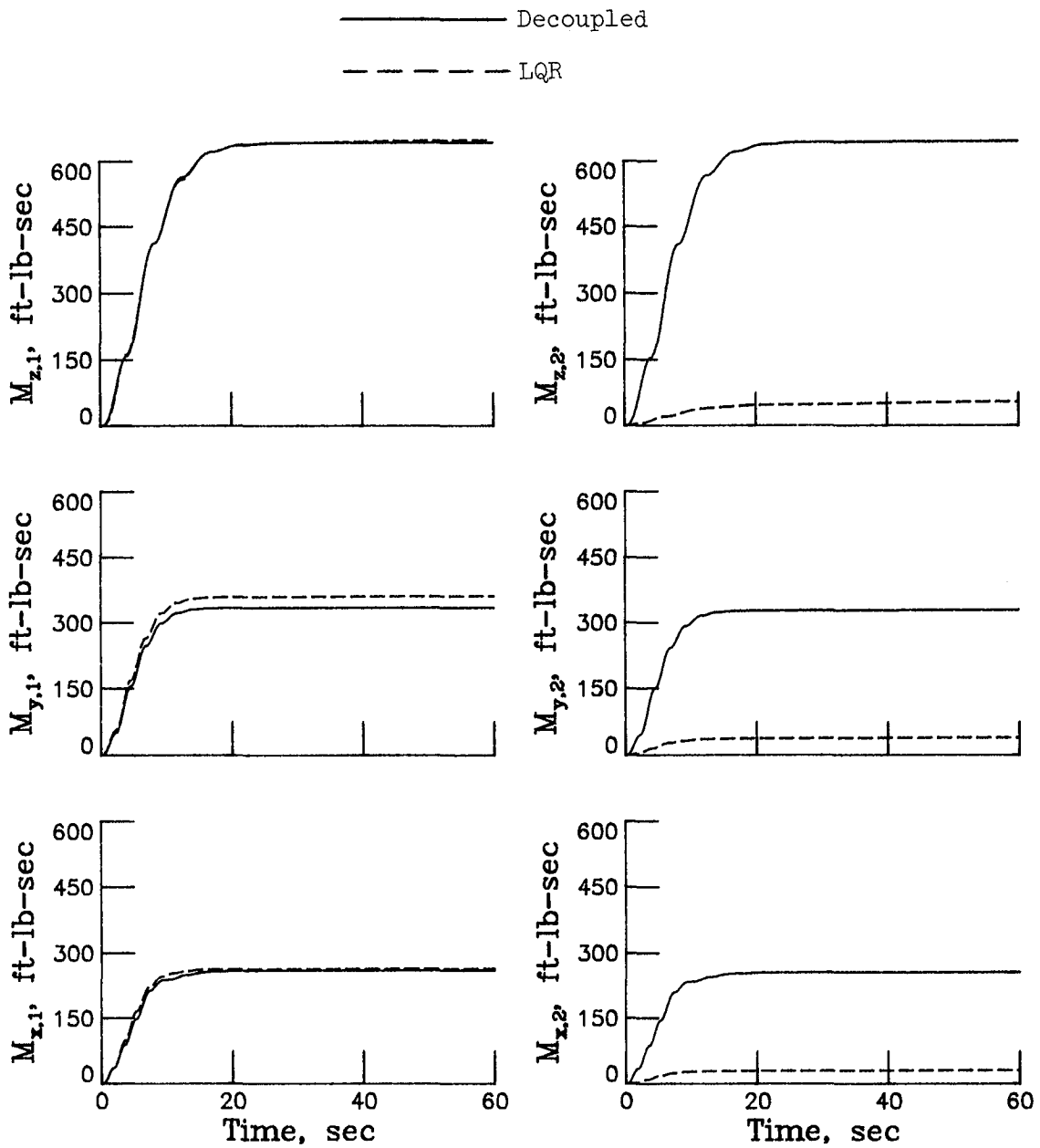
(b) Momentum required.

Figure 22. Concluded.
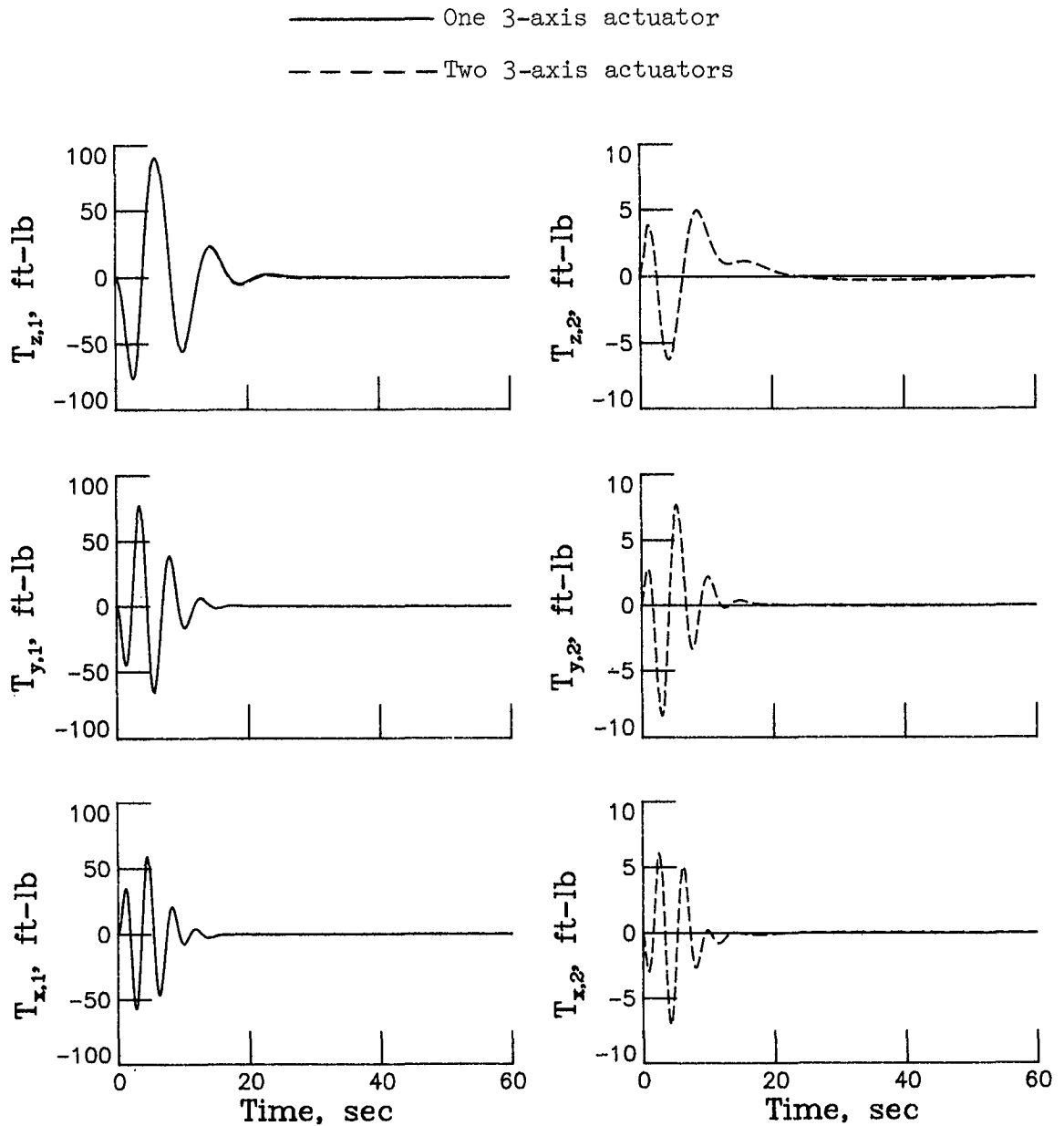
(a) Torque response for LQR control.

Figure 23. Effect of inoperative CMG at bottom of antenna column for flexible-mode control. (Conditions correspond to those of fig. 22.)
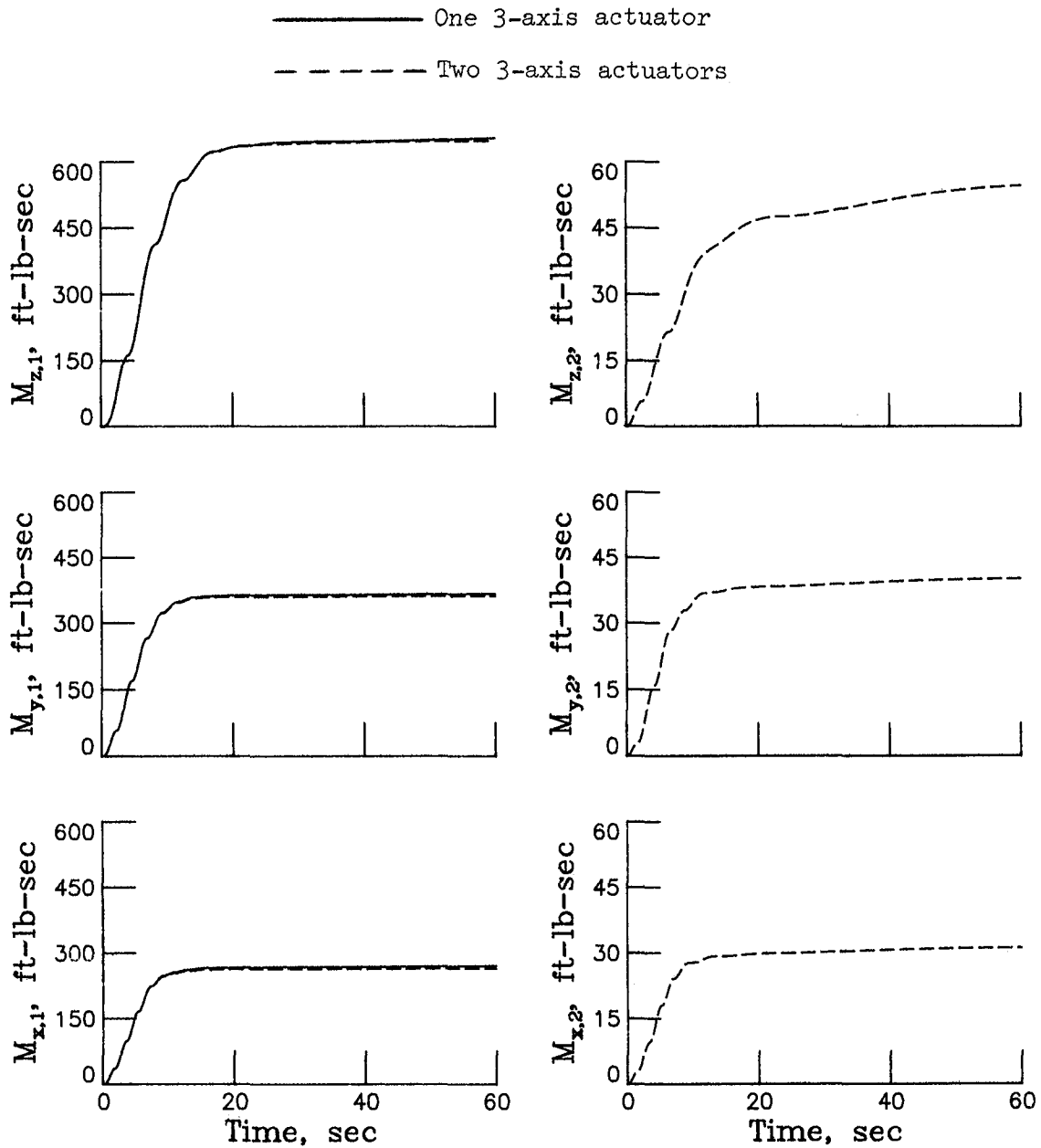
(b) Momentum required for LQR control.
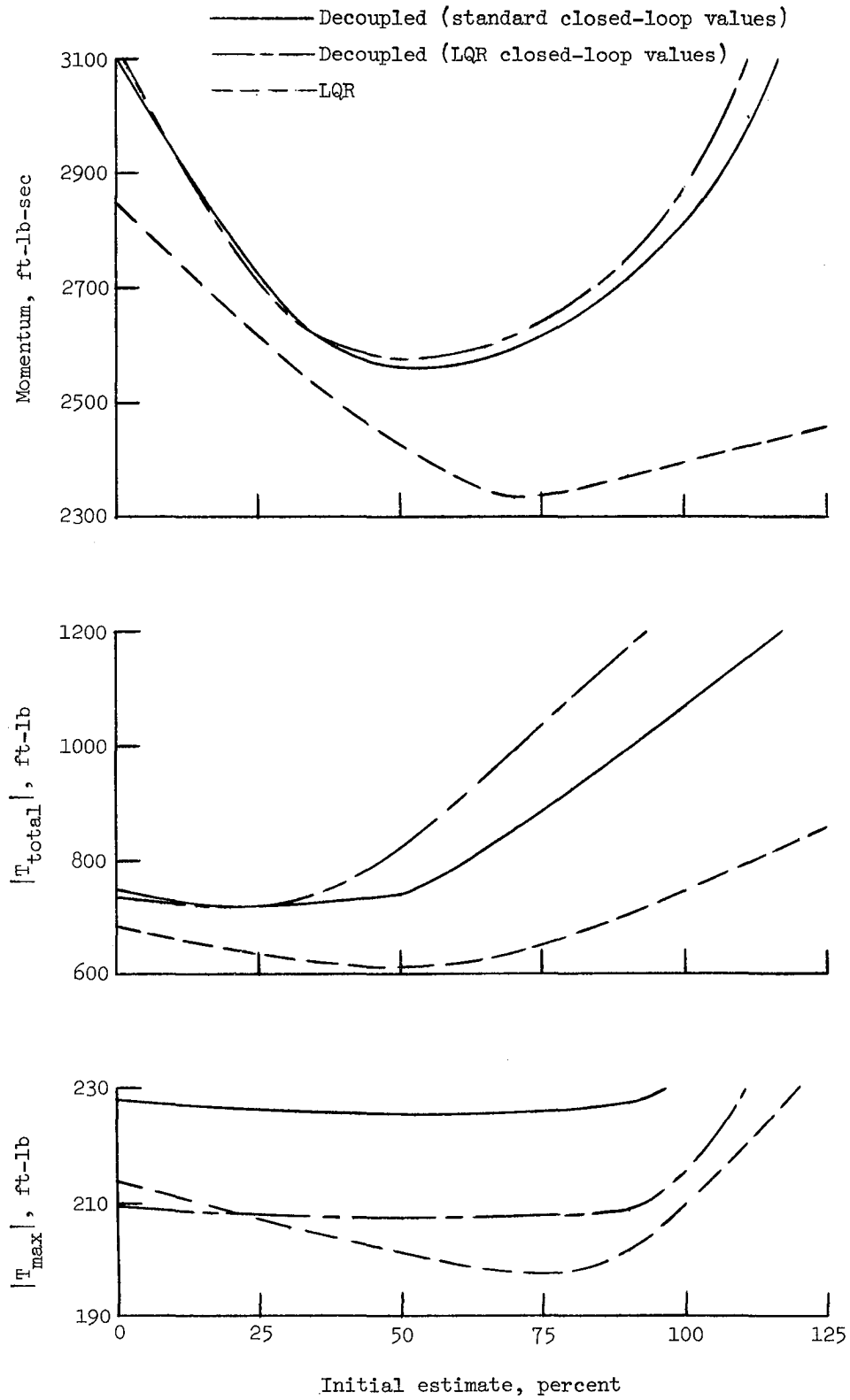
Figure 23. Continued.
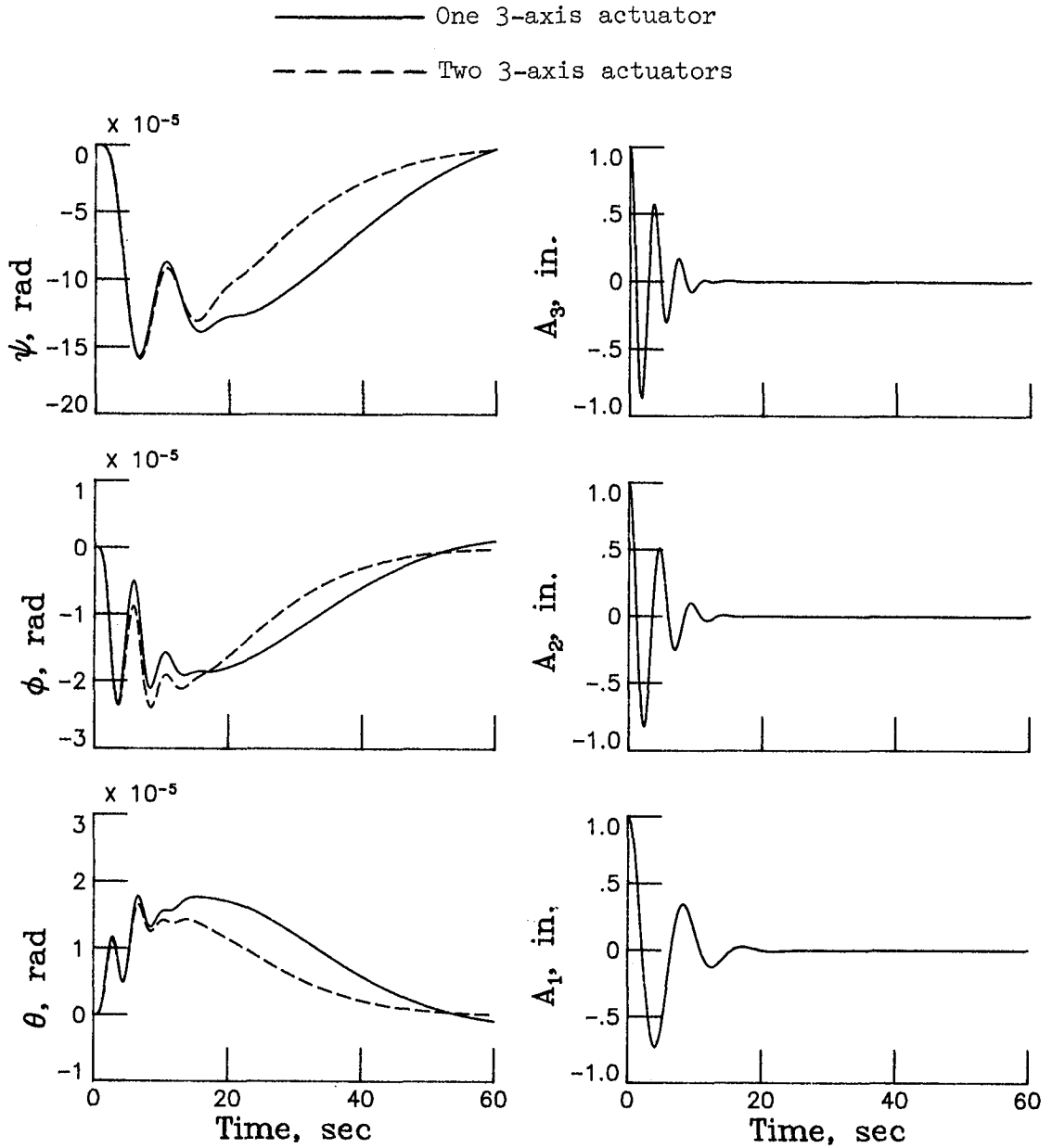
(c) Modal response for LQR control.

Figure 23. Concluded.
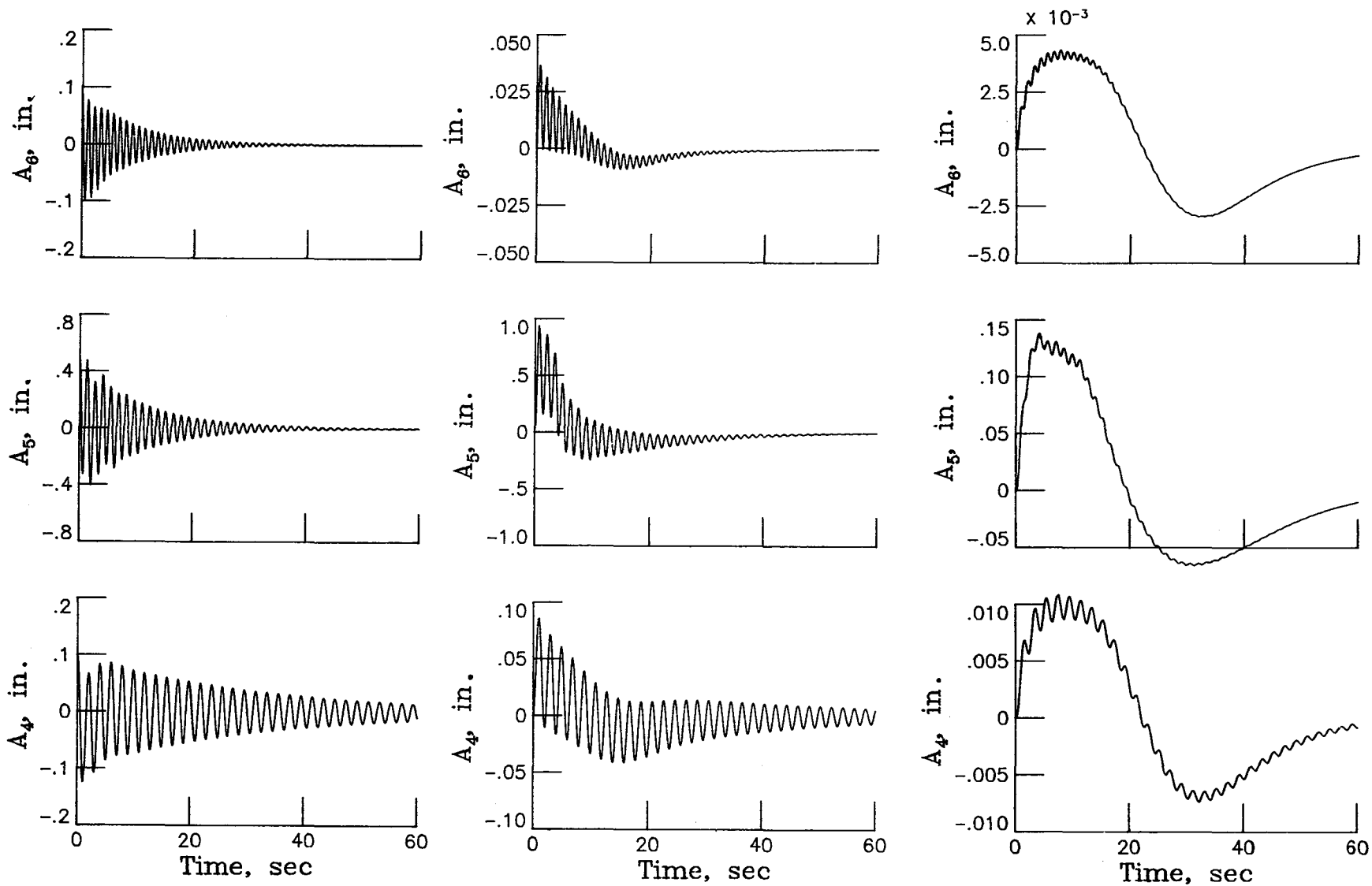
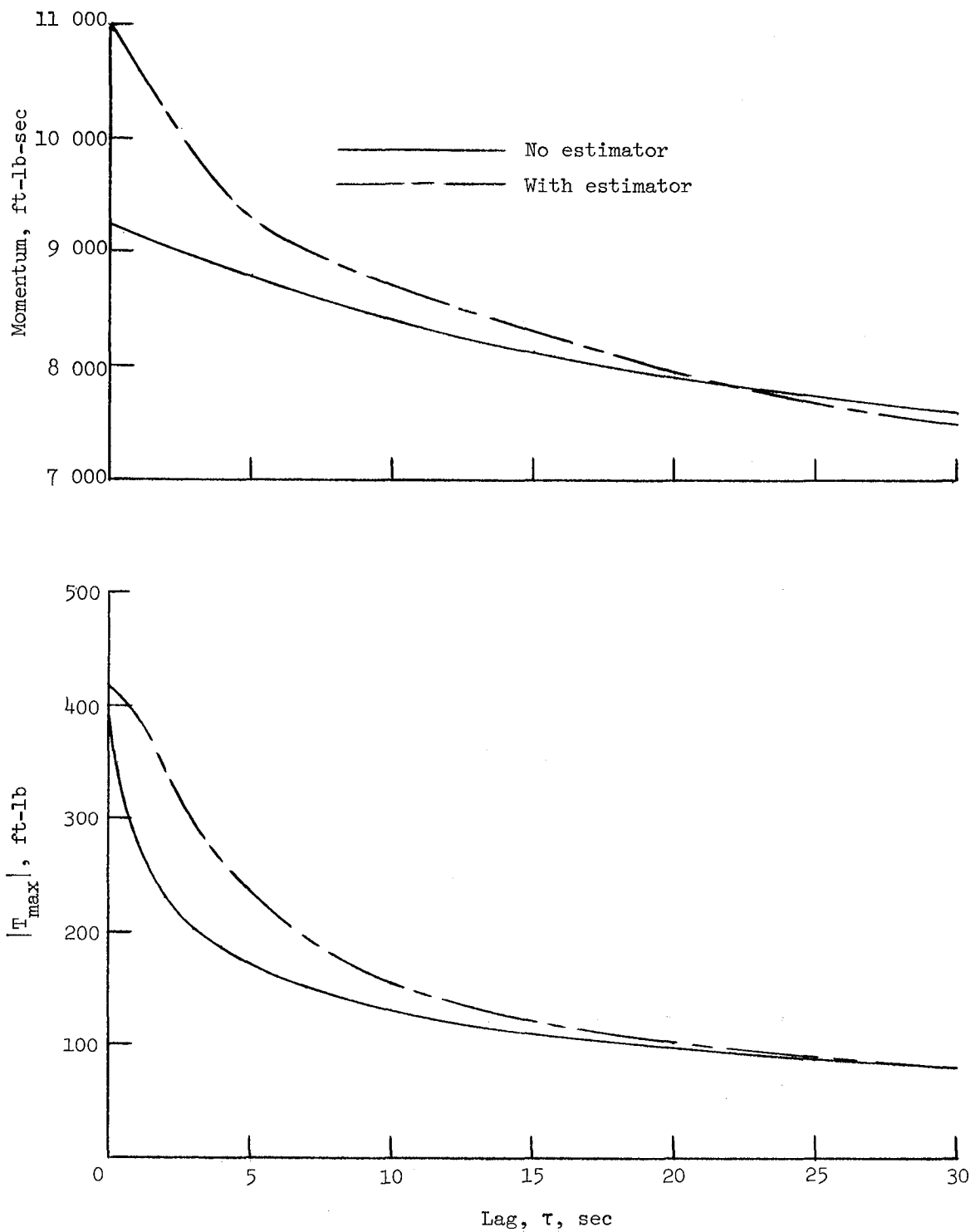Figure 24. Effect of decoupled control on residual modes.
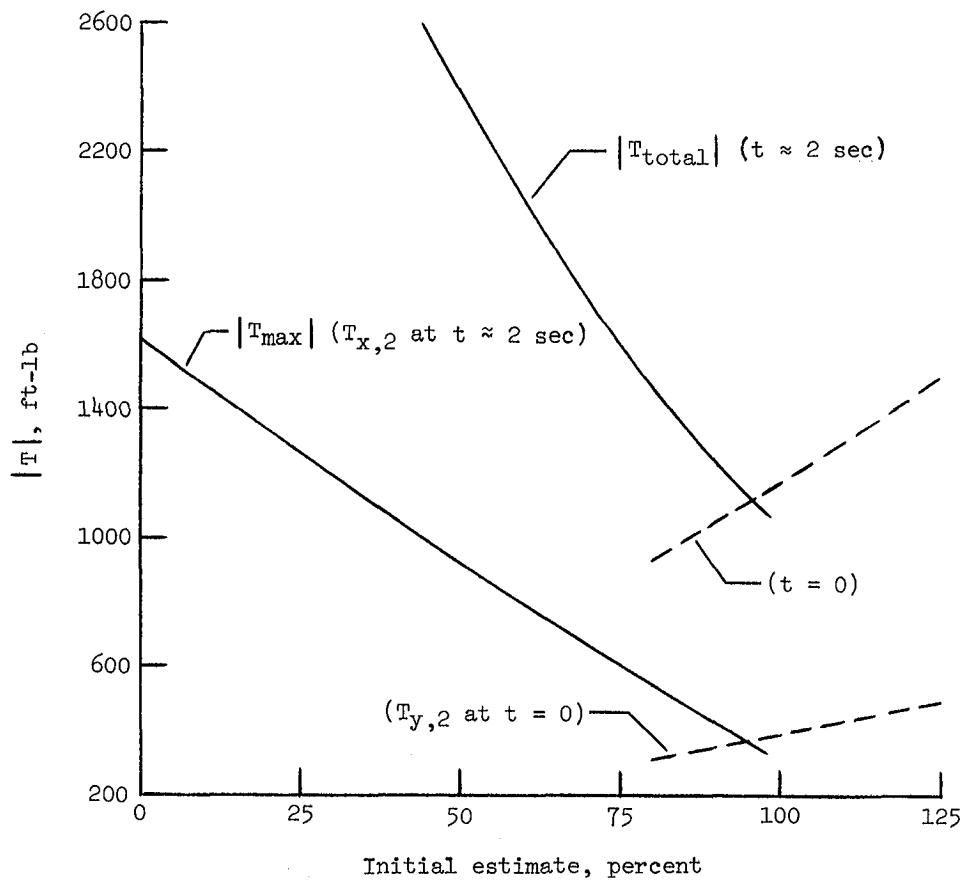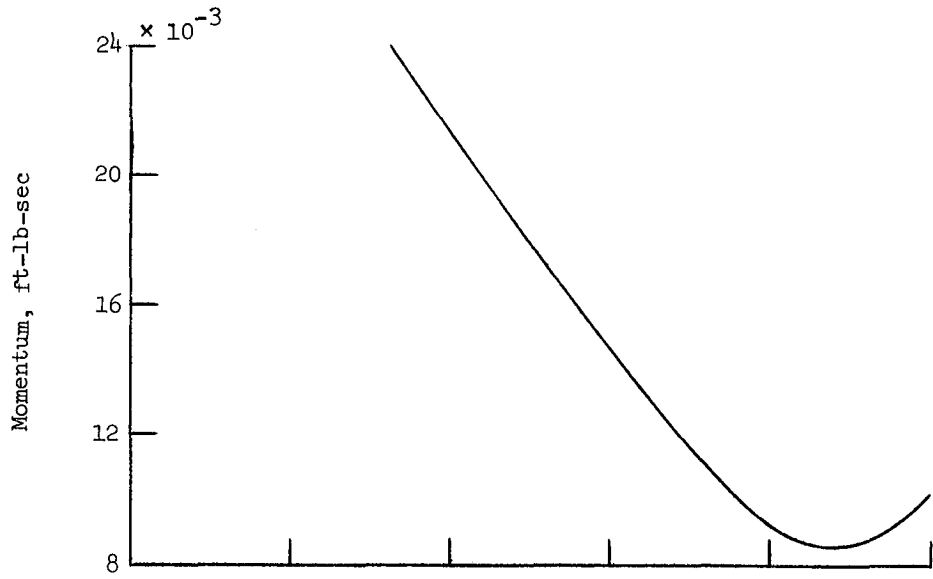
(a) Rigid-body decoupled control. (Decoupled closed-loop dynamics used.)

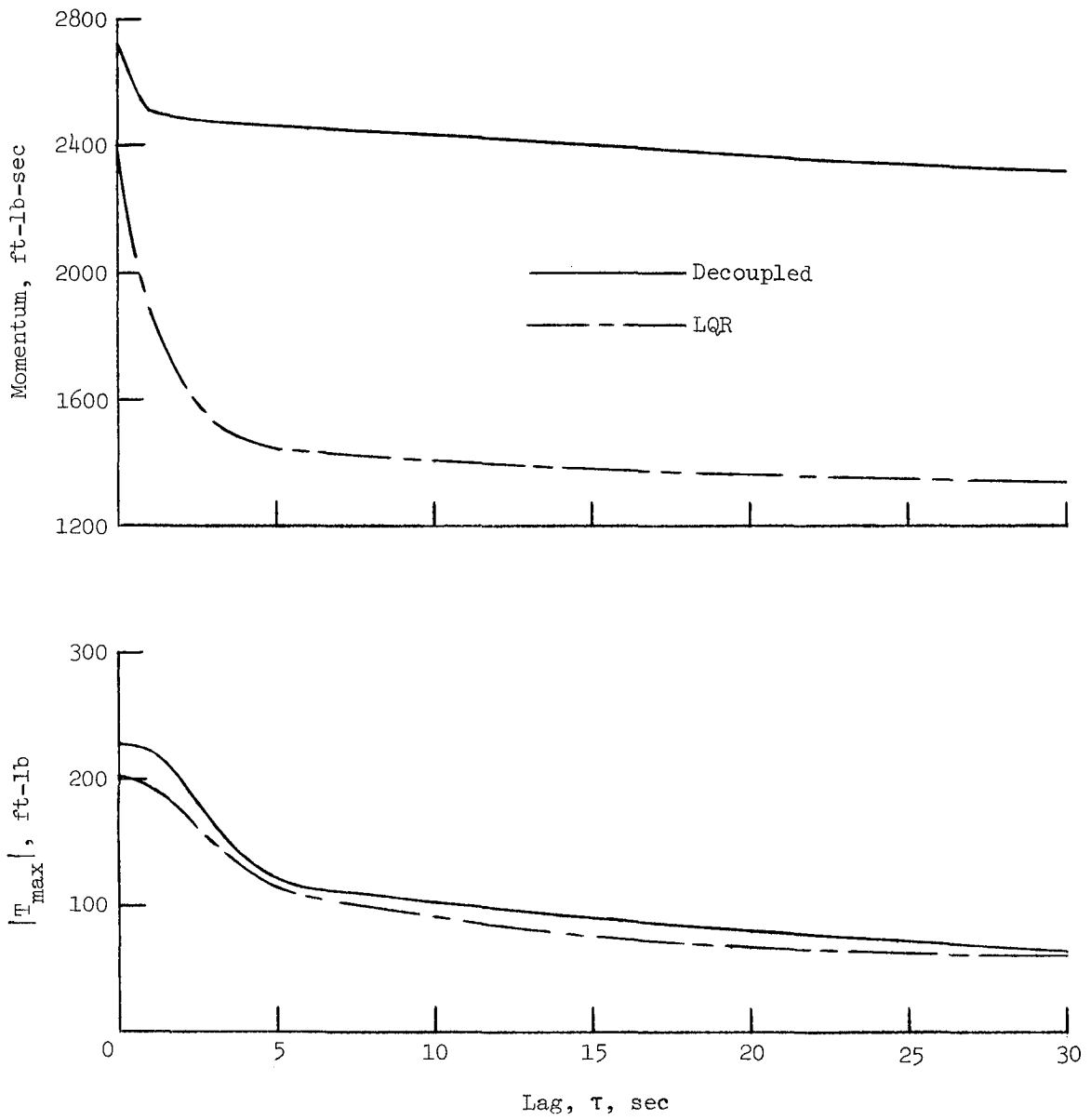Figure 25. Effect of initial estimate on control requirements.

(b) Flexible-mode control.

Figure 25. Concluded.

(a) Rigid-body decoupled control. (One three-axis attitude sensor at location 1. Decoupled closed-loop dynamics used.)

Figure 26. Effect of lag on control requirements.

(b) Flexible-mode control.

Figure 26. Concluded.

Standard Bibliographic Page

1. Report No. NASA TP-2484	2. Government Accession No.	3. Recipient's Catalog No.
4. Title and Subtitle Decoupled and Linear Quadratic Regulator Control of a Large, Flexible Space Antenna With an Observer in the Control Loop		5. Report Date November 1985
		6. Performing Organization Code 506-57-13-03
7. Author(s) Harold A. Hamer, Katherine G. Johnson, and John W. Young		8. Performing Organization Report No. L-15913
9. Performing Organization Name and Address NASA Langley Research Center Hampton, VA 23665-5225		10. Work Unit No.
		11. Contract or Grant No.
12. Sponsoring Agency Name and Address National Aeronautics and Space Administration Washington, DC 20546-0001		13. Type of Report and Period Covered Technical Paper
		14. Sponsoring Agency Code

15. Supplementary Notes

16. Abstract

An analysis was performed to compare decoupled and linear quadratic regulator (LQR) procedures for the control of a large, flexible space antenna. Control objectives involved (1) commanding changes in the rigid-body modes, (2) nulling initial disturbances in the rigid-body modes, or (3) nulling initial disturbances in the first three flexible modes. Control was achieved with two three-axis control-moment gyros located on the antenna column. Results are presented to illustrate various effects on control requirements for the two procedures. These effects include errors in the initial estimates of state variables, variations in the type, number, and location of sensors, and deletions of state-variable estimates for certain flexible modes after control activation. The advantages of incorporating a time lag in the control feedback are also illustrated. In addition, the effects of inoperative-control situations are analyzed with regard to control requirements and resultant modal responses. Comparisons are included which show the effects of perfect state feedback with no residual modes (ideal case). Time-history responses are presented to illustrate the various effects on the control procedures.

17. Key Words (Suggested by Authors(s)) Decoupling Large space structures Linear quadratic regulator Modal control	18. Distribution Statement Unclassified—Unlimited Subject Category 18		
19. Security Classif.(of this report) Unclassified	20. Security Classif.(of this page) Unclassified	21. No. of Pages 72	22. Price A04

National Aeronautics and
Space Administration
Code NIT-3

Washington, D.C.
20546-0001

BULK RATE
POSTAGE & FEES PAID
NASA Washington, DC
Permit No. G-27

NASA

POSTMASTER: If Undeliverable (Section 158
Postal Manual) Do Not Return